PRACTICAL SOLUTIONS TO THE NON-MINIMUM PHASE AND VIBRATION PROBLEMS UNDER THE DISTURBANCE REJECTION PARADIGM

SHEN ZHAO

Bachelor of Engineering in Electrical Engineering

Southeast University, China

June, 1999

Master of Engineering in Electrical Engineering

National University of Defense Technology, China

May, 2006

submitted in partial fulfillment of requirements for the degree

DOCTOR OF ENGINEERING

at the

CLEVELAND STATE UNIVERSITY

May, 2012

This dissertation has been approved for the

Department of ELECTRICAL AND COMPUTER ENGINEERING

and the College of Graduate Studies by

Zhiqiang Gao

Dissertation Committee Chairperson, Dr. Zhiqiang Gao

ECE 4-13-2012

Department / Date

Dan Simon

Dissertation Committee Member, Dr. Dan Simon

ECE / 4-13-2012

Department / Date

Dissertation Committee Member, Dr. Hanz Richter

MCE, 4/13/12

Department / Date

Dissertation Committee Member, Dr. Yung-Tse Hung

Civil Engr Dept 4-13-12

Department / Date

Sally Shao

Dissertation Committee Member, Dr. Sally Shao

Mathematics 4-13-2012

Department / Date

James A. Lock

Dissertation Committee Member, Dr. James Lock

Physics 4/13/12

Department / Date

To the readers...

ACKNOWLEDGEMENTS

First of all, I would like to give the special thanks to my advisor, Dr. Zhiqiang Gao, for his unreserved support on both my academic development and personal life. During the past four years, his eagerness on research has inspired me greatly. I would not accomplish the current achievements and finish this dissertation without his guidance, patience and tolerance. I would give my truly appreciation to Dr. Dan Simon, Dr. Hanz Richter, Dr. Sally Shao, Dr. Yung-Tse Hung and Dr. James Lock for being in my committee, sharing their precious time and providing helpful suggestions. Deepest thanks to Professor Han for introducing me to this great area and sharing his valuable insight.

Also I want to thank: the lab mates Qing Zheng, Gang Tian, Anthony Roberts, Han Zhang, Qinling Zheng and Xiao Wang for enlightening discussions held from time to time; the collaborators on various research projects for their seamless collaboration, including but not limited to Professor Jack Zeller, Mike Neundorfer, Carlo Chico, John Vincent, Dan Morris, Nathan Usher, Wencao Xue, Steve Craig and Leon Hanson; the senior design students Vlad Shtin, Achille Nicoletti, Mike Zandy and Jason Tatsumi for sharing a great experience with them; and other friends Honglei Zhang, Song Cui, Limei Hou, Gu Ouyang, Ning Ge and Maosheng Ye for their help on personal life. Grant support from National Science Foundation is greatly appreciated as well.

My last and deepest gratitude goes to my beloved wife Hui Jin, my lovely daughter Avery Jin-Zhao, and other family members. It is their expectation that supports me to go through this challenging journey and finally finish the program.

PRACTICAL SOLUTIONS TO THE NON-MINIMUM PHASE AND VIBRATION PROBLEMS UNDER THE DISTURBANCE REJECTION PARADIGM

SHEN ZHAO

ABSTRACT

This dissertation tackles two kinds of control problems under the disturbance rejection paradigm (DRP): 1) the general problem of non-minimum phase (NMP) systems, such as systems with right half plane (RHP) zeros and those with time delay; 2) the specific problem of vibration, a prevailing problem facing practicing engineers in the real world of industrial control. It is shown that the DRP brings to the table a refreshingly novel way of thinking in tackling the persistently challenging problems in control. In particular, the problem of NMP has confounded researchers for decades in trying to find a satisfactory solution that is both rigorous and practical. The active disturbance rejection control (ADRC), originated from DRP, provides a potential solution. Even more intriguingly, the DRP provides a new framework to tackle the ubiquitous problem of vibration, whether it is found in the resonant modes in industrial motion control with compliant load, which is almost always the case, or in the microphonics of superconducting radio frequency (SRF) cavities in high energy particle accelerators. That is, whether the vibration is caused by the environment or by the characteristics of process dynamics, DRP provides a single framework under which the problem is better

understood and resolved. New solutions are tested and validated in both simulations and experiments, demonstrating the superiority of the new design over the previous ones. For systems with time delay, the stability characteristic of the proposed solution is analyzed.

TABLE OF CONTENTS

Page

LIST OF TABLES

LIST OF FIGURES

ACRONYMS

ADRC: active disturbance rejection control

CDESO: current discrete extended state observer

CSTR: continuous stirred tank reactor

DDC: disturbance decoupling control

DOB: disturbance observer

DOE: Department of Energy

DRP: disturbance rejection paradigm

ESO: extended state observer

FOPTD: first order plus time delay

FRIB: Facility for Rare Isotope Beams

IAE: integral absolute error

IEC: International Electrotechnical Commission

LINAC: linear accelerator

LLRF: low level radio frequency

LMI: linear matrix inequality

MEMS: micro-electro-mechanical system

MIMO: multi input multi output

MSU: Michigan State University

NMP: non-minimum phase

NSCL: National Superconducting Cyclotron Laboratory

NSF: National Science Foundation

PID: proportional-integral-derivative

PLC: programmable logic controller

POB: perturbation observer

ReA3: 3 MeV/u re-accelerator

RESO: reduced order extended state observer

RF: radio frequency

RHP: right half plane

SISO: single input single output

SOPTD: second order plus time delay

SRF: superconducting radio frequency

UIO: unknown input observer

UPAC: universal programmable automation controller

ZOH: zero order hold

CHAPTER I

INTRODUCTION

Control as a technology is almost everywhere in engineering. It was developed by the people who tried to solve various problems in practice over thousands of years. For example, around 300 BC Greeks invented a float regulator for a water clock to accurately determine the time [1]. One of the most significant inventions in the control history may be the fly-ball governor designed by James Watt in 1788 to regulate the power output of the steam engine [2], after which the Industrial Revolution started. The mostly used proportional-integral-derivative (PID) controller was proposed by Nicholas Minorsky in 1922 [3] to control the steering of ships and it is still a tool of choice today. The empirical approach to design and its variations can be characterized under the *industrial paradigm* [4-6].

On the other hand, control as a science is a branch of applied mathematics. The stability of the control systems was first analyzed by mathematicians around 1850s [1]. In

1930s the frequency domain approaches were used to analyze the control system and later on the classical control theory established. The modern control theory which is based on the time domain analysis started to develop in 1960s. Using the approaches mentioned above, a control problem is solved by the strict analysis and synthesis. Since the control design is based on the mathematical descriptions or models of the systems, this approach can be described as the *model paradigm* [4-6].

Though the modern control theory has been applied to many areas such as space vehicles, robots and aircrafts, the industry world is still dominated by the primitive PID controllers. More than 95% of the controllers used in process control are still PID controllers [7]. People may wonder why the gap is so big. By examining the two approaches, one may find the answer. For a PID controller design, no information about the system is required, which means the dynamics of the system is assumed to be unknown. This actually makes it easy to implement and more practical. For a control design using classical or modern control theory, a mathematic model of the system is needed at the very beginning, which means most of the dynamics of the system is assumed to be known. With the model, a rigorous and systematic control design can be carried out. These two approaches seem to be at two extremes. One assumes that no knowledge of the system is available; the other assumes that very good knowledge of the system is available. This may explain why there is a big gap between the two control paradigms.

In most cases we know something about the system dynamics, but not everything. Thus an approach that can take advantage of what is known and also can deal with what is unknown is necessary. The *disturbance rejection paradigm* (DRP) [4-6] is proposed to

meet this need. Under the DRP, the primary dynamics of the system is assumed to be known and all the unknowns are considered as disturbances. The main goal of this approach is then to reject the disturbances. If somehow the effect of the disturbances can be cancelled, the remaining part of the control design will focus on the control of the primary dynamics of the system.

As one can see, the DRP plays a role of connecting the industrial paradigm and the model paradigm as a bridge. It provides another option for solving a control problem between the industrial paradigm and the model paradigm, which may be more practical than the model paradigm and may get better performance than the industrial paradigm.

The fundamental goal in a control system design is to keep the error e between the system output y and the reference input r constantly at zero as shown in Figure 1. In other words, let the error e be invariant to the changes in both the reference input r and the disturbance input d, which can be considered as general disturbances under the DRP. From the traditional perspective, the fundamental goal might be broken down as two separate goals which are tracking the reference (also known as servo) and rejecting disturbances (also known as regulator). To achieve these goals, different methods can be used. The error driven feedback controller can achieve the two goals at the same time, but it is passive since it only reacts to the error. The model based feedforward control, however, can achieve better tracking performance, because it does not have to wait for the error to occur. Similarly better disturbance rejection performance can also be achieved by canceling the disturbance based on direct measurement or estimation. Both feedforward control and disturbance cancellation are active compared to the feedback control, hence both can be considered as active disturbance rejection methods.

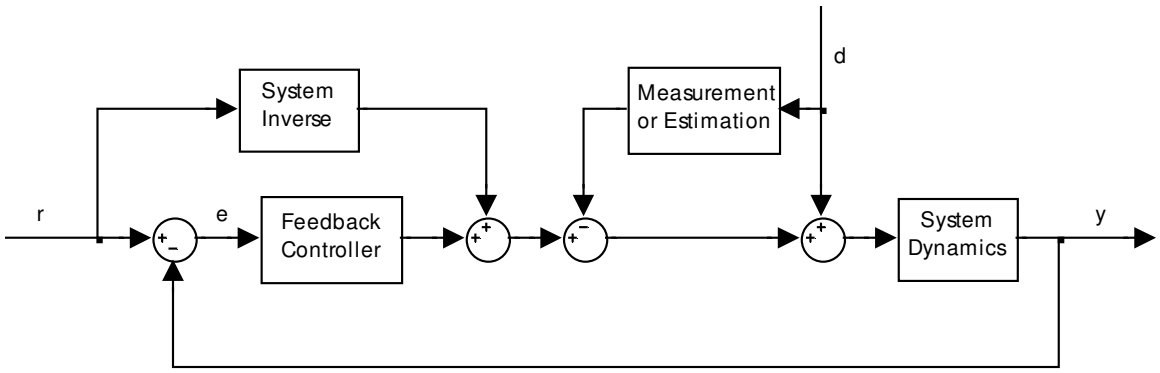

Figure 1 The diagram of a general control design.

The most effective way to cancel the disturbance is obviously to measure it directly. Under situations that the disturbance is not measurable, an estimation of the disturbance can be obtained using various methods; for example, the unknown input observer (UIO) [8, 9], the disturbance observer (DOB) [10, 11], the extended state observer (ESO) [4, 12], the perturbation observer (POB) [13, 14], etc. Among those methods, only ESO does not rely on an accurate system model, which means it can handle the system uncertainties. The active disturbance rejection control (ADRC) is built based on the unique ESO and has been demonstrated to be very effective for systems with both internal uncertainties and external disturbances.

The research work on ADRC, however, has been mainly focus on minimum phase systems. The ADRC design for non-minimum phase (NMP) systems, for example, systems with right half plane (RHP) zeros and systems with time delay, have not been fully addressed. The control design for NMP systems is generally challenging due to the additional phase lag and the achievable closed-loop bandwidth is normally limited. Recall that the feedforward control does not help with the disturbance rejection and the disturbance cancellation does not help with the reference tracking. It is under this

background that we investigate the ADRC design for such systems, hoping for a better solution, and propose the ADRC and feedforward combined design to achieve better performance.

In addition, the control design for two vibration problems in industrial applications is addressed under the DRP using ADRC. One is the ubiquitous vibration suppression problem in motion control; the other is the annoying microphonics problem in superconducting radio frequency (SRF) cavity control. In motion control, the vibration is the result of the resonant modes in system dynamics, which can be treated as internal disturbance, whereas in SRF cavity control the microphonics due to the vibrations from surrounding environment is an external disturbance. In each application, both simulation study and experimental verification are conducted.

The rest of the dissertation is organized as follows. The literature review on disturbance rejection in general and the specific development of ADRC is given in Chapter 2, where the standard linear ADRC design with parameterization is also described. The literature review for each topic addressed in the dissertation is provided in individual chapters. The ADRC design together with the feedforward design for systems with RHP zeros is explored in Chapter 3. The ADRC design for systems with time delay is studied and corresponding stability analysis is provided in Chapter 4. The ADRC solution to the vibration suppression problem in motion control is studied through both simulations and experiments in Chapter 5. In Chapter 6 the microponics problem in SRF cavity control is solved using the ADRC design. As an extension the ability of ADRC to deal with unknown actuator nonlinearities is addressed in Chapter 6 as well. Finally, conclusions and possible future work are given in Chapter 7.

CHAPTER II

THE EMERGENCE OF THE DISTURBANCE REJECTION PARADIGM

In this chapter, a literature review on disturbance rejection is provided. The chapter is organized as follows. Section 2.1 reviews the history of active disturbance rejection. In Section 2.2 the evolution of ADRC towards a practical solution is reviewed from different perspective, including technical development, application and theoretical justification. Section 2.3 discusses the emergence and the benefits of the disturbance rejection paradigm. Section 2.4 describes the standard linear ADRC formulation with the parameterization, which will be used later on. Section 2.5 summarizes the chapter.

2.1 A Historic View of Active Disturbance Rejection

As discussed in Chapter 1, disturbance cancellation as an alternative to the feedback provides better disturbance rejection performance. The idea of disturbance

cancellation is not something new as many people may think. In fact, it has a history just as old as the feedback control. The first application of disturbance cancellation might be the south-pointing chariot [15], a famous Chinese invention, on which a figure points to a constant direction no matter how the chariot turns. In legend, the south-pointing chariot was invented in 2634 BC, but the first recorded invention happened in 235 AD [16]. In this application, the movement of the south-pointing chariot is measured by a special designed mechanism and then the figure is adjusted accordingly to maintain its direction. Over a thousand years later, in 1829, Jean-Victor Poncelet designed a new governor for steam engines using a similar idea [17]. In his design the engine load is measured directly by a spring, and based on the changes in load (disturbances), instead of changes in velocity (errors), the valve is adjusted to maintain a constant speed. The theory behind the idea, however, did not establish until 1939 when G. B. Shchipanov, a scholar of Soviet Union, proposed the theory of invariance [18]. The main problem studied in the theory of invariance is how to make a system variable (e.g. error) invariant to the system inputs (e.g. reference and disturbance). Reference tracking and disturbance rejection are then unified in this manner, and reference tracking can be regarded as another type of disturbance rejection. Hence the core of a control design is disturbance rejection.

In the above two examples, the disturbances are directly measurable. Under situations that the disturbance is not measurable, an estimation of the disturbance is necessary for the cancellation. Different forms of modern control theory based observers have been proposed to meet this need. In 1971, Johnson proposed the UIO [8] to estimate the unknown input of the system. The transfer function based DOB [10], proposed later on by Japanese researchers, can estimate the disturbance as well. The research [11] in

2002 showed the UIO and DOB are equivalent. The POB was proposed by Kwon and Chung in 2002 [13] in the discrete form to estimate the perturbation acted on the system. Above the "unknown input", the "disturbance" and the "perturbation" are just different names for the external disturbance, and the above observers can only deal with it.

The observer design took a leap in 1995, when Han proposed the unique ESO [12] to address not only the external disturbances but also the internal dynamic uncertainties, the whole effect of which is considered as the total disturbance and estimated by the ESO. Once the total disturbance is estimated, it can be cancelled out in the control law, based on which the ADRC was first proposed in 1998 by Han [19] in the nonlinear form. In [20] ADRC has been demonstrated to be very effective for a variety of systems, such as MIMO systems, cascade systems, chaos systems, etc.

2.2 The Evolution of ADRC towards an Engineered Solution

Though powerful, the original nonlinear ADRC is very complicated in implementation, tuning, and analysis, which hinders its application. The simplification and parameterization by Gao [21] in 2003 made it practical and facilitated its development afterward. Much research work has been done on improving the ADRC design since then, which are classified into three categories: technical development, applications and theoretical justification, and summarized in the following subsections.

2.2.1 Technical Development

Since ESO is a key part of the ADRC, extensive work has been done on it. First, a current discrete extended state observer (CDESO) is developed based on the idea of taking advantage of the current measurement to reduce the lag due to the sampling [22,

23]. Its advantage is obvious in systems with slow sampling rate. ESO is then generalized to comprise more than one extended states so that it can accommodates different types of disturbances, such as a ramp or a parabola disturbance [23]. Under a few assumptions, the ESO is combined with a Kalman filter to provide an optimal ESO formulation without increasing the complexity [24]. After that, a reduced order ESO (RESO) is proposed [25] to reduce the phase lag while estimating the total disturbance, but it is more sensitive to the measurement noise. So one should decide when to use RESO based on the acceptable noise level.

In addition to the observer development, a disturbance decoupling control (DDC) [26] is proposed based on the disturbance rejection ability of ADRC. By treating the internal interactions as disturbances, the multi-input-multi-output (MIMO) system is easily decoupled into separate loops.

On the controller design, a study that combines ADRC and H-infinity controller is carried out in [27] and better robustness over the original ADRC design is achieved with the proposed design.

2.2.2 Applications

Besides the technical development, ADRC has also been applied to solve different problems successfully in a variety of applications, such as the web tension control [28, 29], hard disk drive control, DC-DC power converter [30], etc. It also has the ability to deal with the nonlinearity of the actuators, such as hysteresis in the piezoceramic actuator [31, 32]. Several MIMO systems, such as micro-electro-mechanical system (MEMS) [33] and the continuous stirred tank reactor (CSTR) [26], are decoupled and well controlled by

applying DDC. The application of ADRC is no restrict only in control, it has been used for the health monitoring and fault detection purposes as well [24].

The previous applications are mostly within the confine of minimum phase systems. The more challenging control design for systems with RHP zeros and systems with time delay has not been fully investigated. Even in the only book on ADRC [20], the design problem associated with RHP zeros is not addressed. The ADRC design for systems with time delay is only addressed in [20, 34], but the complexity of the design inhibits its application.

2.2.3 Theoretical Justification

Theoretically, since ADRC has been simplified to the linear form, almost all the tools in the classical and modern control theory are readily available to facilitate the analysis of ADRC. An equivalent two degree of freedom transfer function form of ADRC is developed [35], so that the frequency domain analysis can be carried out. The frequency response analysis gives a clearer picture on how well is the total disturbance estimated than in the time domain description.

The stability analysis of ESO and ADRC has been done to enhance the theoretical completeness of the technique. Zheng *et al.* [36, 37] proved the stability of ESO, ADRC and even DDC by solving the state equations directly, assuming that the derivative of the total disturbance $\dot{f}$ is bounded. A later research [38] showed that ESO converges as long as $\dot{f}$ is bounded or f itself is bounded. Freidovich *et al.* [39] proved the stability of an extended high gain observer for a more general nonlinear system. Zhou *et al.* [40] proved the stability of ADRC from the prospective of singular perturbation. A comparison of the

stability properties of different observers is found in [41]. Zhao [42] studied the capability of ADRC for minimum phase systems with unknown orders and uncertain relative degrees. Most recently, Guo *et al.* provided the analysis on the convergence of ESO for nonlinear systems with uncertainty [43]. Huang *et al.* [44] compared ADRC with other control methods that deal with system uncertainties, such as adaptive control, robust control, sliding mode control, etc., and summarized recent theoretical achievements on the ADRC design.

2.3 The Emergence of the Disturbance Rejection Paradigm

After over ten years of significant developments and successful applications of ADRC-based design techniques, the concept of disturbance rejection paradigm (DRP) was crystallized and articulated by Gao in 2010 [6], inspired by the conviction that the essence of control problems is how to deal with uncertainties. There are many kinds of uncertainties in the physical processes. The disturbance commonly seen in the literature comes from the environment in which control systems operate, and is generally independent of the system dynamics. This notion of disturbance is also known as *external disturbance*. Another kind of system uncertainty, considered in robustness control theory in modern control, is associated with the unknown dynamics in the physical process and is "internal" to it. Such uncertainty can be viewed as *internal disturbance*. Central to the mission of control system design is to make the process variables to be controlled "invariant", i.e. independent to, both kinds of uncertainties. Under the DRP, the previously two separated problems of (external) disturbance rejection and robustness with respect to unknown internal dynamics are united into a single framework. That is the

whole effect of the external disturbance and the internal disturbance is defined as the *total disturbance*. Hence, all design methods and concepts are evaluated in terms of how well such total disturbance is mitigated under the DRP.

This unique idea of treating system uncertainties as total disturbances breaks down the boundaries and unifies many previously separate fields of investigation, including but not limited to, linear and nonlinear systems, time varying and time invariant systems, robust control and disturbance rejection, coupled (MIMO) and independent (SISO) control loops. In short, the DRP brings a totally different perspective in how the control problems are perceived and treated, as well as solutions to conventional problems that are "out of box", as will be shown throughout this dissertation. One such solution is ADRC, as discussed below.

2.4 The ADRC Formulation

In this section, the ADRC solution is presented in its linear and parameterized form, which will be used throughout the dissertation unless otherwise noted. Consider the following n th order system

$$y^{(n)} + a_{n-1}y^{(n-1)} + \cdots + a_1\dot{y} + a_0 y = b\left(u + w\right) \tag{2.1}$$

where y is the system output, $y^{(n)}$ denotes the n th order derivative of y, u is the system input, and w is the equivalent input disturbance which is a function of time. The objective of the control design is to make the system output y to follow a given reference signal r.

In the context of active disturbance rejection, the original system (2.1) can be reformulated as

$$y^{(n)} = bu + \left(bw - \sum_{i=0}^{n-1} a_i y^{(i)} \right) = bu + f\left(w, y, \dot{y}, \cdots, y^{(n-1)} \right) \tag{2.2}$$

where f is called the total disturbance which includes not only the external disturbances but also the unknown internal dynamics. Then the state vector of the system is defined as

$$X_{n+1} = \begin{bmatrix} x_1 & x_2 & \cdots & x_n & x_{n+1} \end{bmatrix}^T = \begin{bmatrix} y & \dot{y} & \cdots & y^{(n-1)} & f \end{bmatrix}^T \tag{2.3}$$

which has $(n+1)$ elements. Note that for an n th order system the state vector is normally defined as $X = \begin{bmatrix} y & \dot{y} & \cdots & y^{(n-1)} \end{bmatrix}^T$ with n elements. Here $x_{n+1} = f$ which is called the extended state representing the total disturbance is augmented to the regular design.

The state space representation of (2.2) is

$$\begin{aligned} \dot{X}_{n+1} &= A_{n+1} X_{n+1} + bB_{n+1} u + E_{n+1} \dot{f} \\ y &= C_{n+1} X_{n+1} \end{aligned} \tag{2.4}$$

where $A_{n+1} = \begin{bmatrix} 0 & 1 & 0 & \cdots & 0 \\ 0 & 0 & 1 & \cdots & 0 \\ \vdots & \vdots & \vdots & \ddots & \vdots \\ 0 & 0 & 0 & \cdots & 1 \\ 0 & 0 & 0 & \cdots & 0 \end{bmatrix}_{(n+1)\times(n+1)}$, $B_{n+1} = \begin{bmatrix} 0 \\ 0 \\ \vdots \\ 1 \\ 0 \end{bmatrix}_{(n+1)\times 1}$, $E_{n+1} = \begin{bmatrix} 0 \\ 0 \\ \vdots \\ 0 \\ 1 \end{bmatrix}_{(n+1)\times 1}$, and

$C_{n+1} = \begin{bmatrix} 1 & 0 & 0 & \cdots & 0 \end{bmatrix}_{1\times(n+1)}$. An ESO is designed for system (2.4) accordingly as

$$\dot{\hat{X}}_{n+1} = A_{n+1} \hat{X}_{n+1} + \hat{b} B_{n+1} u + L_{n+1} \left(x_1 - \hat{x}_1 \right) \tag{2.5}$$

where $\hat{X}_{n+1} = \begin{bmatrix} \hat{x}_1 & \hat{x}_2 & \cdots & \hat{x}_n & \hat{x}_{n+1} \end{bmatrix}^T$ is the observer state vector which provides an estimation of the system state vector X_{n+1}, $\hat{b}$ is an estimation of b, and $L_{n+1} = \begin{bmatrix} l_1 & l_2 & \cdots & l_n & l_{n+1} \end{bmatrix}^T$ is the observer gain vector. The controller is designed as

$$u = \frac{K_{n+1}\left(R_{n+1} - \hat{X}_{n+1}\right)}{\hat{b}} \tag{2.6}$$

where $R_{n+1} = \begin{bmatrix} r & \dot{r} & \cdots & r^{(n-1)} & r^{(n)} \end{bmatrix}^T$, $r^{(n)}$ denotes the n th order derivative of r, and $K_{n+1} = \begin{bmatrix} k_1 & k_2 & \cdots & k_n & 1 \end{bmatrix}$ is the controller gain vector. In practice, $r^{(i)}$ $\left(i = 1, 2, \ldots, n\right)$ is set to zero if it is either not available or unbounded.

The above ADRC design is for the general n th system, hence called the n th order ADRC; though the observer has $\left(n+1\right)$ states.

According to the parameterization technique proposed in [21], the individual observer gains l_i $\left(i = 1, 2, \ldots, n, n+1\right)$ are selected such that all eigenvalues of $A_{n+1} - L_{n+1}C_{n+1}$ are placed at $-\omega_o$, and they are found to be

$$l_i = \binom{n+1}{i} \omega_o^i \quad \left(i = 1, 2, \ldots, n, n+1\right) \tag{2.7}$$

where $\binom{n}{k}$ denotes the number of k -combinations from a given set of n elements. Similarly, the individual controller gains k_i $\left(i = 1, 2, \ldots, n\right)$ are selected such that all eigenvalues of matrix $\tilde{A}_{n\times n}$ are placed at $-\omega_c$, where $\tilde{A}_{n\times n}$ is defined as

$$\begin{bmatrix} \tilde{A}_{n\times n} & 0 \\ 0 & 0 \end{bmatrix}_{(n+1)\times(n+1)} = A_{n+1} - B_{n+1}K_{n+1} \tag{2.8}$$

and they are found to be

$$k_i = \binom{n}{n+1-i} \omega_c^{n+1-i} \quad \left(i = 1, 2, \ldots, n\right) \tag{2.9}$$

Above, ω_o and ω_c are referred to as observer and controller bandwidth respectively, and are the tuning parameters of the ADRC design. Furthermore, the ratio between the observer and controller bandwidth $\alpha = \omega_o / \omega_c$ can be fixed, so that the controller bandwidth ω_c becomes the only tuning parameter of the design. In most applications α can be chosen from two to ten.

In practice, observer and controller bandwidth are selected based on following considerations: 1) the controller bandwidth should be higher than the required bandwidth given in the specification; 2) the observer bandwidth should be two to five times higher than the controller bandwidth; 3) the observer bandwidth should be five to ten times less than the sampling rate. Normally, the higher the bandwidth is, the better the performance is; the cost is that the system is more susceptible to noise and has less robustness.

2.5 Summary

By reviewing the history of active disturbance rejection, the evolution of ADRC and the emergence of the DRP, shows that the research work addressing the disturbance rejection in NMP systems is of great importance and needs to be addressed timely.

CHAPTER III

DISTURBANCE REJECTION IN SYSTEMS WITH RHP ZEROS

Systems with right half plane (RHP) zeros belongs to a class of system known as non-minimum phase (NMP) systems. Hence the RHP zeros are also call NMP zeros. The control design for such NMP systems is quite challenging due to the additional phase lag introduce by the RHP zeros. At the same time, controlling such NMP systems is also a rather important practical concern as we find it alike in industrial processes such as hydro power plants as well as military applications such as the aircraft pitch angle control. In this chapter, several control designs were carried out to address the disturbance rejection as well as the tracking performance of such systems.

The chapter is organized as follows. Starting in Section 3.1 some preliminaries and the literature review are provided. The ADRC design for systems with RHP zeros is addressed in Section 3.2. The feedforward control designs including the time optimal control solution and a novel solution that achieves minimum settling time subject to

undershoot constraint are presented in Section 3.3. An example adopting the feedforward and feedback combined design is given in Section 3.4 to demonstrate the effectiveness of the proposed solutions. At the end Section 3.5 summarizes this chapter.

3.1 Background

There are different causes for the RHP zeros. Physical non-collocation of sensing and actuation [45] or linearization of nonlinear systems around an operating point may produce RHP zeros in a continuous single-input-single-output system (SISO), such as the four-wheeled car and the inverted pendulum on a cart given in [46]; in a multi-input-multi-output (MIMO) system, however, the RHP zeros are the effects of competing slow and fast dynamics which have opposite signs [47]; systems originally having stable zeros may possess RHP zeros as well after discretization using the zero-order hold (ZOH) method [48].

Systems with RHP zeros have a unique behavior in the step response known as undershoot or "wrong way response," and it has been studied for many decades [45, 49-53]. A rather comprehensive review on NMP zeros can be found in [46] where some important properties, for example, the condition for the initial undershoot and the number of zero crossings, of such systems are discussed. The NMP zeros in MIMO systems and discrete systems are also briefly mentioned at the end of [46].

Perfect tracking for systems with RHP zeros requires either the unstable pole-zero cancellation which should be avoided because it will make the system internally unstable, or a non-causal controller [47]. Neither is practical; hence perfect tracking should not be expected for such systems. Theoretical analysis on performance limitations imposed by

RHP zeros have been studied and presented [47, 54, 55]. It is shown that the closed-loop bandwidth ω_{cl} is limited to $\omega_{cl} < z/2$, where z is a real RHP zero [47]. To overcome this constraint and achieve better, faster transient response, the only recourse seems to be the open loop compensation, known as the feedforward method. See, for example, [56] where various feedforward methods [57-60] for discrete systems with RHP zeros are considered in the context of a hard disk drive application to reduce the settling time.

Even with the feedforward design, the task of control design for these problems is still complicated, because in general the faster the response the larger the undershoot; there is only so far the wrong way response can go before it endangers the physical integrity of the system. The well known time optimal control solution for a specific system with RHP zero will be derived in Section 3.3.1, but the associated undershoot tends to be overwhelming. Although some vague ideas of the connection between the settling time and the undershoot has been given in [53] and [61], what has not been adequately addressed in the literature is how to systematically make the proper design tradeoff between the settling time and the undershoot. In particular, the theoretical minimum settling time for a given undershoot constraint can be calculated based on the results in [53] and [61], but the corresponding control signal that achieves such settling time has not been found yet. In Section 3.3.2 the control law that achieves the minimum settling time for systems with either a single real RHP zero or two distinct real RHP zeros subject to a specific undershoot constraint will be constructed.

In this chapter, we focus on the control design for continuous SISO systems with RHP zeros. Some related preliminaries which will be used in Section 3.3.2 are presented below. The transient response for linear time invariant NMP systems, with input u,

output y and transfer function $P(s)=Y(s)/U(s)$, is addressed in [53], from its initial condition ($y=0$) to final destination ($y=y_d>0$). It is shown that for such systems the undershoot, while unavoidable in systems with real RHP zeros, has a tradeoff relationship with the settling time. Specifically, the relative undershoot r_{us} and the settling time t_s are defined in [53] as

$$r_{us}=-\inf_{t\in[0,\infty)}\left\{\frac{y(t)}{y_d}\right\} \tag{3.1}$$

$$t_s=\inf_{\tau\in[0,\infty)}\left\{\tau\middle|y(t)=y_d,\ \ t\in[\tau,\infty)\right\} \tag{3.2}$$

Note that t_s is defined as the *exact settling time* to simplify the analysis, as stated in [53]. With these definitions, the relations between the undershoot and the settling time are obtained for systems with one real RHP zero or two distinct real RHP zeros, as restated in the following lemmas.

Lemma 3.1 [53]**:** *For a NMP system with one RHP zero* $z>0$*, and for any bounded input signal* u*,*

$$r_{us}\geq r_{us}^*=\frac{1}{e^{zt_s}-1}\ \text{ or }\ t_s\geq t_s^*=\frac{\ln(1/r_{us}+1)}{z} \tag{3.3}$$

Lemma 3.2 [53]**:** *For a NMP system with two RHP zeros* z_1 *and* z_2*, with* $z_2>z_1>0$*, and for any bounded input signal* u*,*

$$r_{us}\geq r_{us}^*=\frac{z_1e^{-z_2t_s}-z_2e^{-z_1t_s}}{z_1\left(1-e^{-z_2t_s}\right)-z_2\left(1-e^{-z_1t_s}\right)}=f(t_s,z_1,z_2)\ \text{ or }\ t_s\geq t_s^*=f^{-1}(r_{us},z_1,z_2) \tag{3.4}$$

That is, for a given settling time t_s, there exists a minimum undershoot r_{us}^*; conversely, for a given undershoot r_{us}, there exists a minimum settling time t_s^*.

Furthermore we can infer from (3.3) and (3.4) that there is an inverse relationship between the two, i.e. the shorter the settling time, the larger the undershoot and vice versa. The challenge is to find the specific input signal u such that the output y achieves the minimum settling time, or at least close to, for a given undershoot constraint.

Before turning to the feedforward design, the unsolved ADRC design for systems with RHP zeros will be addressed first.

3.2 ADRC Design for Systems with RHP Zeros

Consider the following second order system with a RHP zero in the transfer function form

$$G_p(s) = \frac{k(1-s/z)}{(1+s/p_1)(1+s/p_2)} = \frac{b_1 s + b_0}{s^2 + a_1 s + a_0} \tag{3.5}$$

where $a_0 = p_1 p_2$, $a_1 = p_1 + p_2$, $b_0 = k p_1 p_2$ and $b_1 = -k p_1 p_2 / z$. All parameters (z, p_1, p_2, k, b_0, a_0 and a_1) in (3.5) are positive numbers; except b_1 is negative. Normally in the ADRC framework, system (3.5) can be treated either as a first order system using the relative degree formulation or as a second order system by ignoring the RHP zero. Since the former uses the high frequency gain and the latter uses the low frequency gain in the design, they are referred to as high frequency gain formulation and low frequency gain formulation respectively. The ADRC design based on those two formulations will be carried out in the subsequent two subsections.

3.2.1 High Frequency Gain Formulation

The corresponding differential equation for system (3.5) is

$$\ddot{y} + a_1 \dot{y} + a_0 y = b_1 \dot{u} + b_0 u \tag{3.6}$$

with a relative degree of one. Therefore by integrating (3.6) and manipulating the terms, a first order system is obtained as follows

$$\dot{y} = \underbrace{b_1}_{b} u + \underbrace{b_0 \int u dt - a_1 y - a_0 \int y dt}_{f} = bu + f \tag{3.7}$$

which is in the standard ADRC form. Following the ADRC design procedure described in Section 2.4, the state space representation of (3.7), the observer, and the controller are given below.

$$\dot{X}_2 = A_2 X_2 + b B_2 u + E_2 \dot{f} \tag{3.8}$$

$$\dot{\hat{X}}_2 = A_2 \hat{X}_2 + \hat{b} B_2 u + L_2 \left(x_1 - \hat{x}_1 \right) \tag{3.9}$$

$$u = \frac{K_2 \left(R_2 - \hat{X}_2 \right)}{\hat{b}} \tag{3.10}$$

The ADRC design so far is almost the same as it normally is, except $\hat{b} = b_1$ here is negative.

Simulations are run for a specific system with $z = 1$, $p_1 = 2$, $p_2 = 5$, $k = 1$, $a_0 = 10$, $a_1 = 7$, $b_0 = 10$ and $b_1 = -10$, which is also used for the rest part of Section 3.2 unless specified. The ratio between the observer and controller bandwidth α is set to 2 for the rest of the chapter. Different values of the controller bandwidth have been chosen over quite a big range to simulate the system responses, but none of them gives a stable result. One of the simulation results with $\hat{b} = b_1 = -10$ and $\omega_c = 50$ is shown in Figure 2.

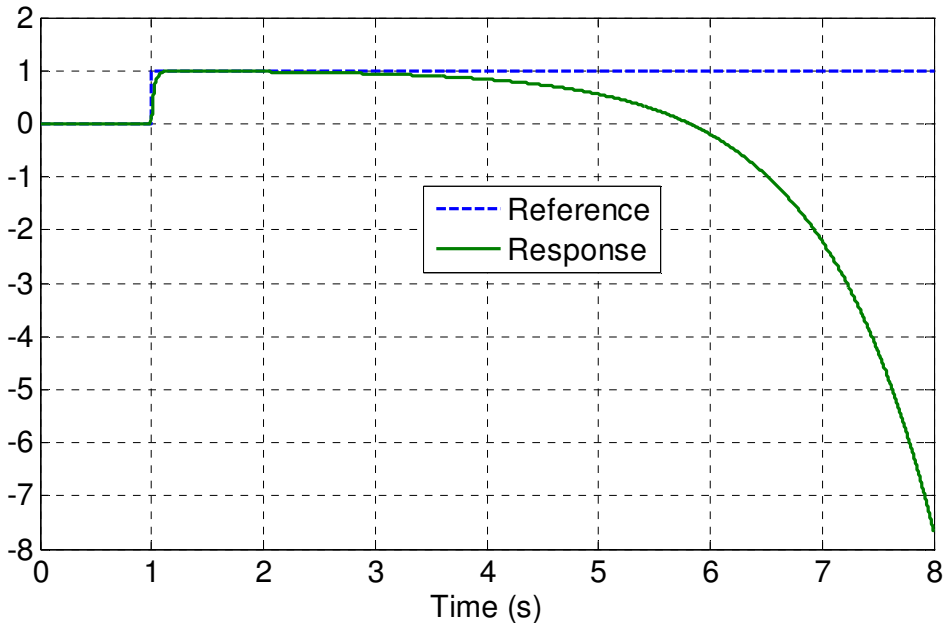

Figure 2 Simulation results for high frequency gain formulation.

As one can see, the transient part of the response is almost perfect without any undershoot. However, when the system goes near to the steady state it becomes unstable. An intuitive explanation of this is that since $\hat{b}$ is negative, for the high frequency part the system is a negative feedback which explains why the transient response is very good. On the other hand, for the low frequency part the system is a positive feedback which leads to an undesired result. More detailed analysis will be conducted in Section 3.2.3 to give more insights to this problem.

3.2.2 Low Frequency Gain Formulation

Another possible way to formulate this problem is ignoring the unstable zero and considering system (3.5) as a system with a relative degree of two represented by the following equation.

$$\ddot{y} = \underbrace{b_0}_{b} u + \underbrace{\left(b_1 \dot{u} - a_1 \dot{y} - a_0 y\right)}_{f} = bu + f \tag{3.11}$$

The corresponding ADRC design for (3.11) is given as

$$\dot{X}_3 = A_3 X_3 + bB_3 u + E_3 \dot{f} \tag{3.12}$$

$$\dot{\hat{X}}_3 = A_3 \hat{X}_3 + \hat{b} B_3 u + L_3 \left(x_1 - \hat{x}_1\right) \tag{3.13}$$

$$u = \frac{K_3 \left(R_3 - \hat{X}_3\right)}{\hat{b}} \tag{3.14}$$

Again simulations were run to find an appropriate solution to this problem. Similar results are found that for most values of the controller bandwidth, the system is unstable. Only a very small stable range for the controller bandwidth is found, with which a very slow and oscillatory system response is obtained. A particular response with $\hat{b} = b_0 = 10$, $\omega_c = 1.2$ and $\alpha = 2$ is shown in Figure 3. A disturbance of magnitude 0.1 is introduced at 60 seconds.

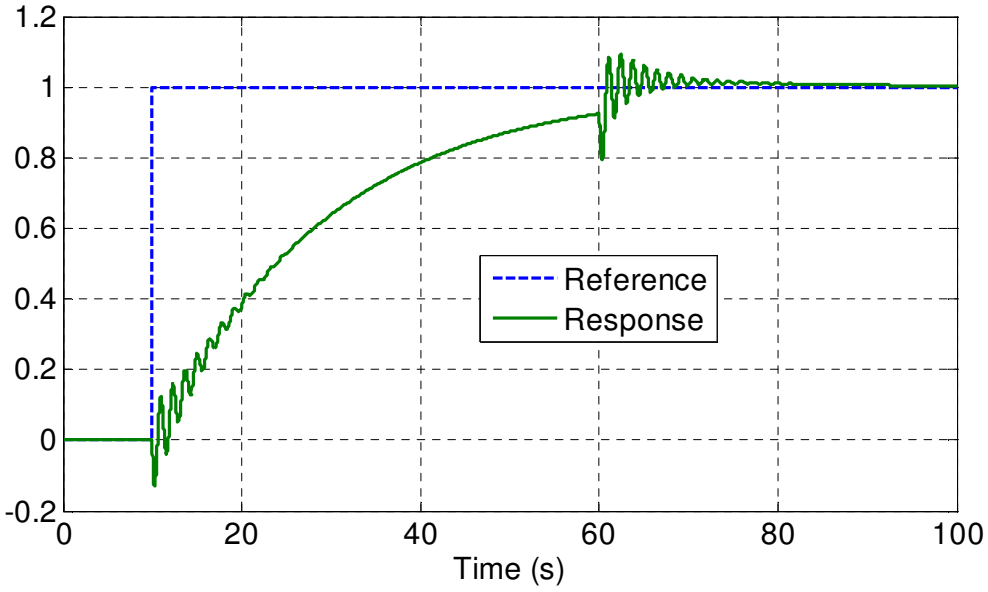

Figure 3 Simulation results for low frequency gain formulation.

As shown above, the two design formulations of ADRC do not fit the NMP zeros problem quite well. More researches based on frequency domain analysis are carried out in the next section to find the reasons behind it and the applicable approaches.

3.2.3 Frequency Domain Analysis

It is easy to take the advantage of the classical control theory and perform the frequency domain analysis for the linear ADRC design [35]. To do so, we need to put the ESO into the transfer function form. A schematic of the ADRC design with state feedback is shown in Figure 4.

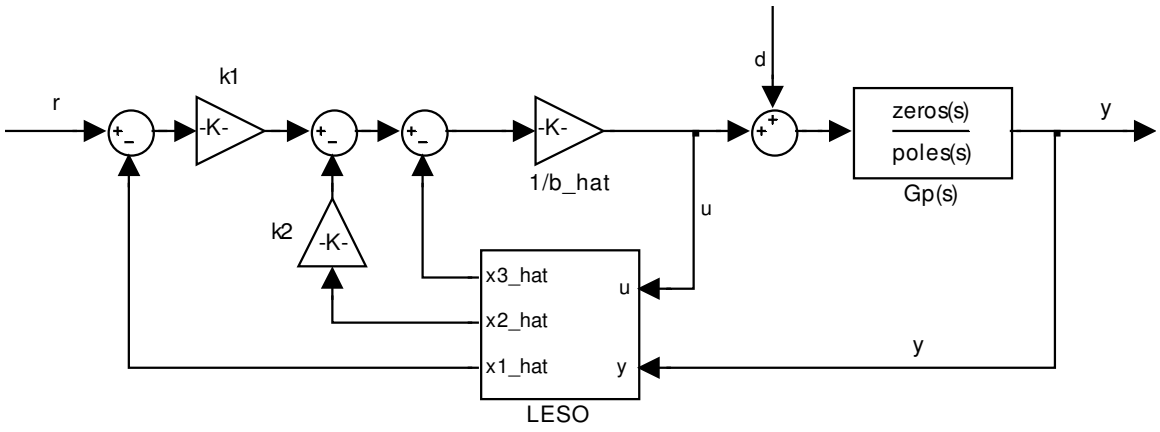

Figure 4 Diagram of the ADRC structure with state feedback.

This design can be transformed into an equivalent two degree of freedom transfer function form as shown in Figure 5, where $H(s)$ is the pre-filter transfer function and $C(s)$ is the controller transfer function.

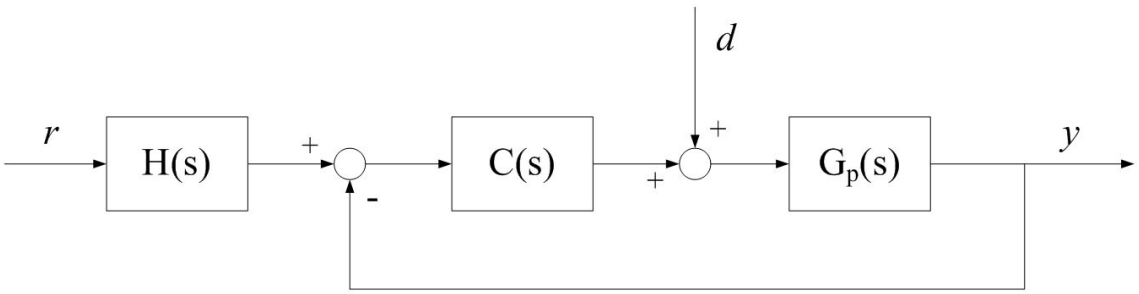

Figure 5 Equivalent transfer function structure of ADRC.

It is not difficult to derive the transfer functions using linear system theory. The equivalent transfer functions for a first order ADRC with state feedback are given in (3.15) and (3.16); and those for a second order ADRC with state feedback are given in (3.17) and (3.18) as well.

$$H(s)=\frac{k_1\left(s^2+l_1s+l_2\right)}{\left(k_1l_1+l_2\right)s+k_1l_2} \tag{3.15}$$

$$C(s)=\frac{\left(k_1l_1+l_2\right)s+k_1l_2}{\hat{b}\left[s^2+\left(l_1+k_1\right)s\right]} \tag{3.16}$$

$$H(s)=\frac{k_1\left(s^3+l_1s^2+l_2s+l_3\right)}{\left(k_1l_1+k_2l_2+l_3\right)s^2+\left(k_1l_2+k_2l_3\right)s+k_1l_3} \tag{3.17}$$

$$C(s)=\frac{\left(k_1l_1+k_2l_2+l_3\right)s^2+\left(k_1l_2+k_2l_3\right)s+k_1l_3}{\hat{b}\left[s^3+\left(l_1+k_2\right)s^2+\left(l_2+k_2l_1+k_1\right)s\right]} \tag{3.18}$$

Reconsidering the high frequency formulation presented in Section 3.2.1, the characteristic equation of the closed-loop transfer function can be obtained from (3.5) and (3.16) as

$$\begin{aligned}&s^4+\left(a_1+l_1+k_1\right)s^3+\left[a_0+a_1\left(l_1+k_1\right)+\left(k_1l_1+l_2\right)b_1/\hat{b}\right]s^2\\&+\left[a_0\left(l_1+k_1\right)+\left(k_1l_1+l_2\right)b_0/\hat{b}+k_1l_2b_1/\hat{b}\right]s+k_1l_2b_0/\hat{b}=0\end{aligned} \tag{3.19}$$

Note that here $\hat{b} \approx b_1$ is negative. It is noticed that for any ω_c, the coefficients of the highest order term and lowest order term will have the opposite signs. Therefore the system will have at least one pole located in the RHP making it unstable. This could also be explained intuitively, by examining (3.16), where $C(s)$ is found having a negative sign due to the negative $\hat{b}$, which makes the loop a positive feedback loop according to Figure 5.

Though with a negative $\hat{b}$ the transient response is perfect without any undershoot, for systems with RHP zeros, the control design should focus on stabilizing the low frequency part first, hence the undershoot is unavoidable because the high frequency part always has a different sign from the low frequency part.

Remark 3.1: Never use a negative $\hat{b}$ in the ADRC design if the low frequency gain of the system is positive; doing so will lead to a positive feedback loop for the system.

For the low frequency formulation provided in Section 3.2.2, the characteristic equation of the closed-loop transfer function derived from (3.5) and (3.18) is more complicated as

$$\begin{aligned} &s^5 + (a_1 + l_1 + k_2)s^4 + \left[a_0 + a_1(l_1 + k_2) + l_2 + k_2 l_1 + k_1 + \underline{(k_1 l_1 + k_2 l_2 + l_3) b_1 / \hat{b}}\right] s^3 \\ &+ \left[a_0(l_1 + k_2) + a_1(l_2 + k_2 l_1 + k_1) + (k_1 l_1 + k_2 l_2 + l_3) b_0 / \hat{b} + \underline{(k_1 l_2 + k_2 l_3) b_1 / \hat{b}}\right] s^2 \\ &+ \left[a_0(l_2 + k_2 l_1 + k_1) + (k_1 l_2 + k_2 l_3) b_0 / \hat{b} + \underline{k_1 l_3 b_1 / \hat{b}}\right] s + k_1 l_3 b_0 / \hat{b} = 0 \end{aligned} \quad (3.20)$$

Note that $\hat{b} \approx b_0$ is positive in this case. For the system to be stable, at least all of the coefficients should be positive. It is noticed that all of the system parameters as well as the observer and controller bandwidths are positive, except b_1. Thus only the last terms

in the coefficients of s^3, s^2 and s terms have negative values which may result in negative coefficients. According to the selection of the individual gains of the observer and the controller, the negative terms have a higher order in terms of ω_c than the positive terms, which means when ω_c goes beyond a certain value the coefficients will become negative and the system will be unstable.

This is reasonable if we recall the classical control theory. From the root locus point of view, as the feedback gain k increases from zero to infinity, the closed-loop poles go from the open loop poles to the open loop zeros or infinity. Since there is an unstable zero in the system, k must have an upper limit. This is also true for the ADRC design.

Remark 3.2: In the ADRC design for systems with RHP zeros, the controller bandwidth will have an upper limit in order to keep the system stable.

Through the frequency domain analysis, the reason why those two design formulations do not work for systems with RHP zeros becomes clearer. The solutions to this problem are discussed in the following section.

3.2.4 Proposed Solution

Based on the frequency domain analysis in the previous section, it can be seen from (3.20) that by increasing $\hat{b}$ the effects of the negative terms get smaller. This means that the system tends to be more stable or with the same stability margin a higher controller bandwidth can be achieved. To analytically derive the upper limit for the controller bandwidth is non-trivial, hence a computer program is written to find the upper limits of the controller bandwidth according to different $\hat{b}$ values. Figure 6 is a plot of

the result. The part below the curve represents the stable region, while the part above the curve represents the unstable region.

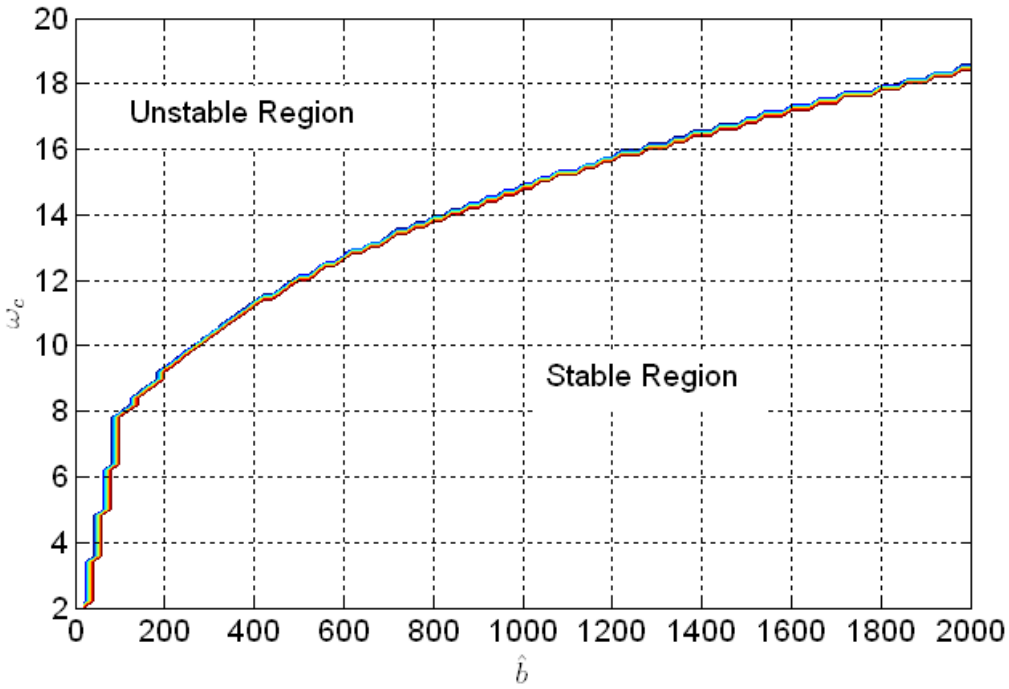

Figure 6 Stable region search result.

Simulations are run to demonstrate the effectiveness of this solution. As shown in Figure 7, with a larger $\hat{b}$ value, 100 times of its nominal value, the allowable controller bandwidth is increased from 1.2 to 10. The performance is much better than the result obtained in Section 3.2.2, and is acceptable now.

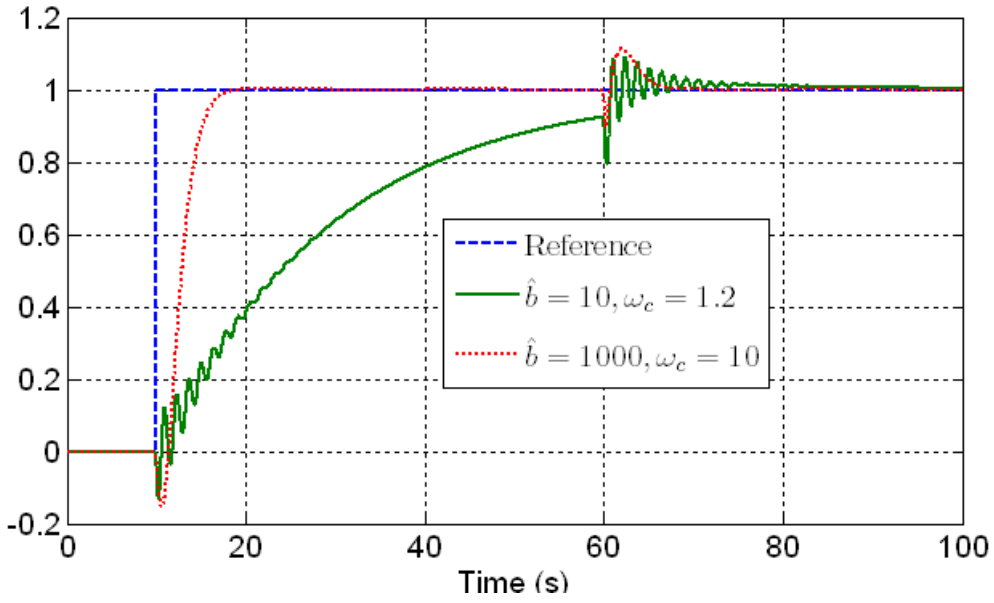

Figure 7 Simulation results for low frequency gain formulation – comparison between original $\hat{b}$ and increased $\hat{b}$.

Increasing $\hat{b}$ further, even higher controller bandwidth can be achieved; but overshoot and oscillation come into play when the bandwidth is set too high. Simulation results show that not much improvement on reducing the response time is obtained from further increasing $\hat{b}$. Based on a large amount of simulations, a range of 20 to 100 times of its nominal value is suggested for $\hat{b}$.

3.3 Open Loop Design for Systems with RHP Zeros

In Section 3.2, the ADRC design solution for systems with RHP zeros is provided. The tracking performance, however, is still not comparable to the performance limit indicated by Lemma 3.1 and 3.2. Hence in this section, the open loop design is carried out to further improve the tracking performance, and hopefully reach the performance

limit. In Section 3.3.1, the time optimal control solutions is obtained with the control effort constraint. The more practical minimum settling time solution subject to undershoot constraint is presented in Section 3.3.2.

3.3.1 Time Optimal Control Solution

Consider the system given in (3.5), repeated here as (3.21)

$$G_p(s) = \frac{k(1 - s/z)}{(1 + s/p_1)(1 + s/p_2)} = \frac{b_1 s + b_0}{s^2 + a_1 s + a_0} \tag{3.21}$$

The control input subjects to the constraint $|u| \le r \ \ (r > 0)$.

Putting (3.21) into the observable canonical form

$$\begin{aligned} \dot{x} &= \underbrace{\begin{bmatrix} -a_1 & 1 \\ -a_0 & 0 \end{bmatrix}}_{A} x + \begin{bmatrix} b_1 \\ b_0 \end{bmatrix} u = a(x,u) \\ y &= \begin{bmatrix} 1 & 0 \end{bmatrix} x \end{aligned} \tag{3.22}$$

According to the Theorem 5.4-1 and Theorem 5.4-2 in [62], the time optimal solution for the above system exists and is unique as long as *A* is Hurwitz. For time optimal control, the cost function is defined as

$$J(u) = \int_{t_0}^{t_f} dt \tag{3.23}$$

The Hamiltonian is then formed below

$$\mathcal{H} = g + \lambda^T a = 1 + \lambda_1(-a_1 x_1 + x_2 + b_1 u) + \lambda_2(-a_0 x_1 + b_0 u) \tag{3.24}$$

Solving the co-state equation

$$\begin{bmatrix} \dot{\lambda}_1 \\ \dot{\lambda}_2 \end{bmatrix} = \begin{bmatrix} a_1\lambda_1 + a_0\lambda_2 \\ -\lambda_1 \end{bmatrix} \Rightarrow \begin{cases} \lambda_1 = c_1 e^{p_1 t} + c_2 e^{p_2 t} \\ \lambda_2 = -\dfrac{c_1}{p_1} e^{p_1 t} - \dfrac{c_2}{p_2} e^{p_2 t} \end{cases} \tag{3.25}$$

$$\left(b_1\lambda_1 + b_0\lambda_2\right)u^*(t) \le \left(b_1\lambda_1 + b_0\lambda_2\right)u(t) \tag{3.26}$$

$$\begin{aligned} u^*(t) &= \begin{cases} -r, & b_1\lambda_1 + b_0\lambda_2 > 0 \\ +r, & b_1\lambda_1 + b_0\lambda_2 < 0 \end{cases} \\ &= -r\,\mathrm{sgn}\left(b_1\lambda_1 + b_0\lambda_2\right) \end{aligned} \tag{3.27}$$

Since $b_1\lambda_1 + b_0\lambda_2$ will cross zero at most once depending on the values of c_1 and c_2, the optimal control for a specified initial state must be one of the form:

$$u = \begin{cases} +r, \text{ for all } t \in [t_0, t^*], \text{ or} \\ -r, \text{ for all } t \in [t_0, t^*], \text{ or} \\ +r, \text{ for } t \in [t_0, t_1), \text{ and } -r, \text{ for } t \in [t_1, t^*], \text{ or} \\ -r, \text{ for } t \in [t_0, t_1), \text{ and } +r, \text{ for } t \in [t_1, t^*]. \end{cases} \tag{3.28}$$

$$u = \pm r: \quad \begin{cases} x_1(t) = c_1 e^{-p_1 t} + c_2 e^{-p_2 t} \pm \dfrac{b_0}{p_1 p_2} r \\ x_2(t) = p_2 c_1 e^{-p_1 t} + p_1 c_2 e^{-p_2 t} \pm \left(\dfrac{(p_1 + p_2) b_0}{p_1 p_2} - b_1 \right) r \end{cases} \tag{3.29}$$

Without loss of generality, assuming that the trajectory passes through the origin at time zero, c_1 and c_2 are solved below.

$$\begin{aligned} u = \pm r: \quad & \begin{cases} x_1(0) = 0 \\ x_2(0) = 0 \end{cases} \Rightarrow \begin{cases} c_1 + c_2 \pm \dfrac{b_0}{p_1 p_2} r = 0 \\ p_2 c_1 + p_1 c_2 \pm \left(\dfrac{(p_1 + p_2) b_0}{p_1 p_2} - b_1 \right) r = 0 \end{cases} \\ \Rightarrow & \begin{cases} c_1 = \pm \dfrac{(b_0 - p_1 b_1)}{p_1 (p_1 - p_2)} r \\ c_2 = \pm \dfrac{(b_0 - p_2 b_1)}{p_2 (p_2 - p_1)} r \end{cases} \end{aligned} \tag{3.30}$$

Next solving for t and eliminate it from (3.29), we get the relationship between x_1 and x_2, representing the switching curve in the phase plane.

$$u=\pm r:\quad x_1=\pm\frac{(b_0-p_1b_1)r}{p_1(p_1-p_2)}\left(1\pm\frac{p_2(p_2x_1-x_2)}{(b_0-p_2b_1)r}\right)^{p_1/p_2}$$
$$\pm\frac{(b_0-p_2b_1)r}{p_2(p_2-p_1)}\left(1\pm\frac{p_2(p_2x_1-x_2)}{(b_0-p_2b_1)r}\right)\pm\frac{b_0r}{p_1p_2} \tag{3.31}$$

The magenta switching curve is shown in Figure 8. The parameters of the system are chosen as: $a_1=7$, $a_0=10$, $b_1=-1$, $b_0=1$ and $r=10$. As shown in Figure 8 the system trajectories are confined within an ellipse-like region, due to the fact that the system has no pure integrators. For system starts with initial states below the switching curve to reach the origin, $u=+r$ will be applied first; Once the trajectory reaches the switching curve, the control is switched to $u=-r$. Similar result can be found easily for initial states above the switching curve.

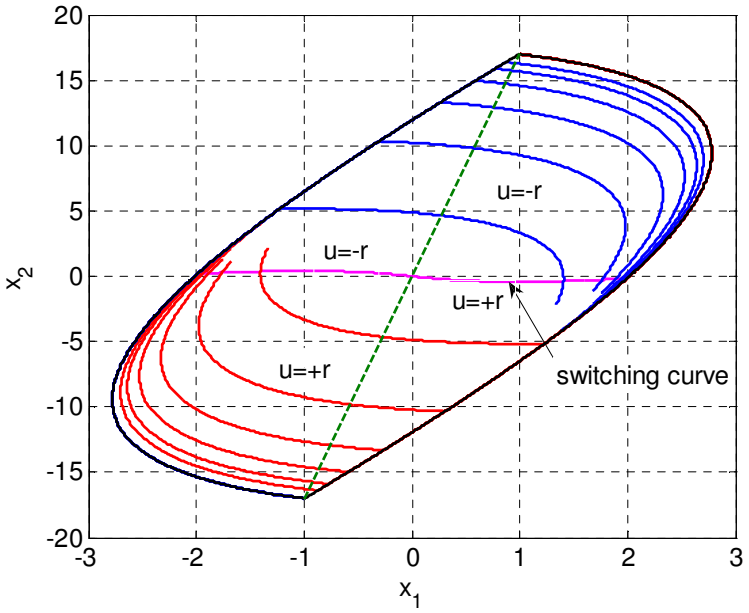

Figure 8 Phase plane trajectories of the time optimal control.

Figure 9 shows the time optimal control that transfers the system states from (0, 0) to (0.5, 8.5). Here we see that the time optimal control solution has an undershoot

that is close to 180%, which is not desirable and urges us to find a more practical solution with the undershoot constraint.

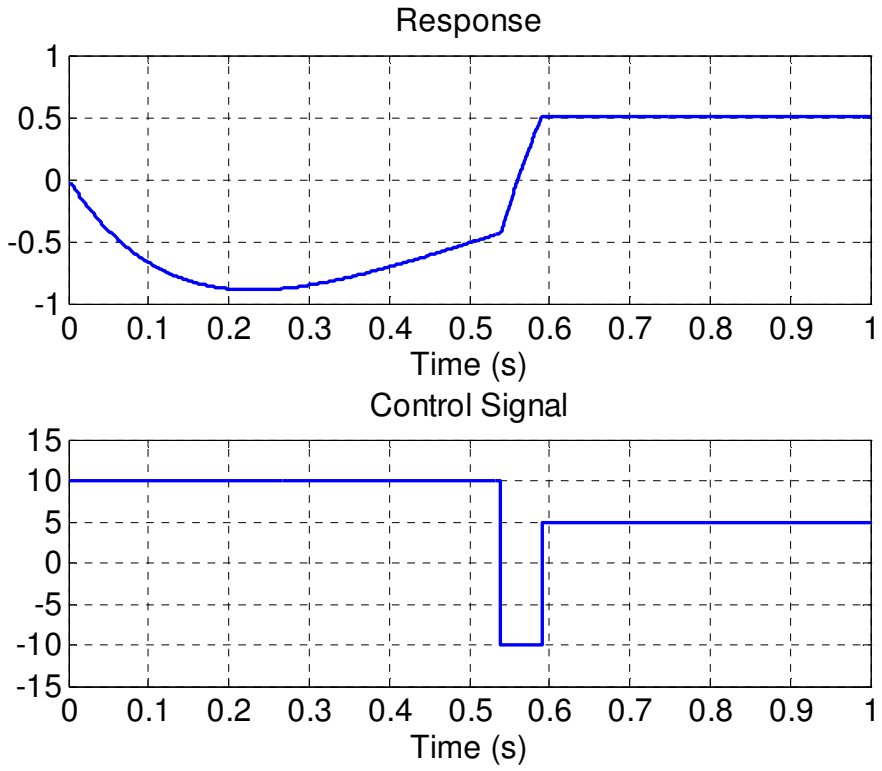

Figure 9 Time domain response of the time optimal control.

3.3.2 Minimum Settling Time Solution with Undershoot Constraint

In this section, the control signals that minimize the settling time subject to undershoot constraint are synthesized for systems with one and two real RHP zeros, respectively, using the clues demonstrated in the proof of the two lemmas in [53].

One Positive Zero Case

The ideal response for the system with just one positive zero can be deduced from the proof of Lemma 3.1 in [53] as

$$y^*(t)=\begin{cases}0, & t=0\\ -y_d r_{us}, & t\in\left(0,t_s^*\right)\\ y_d, & t\in\left[t_s^*,\infty\right)\end{cases} \tag{3.32}$$

which yields the minimum settling time, $t_s = t_s^*$ in (3.3) and complies with the undershoot constraint $-y(t)/y_d \le r_{us}$, $t\in[0,\infty)$. But such response has two jumps at $t=0$ and $t=t_s^*$ respectively, and this requires either an unbounded input which is ruled out in [53] or an infinitely fast system. Neither is practical but the latter gives us a starting point. Let us construct a bounded control law first for the ideal, i.e. infinitely fast, system. Without loss of generality, an nth order linear time invariant NMP system with one positive zero can be represented as

$$\frac{Y(s)}{U(s)}=P(s)=\frac{(1-s/z)}{(1+s/p)^n},\ z>0,\ p>0 \tag{3.33}$$

This system becomes infinitely fast as $p\to\infty$. Now define

$$\tilde{U}(s)=(1-s/z)U(s) \tag{3.34}$$

or equivalently

$$\tilde{u}(t)=u(t)-\dot{u}(t)/z \tag{3.35}$$

where $\tilde{U}(s)$ is the Laplace transformation of $\tilde{u}(t)$. Then (3.33) becomes

$$\frac{Y(s)}{\tilde{U}(s)}=\tilde{P}(s)=\frac{1}{(1+s/p)^n} \tag{3.36}$$

For the infinitely fast system $\tilde{P}(s)$ in (3.36), i.e. $p\to\infty$, $Y(s)=\tilde{U}(s)$ or equivalently $y(t)=\tilde{u}(t)$. Thus according to (3.32), for $y(t)=y^*(t)$,

$$\tilde{u}(t) = u(t) - \dot{u}(t)/z = \begin{cases} 0, & t = 0 \\ -y_d r_{us}, & t \in (0, t_1) \\ y_d, & t \in [t_1, \infty) \end{cases} \tag{3.37}$$

with the following initial condition and boundary condition.

$$u(0) = 0 \tag{3.38}$$

$$u(t_1) = y_d \tag{3.39}$$

Solving (3.37) subject to (3.38) and (3.39) yields

$$\begin{cases} u(t) = \begin{cases} \left(e^{zt} - 1\right) y_d r_{us}, & t \in [0, t_1) \\ y_d, & t \in [t_1, \infty) \end{cases} \\ t_1 = \dfrac{\ln\left(1/r_{us} + 1\right)}{z} \end{cases} \tag{3.40}$$

It is obvious that $t_1 = t_s^*$, thus

$$\lim_{p \to \infty} t_s = t_s^* \tag{3.41}$$

Therefore, the following theorem has been constructively proven.

Theorem 3.1: *Given the undershoot constraint* $-y(t)/y_d \le r_{us}$, $t \in [0, \infty)$, *if the transfer function of the system satisfies (3.33), then the control law (3.40) achieves the minimum settling time for the system as* $p \to \infty$.

Example 3.1: Consider the system with one positive zero.

$$Q(s) = \frac{(1 - s)}{(1 + s/10)^2} \tag{3.42}$$

Applying the constructed control law (3.40) to system (3.42) with three different undershoot constraints: 2%, 5%, and 10%, the system responses are shown in Figure 10.

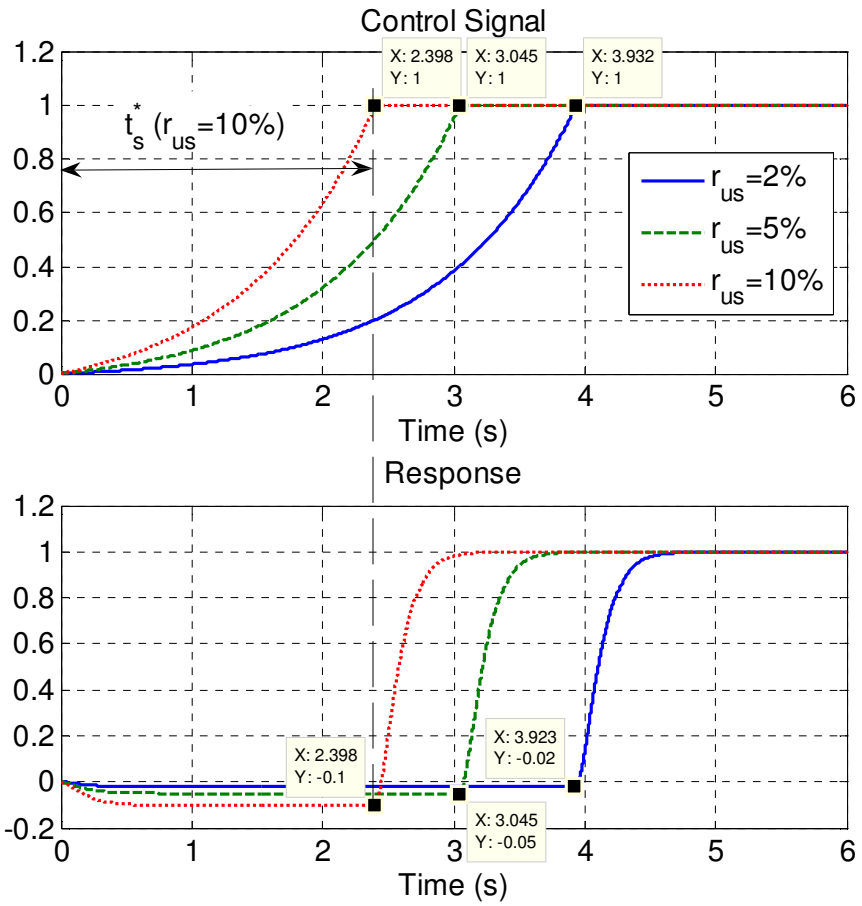

Figure 10 Input and output signals in Example 3.1.

As can be seen from the results, the larger undershoot allowed the shorter settling time can be achieved. The minimum settling time of system (3.42) can be calculated from (3.3) for each undershoot constraint with $z=1$, and they are 3.932 seconds for 2% undershoot, 3.045 seconds for 5% undershoot, and 2.398 seconds for 10% undershoot. We see that the control signals reach their final value at exactly the minimum settling time. The responses, however, take a little longer to settle due to the finite poles at -10. For example, for the 5% undershoot case (green dashed line) the actual settling time is 3.634 seconds. The settling time can be reduced by replacing the original system poles with larger ones, using the compensator (3.43) below with $p>10$. But too large poles

may result in larger control effort and drastic changes in the control signal, which are to be avoided in practice.

$$C(s)=\frac{(1+s/10)^2}{(1+s/p)^2} \tag{3.43}$$

Two Positive Zeros Case

Consider NMP system with two positive zeros

$$P(s)=\frac{(1-s/z_1)(1-s/z_2)}{(1+s/p)^n},\ \ z_2>z_1>0,\ p>0 \tag{3.44}$$

The ideal response for system (3.44) with $p\to\infty$ can also be deduced from the proof of Lemma 3.2 in [53] and it is the same as in (3.32). Consider that a continuous response of system (3.44) must have at least two zero crossings (see [63], pp. 154-156), the ideal response for it can be similarly constructed as

$$y^*(t)=\begin{cases}0, & t=0\\ A_1>0, & t\in(0,t_1)\\ -y_d r_{us}, & t\in[t_1,t_2)\\ y_d, & t\in[t_2,\infty)\end{cases}\ \text{with } t_1\to 0 \tag{3.45}$$

where A_1 and t_2 are design parameters to be determined as shown below. Define

$$\tilde{U}(s)=(1-s/z_1)(1-s/z_2)U(s) \tag{3.46}$$

or equivalently

$$\tilde{u}(t)=u(t)-(1/z_1+1/z_2)\dot{u}(t)+\ddot{u}(t)/z_1z_2 \tag{3.47}$$

where $\tilde{U}(s)$ is the Laplace transformation of $\tilde{u}(t)$. Then (3.44) becomes

$$\frac{Y(s)}{\tilde{U}(s)}=\tilde{P}(s)=\frac{1}{(1+s/p)^n} \tag{3.48}$$

For the infinitely fast system $\tilde{P}(s)$ in (3.48), i.e. $p \to \infty$, $Y(s) = \tilde{U}(s)$ or equivalently $y(t) = \tilde{u}(t)$. Thus according to (3.45), for $y(t) = y^*(t)$,

$$\begin{aligned}\tilde{u}(t) &= u(t) - (1/z_1 + 1/z_2)\dot{u}(t) + \ddot{u}(t)/z_1 z_2 \\ &= \begin{cases} 0, & t = 0 \\ A_1 > 0, & t \in (0, t_1) \\ -y_d r_{us}, & t \in [t_1, t_2) \\ y_d, & t \in [t_2, \infty) \end{cases} \qquad \text{with } t_1 \to 0 \end{aligned} \tag{3.49}$$

with the following initial conditions and boundary conditions.

$$u(0) = \dot{u}(0) = 0 \tag{3.50}$$

$$u(t_2) = y_d,\ \dot{u}(t_2) = 0 \tag{3.51}$$

Solving (3.49) subject to (3.50) and (3.51) yields

$$\begin{cases} \dfrac{z_1 z_2}{(z_2 - z_1)}\left(\dfrac{e^{z_2 t_2} - e^{z_2 T}}{z_2} - \dfrac{e^{z_1 t_2} - e^{z_1 T}}{z_1}\right) A_1 + \dfrac{z_1 z_2}{(z_2 - z_1)}\left(\dfrac{e^{z_2 T} - 1}{z_2} - \dfrac{e^{z_1 T} - 1}{z_1}\right)(-y_d r_{us}) = y_d \\ \dfrac{z_1 z_2}{(z_2 - z_1)}\left(\left(e^{z_2 t_2} - e^{z_2 T}\right) - \left(e^{z_1 t_2} - e^{z_1 T}\right)\right) A_1 + \dfrac{z_1 z_2}{(z_2 - z_1)}\left(e^{z_2 T} - e^{z_1 T}\right)(-y_d r_{us}) = 0 \end{cases} \tag{3.52}$$

where $T = t_2 - t_1$. Eliminating A_1 in (3.52) yields

$$r_{us} = \frac{\left(e^{z_2 t_2} - e^{z_2 T}\right) - \left(e^{z_1 t_2} - e^{z_1 T}\right)}{\left(e^{z_1 t_2} - e^{z_1 T}\right) - \left(e^{z_2 t_2} - e^{z_2 T}\right) + e^{z_1 T + z_2 t_2} - e^{z_2 T + z_1 t_2}} \tag{3.53}$$

With $t_1 \to 0$ or equivalently $T \to t_2$ and applying the L'Hopital's rule to (3.53)

$$\begin{aligned} r_{us} &= \lim_{\substack{t_1 \to 0 \\ \text{or} T \to t_2}} \frac{\left(e^{z_2 t_2} - e^{z_2 T}\right) - \left(e^{z_1 t_2} - e^{z_1 T}\right)}{\left(e^{z_1 t_2} - e^{z_1 T}\right) - \left(e^{z_2 t_2} - e^{z_2 T}\right) + e^{z_1 T + z_2 t_2} - e^{z_2 T + z_1 t_2}} \\ &= \frac{z_1 e^{-z_2 t_2} - z_2 e^{-z_1 t_2}}{z_1\left(1 - e^{-z_2 t_2}\right) - z_2\left(1 - e^{-z_1 t_2}\right)} \end{aligned} \tag{3.54}$$

Consequently in light of (3.4),

$$\lim_{\substack{p\to\infty \\ t_1\to 0}} t_s = t_s^* \tag{3.55}$$

Therefore, the following theorem has been constructively proven.

Theorem 3.2: *Given the undershoot constraint* $-y(t)/y_d \le r_{us}$, $t \in [0,\infty)$, *if the transfer function of the system satisfies (3.44), then the control law determined by (3.49), (3.50) and (3.51) achieves the minimum settling time for the system as* $p \to \infty$.

Remark 3.3: Practically speaking t_1 can be chosen to be an appropriate small number, then A_1 and t_2 can be solved from (3.52). Due to the complexity of (3.52), the analytical solution may not be easily found but numerical algorithms, for example in MATLAB, are readily available to solve for A_1 and t_2.

Remark 3.4: For NMP systems with more than two positive zeros, the relation between the undershoot constraint and the settling time is not yet known, to our knowledge. But based upon the results obtained above, a control law for *m* positive zeros case can be constructed similarly. Consider the NMP system in the form of

$$\frac{Y(s)}{U(s)} = P(s) = \frac{\prod_{i=1}^{m}(1-s/z_i)}{(1+s/p)^n}, \quad z_m > z_{m-1} > \cdots > z_2 > z_1 > 0, \; p > 0, \; n > m \tag{3.56}$$

Define

$$\tilde{U}(s) = \prod_{i=1}^{m}(1-s/z_i)U(s) \tag{3.57}$$

or equivalently,

$$\tilde{u}(t) = u(t) - \sum_{i=1}^{m}\frac{1}{z_i}\dot{u}(t) + \sum_{i\neq j,1\le i,j\le m}\frac{1}{z_i z_j}\ddot{u}(t) - \ldots(-1)^m\frac{1}{z_1 z_2 \ldots z_m}u^{(m)}(t) \tag{3.58}$$

where $\tilde{U}(s)$ is the Laplace transformation of $\tilde{u}(t)$. Given the undershoot constraint $-y(t)/y_d \le r_{us}$, $t \in [0,\infty)$ the control law $u(t)$ can be constructed, as in the case of $m = 1, 2$, by solving (3.58) and (3.59) subject to the initial conditions (3.60) and the boundary conditions (3.61). Many solutions exist. To obtain a particular $u(t)$ the following design parameters $\Delta t_i = t_i - t_{i-1}$, ($i = m - 2k + 1, k = 1, \ldots, \lfloor m/2 \rfloor$), where $\lfloor m/2 \rfloor$ denotes the greatest integer less than or equal to $m/2$, need to be selected.

$$\begin{aligned} &\tilde{u}(t) = \begin{cases} A_i, & t \in [t_{i-1}, t_i),\ i = 1, 2, \ldots m,\ t_0 = 0 \\ y_d, & t \in [t_m, \infty) \end{cases} \\ &\text{if } (-1)^{m-i} > 0,\ A_i = -y_d r_{us} \\ &\text{if } (-1)^{m-i} < 0,\ A_i > 0 \end{aligned} \tag{3.59}$$

$$u^{(i)}(0) = 0,\ i = 0, 1, \ldots, m-1 \tag{3.60}$$

$$u(t_m) = y_d,\ u^{(i)}(t_m) = 0,\ i = 1, 2, \ldots, m-1 \tag{3.61}$$

In the case of $m = 2$, if $\Delta t_1 \to 0$ and $p \to \infty$, it is shown above that the corresponding control law $u(t)$ achieves the minimum settling time. The mathematically analysis for the case of $m > 2$, however, seems prohibitively complex. In practical applications, it is suggested that Δt_i ($i = m - 2k + 1,\ k = 1, \ldots, \lfloor m/2 \rfloor$) be kept small for shorter settling time.

Example 3.2: Consider the system with two positive zeros.

$$Q(s) = \frac{(1 - s/2)(1 - s/5)}{(1 + s/20)^3} \tag{3.62}$$

Appling the control signal determined by (3.49), (3.50) and (3.51) to system (3.62) with the following values for the parameters: $z_1 = 2$, $z_2 = 5$, $p = 20$, $y_d = 1$ and

$r_{us} = 5\%$. With t_1 chosen to be 0.2 seconds, $A_1 = 0.0289660085$ is obtained numerically from solving (3.52). The system response is shown in Figure 11, with the actual settling time measured to be 2.28 seconds, which is very close to the minimum settling time, calculated from (3.4) to be 1.78 seconds. In this case, the settling time can be further reduced not only by assigning larger poles but also reducing t_1 as indicated by Theorem 3.2. The decrease in t_1 corresponds, however, to a larger A_1.

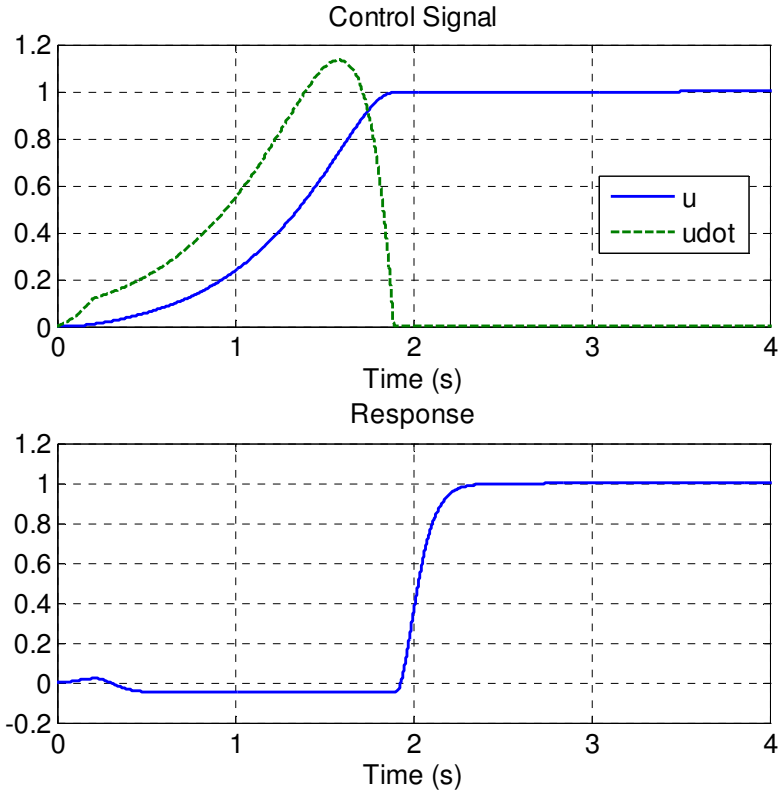

Figure 11 Control signal, its derivative and the output response in Example 3.2.

Remark 3.5: It is noticed that for a given t_1, A_1 has to be very precise such that the two boundary conditions required in (3.51) can be satisfied at the same time. Even in the above simulation with very accurate A_1, $\dot{u}(t)$ is not exactly zero (slightly greater than

zero) when $u(t) = y_d$. That is why the control signal keeps increasing slowly. A practical solution will be forcing $\dot{u}(t)$ to be zero when $u(t) = y_d$ so that A_1 does not have to be very accurate. The cost is that the undershoot constraint may be slightly violated. For example, with $A_1 = 0.0289661$ the actual undershoot increases from 5% to 5.3%, which is still acceptable in most applications.

3.4 The Combined Feedforward-Feedback Design

In this section a realistic hydraulic turbine control problem is used to demonstrate the practical significance of the above solution, where a feedforward and feedback combined design [7, 18] is adopted. The overall transfer function of the hydraulic turbine generator is given in [64] as

$$\begin{aligned} Q(s) &= \frac{-5.25s^2 + 4.2s + 1.05}{1.14s^4 + 8.2s^3 + 7.945s^2 + 6.235s + 1.05} \\ &= \frac{\left(1 - \frac{s}{1}\right)\left(1 + \frac{s}{0.2}\right)}{\left(1 + \frac{s}{6.2085}\right)\left(1 + \frac{s}{0.2144}\right)\left(1 + \frac{s}{0.385 + 0.7373i}\right)\left(1 + \frac{s}{0.385 - 0.7373i}\right)} \end{aligned} \tag{3.63}$$

A block diagram of the combined design is shown in Figure 12. The feedforward control signal is generated based on the reference signal. Before being sent to the real system as well as the system model, it passes through a compensator which is used to reassign the system poles or convert the system transfer function into the standard form in (3.33) or (3.44). The actual response is compared to the reference response coming out from the system model to produce the error signal. The error signal may not be zero due

to the disturbances and/or the model uncertainties. The output deviation is then corrected by the feedback controller.

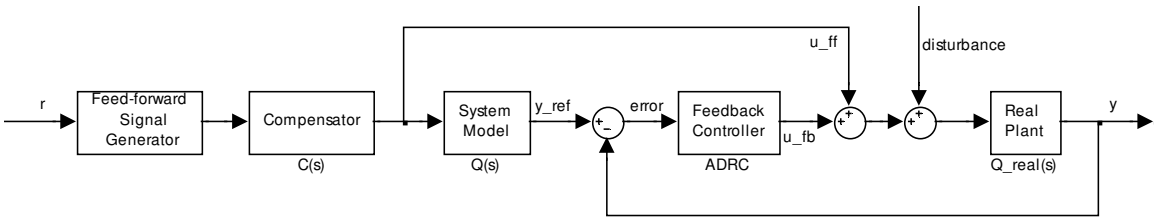

Figure 12 The feedforward and feedback combined control design.

The feedforward control is constructed based on Theorem 3.1 with a 5% undershoot constraint applied. The compensator (3.64) is used to convert system (3.63) into the standard form (3.33) and replace the small poles.

$$C(s)=\frac{\left(1+\frac{s}{6.2085}\right)\left(1+\frac{s}{0.2144}\right)\left(1+\frac{s}{0.385+0.7373i}\right)\left(1+\frac{s}{0.385-0.7373i}\right)}{\left(1+\frac{s}{0.2}\right)\left(1+\frac{s}{4}\right)^{3}} \quad (3.64)$$

If the system model matches the real system exactly and no disturbance exists, the feedforward control would work perfectly (see Figure 13, blue dashed curve) as in Example 3.1. In reality, however, model uncertainties and disturbances do exist. Suppose that the real system dynamic is

$$Q_{real}(s)=\frac{\left(1-\frac{s}{1.05}\right)\left(1+\frac{s}{0.22}\right)}{\left(1+\frac{s}{6.8285}\right)\left(1+\frac{s}{0.1944}\right)\left(1+\frac{s}{0.385+0.7373i}\right)\left(1+\frac{s}{0.385-0.7373i}\right)} \quad (3.65)$$

and a step disturbance with a magnitude of 0.2 is introduced to the system at 50 seconds. In such situations, the feedforward control alone is insufficient (see Figure 13, magenta dotted curve), thus the feedback control is needed to correct the deviation. Note that the

control signals are identical for the first two simulations. For the feedback design, the ADRC design proposed in Section 3.2 is adopted with the parameters chosen as $\hat{b} = 460$, $\omega_c = 5$ and $\alpha = 2$. The simulation result of the combined feedforward and feedback design is shown in Figure 13 (green solid curve). The integral absolute error (IAE) for tracking reduces from 6.595 to 4.792 compared to the result of a pure ADRC design with the same parameters (see Figure 13, red dash-dotted curve). The system response settles in 20 seconds after the disturbance is introduced.

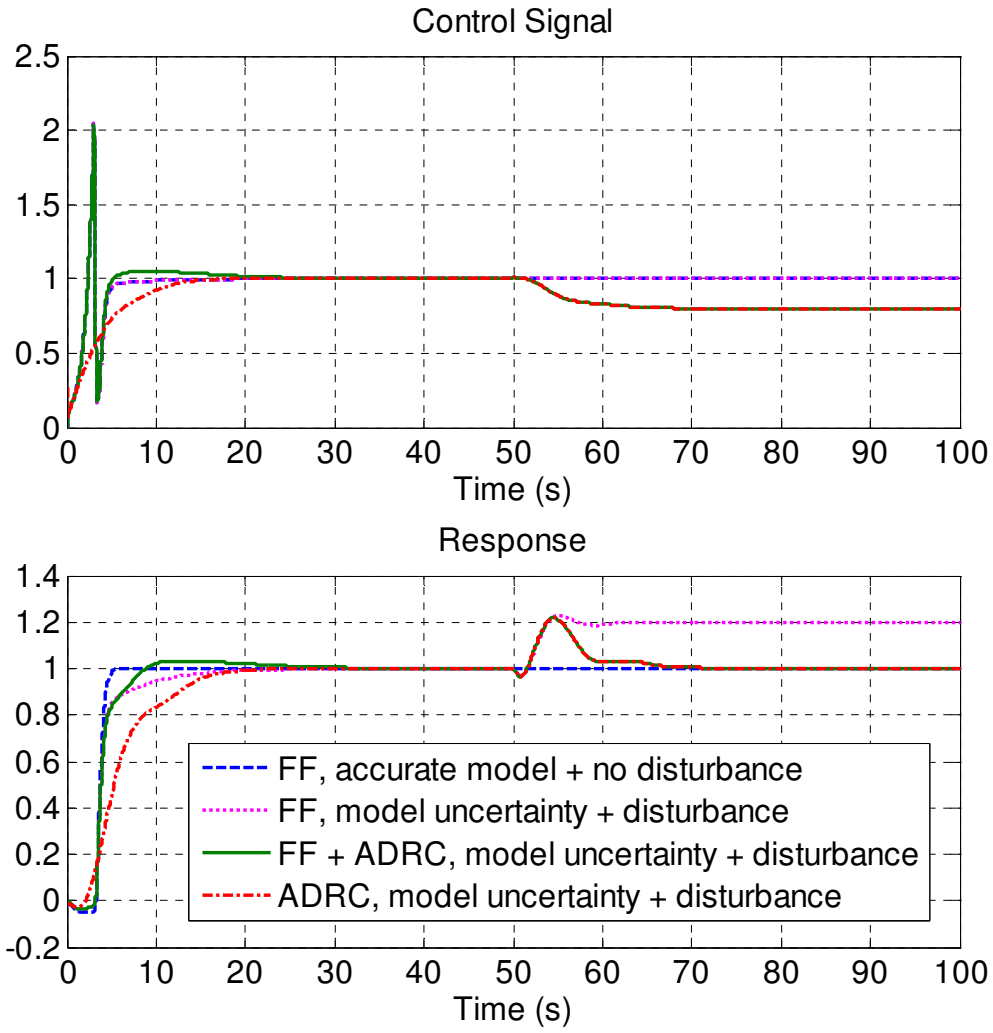

Figure 13 Control signals and output responses.

3.5 Summary

The main contributions of this chapter are: 1) provided an applicable ADRC design for systems with RHP zeros; 2) obtained the feedforward control that achieves the minimum settling time subject to undershoot constraint. Based on those a comprehensive control solution for systems with RHP zeros is made available. The time optimal solution is derived as well and may be applied to the cases where the undershoot is not an issue.

CHAPTER IV

DISTURBANCE REJECTION IN SYSTEMS WITH TIME DELAY

Most industrial processes, e.g. combustion, distillation, waste water treatment, are modeled as systems with time delay, either first order plus time delay (FOPTD) or second order plus time delay (SOPTD). The time delay, also known as dead time, is generally associated with the transportation of the material or energy in the processes [65]. In addition, it can be the result of an approximation of higher order dynamics with a lower order one, which is not the main focus of this chapter. Generally speaking, systems with time delay are another class of NMP systems. In this chapter, we modify the existing ADRC structure to better accommodate the time delay, and demonstrate the effectiveness of the proposed method through simulations and experiments. The stability analysis for the closed-loop system is provided as well.

The chapter is organized as follows. The control design for systems with time delay is briefly reviewed in Section 4.1, followed by the proposed modification to the

ADRC design given in Section 4.2. In Section 4.3, simulation and experimental results are provided to demonstrate the effectiveness of the proposed method. The stability analysis for the closed-loop system with the proposed design is done in Section 4.4. Section 4.5 summarizes the chapter.

4.1 Background

The control design for systems with time delay is very challenging due to the fact that the time delay introduces additional phase lag, which also increases as frequency gets higher, to the system. Hence, the achievable closed-loop bandwidth is normally limited to $1/\tau$, where τ is the time delay [47]. The well-known Smith predictor [66], however, can increase the closed-loop bandwidth providing an accurate system model is available; otherwise the high bandwidth may cause instability due to model uncertainties. The disturbance rejection performance of the original Smith predictor is found to be poor. In addition, it cannot deal with time-delay systems which have right half plane poles, because an unstable cancellation will be involved in such case. Therefore numerous efforts have been made to modify the original Smith predictor and improve its performance [67]. Especially, the control of integral processes with time delay seems to attract much attention [68-71] due to the critical stability. Zhong *et al.* even wrote a series of four papers on this topic [72-75], proposing a disturbance observer based approach. All of the above Smith predictor based methods would require an accurate mathematical model of the system. Hence the control design of ADRC, which is known for its ability to accommodate uncertainties, for systems with time delay is investigated.

As mentioned earlier in Chapter 2, the application of ADRC to systems with time delay has been studied by other researchers [20, 34]. Several methods was proposed in [20] to deal with time delay within ADRC. The first one is to ignore the time delay and design the ADRC for the dynamics without time delay. This leads to limited performance. The second method approximates the time delay with a first order dynamic using the relation $e^{-\tau s} \approx 1/(\tau s+1)$ and adopts a higher order ADRC design. Other methods try to predict the system output or the control signal based on $g(t+\tau) = g(t) + \dot{g}(t)\tau$. Such prediction may not be accurate when the time delay τ is big. The ADRC design for a multivariable system with time delay is studied in [34], where the approximation method is adopted. The original nonlinear ADRC designs in [20, 34] though provide satisfactory performance, the complexity inhibits their applications. It is the aim of this chapter to provide a simple, easy to implement ADRC solution to the prevailing industrial process control applications.

4.2 Proposed Solution

The modification to the regular ADRC design is straightforward and intuitive. A time delay block is added, as shown in Figure 14, to delay the control signal before it goes into the extended state observer. Since the system output is already delayed due to the system dynamic, this will synchronize the signals that go into the observer and let it provide meaningful estimations of the system states and disturbances[1].

[1] This synchronization technique not only works for the ADRC design discussed in this chapter, but also applies to the general observer design for systems with time delay. After the synchronization of the observer inputs, the outputs of the observer then have physical meanings, which are delayed states.

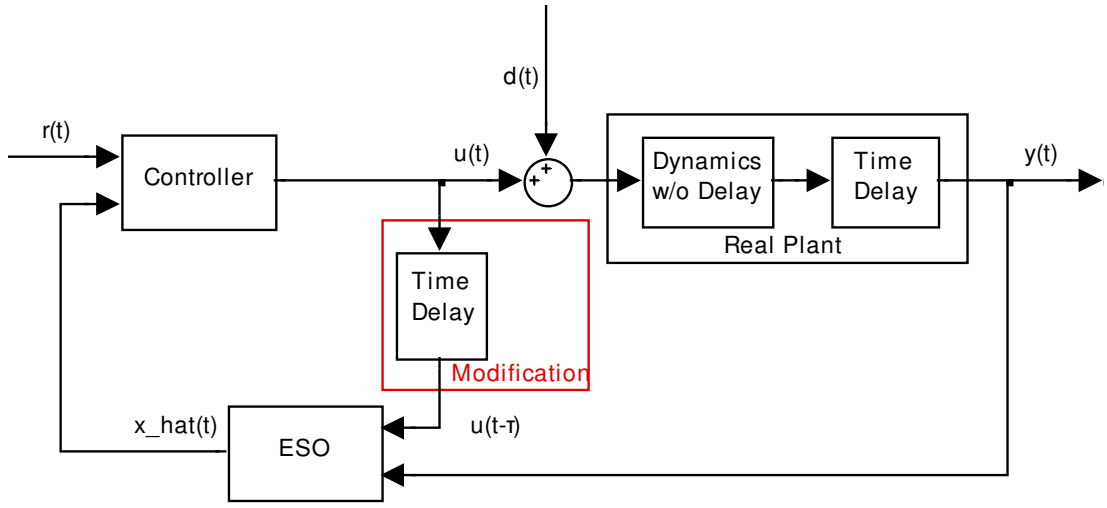

Figure 14 Modified ADRC for systems with time delay.

Compare to the standard ADRC design described in Section 2.4, the proposed ADRC can be implemented easily by replacing (2.5) with the following.

$$\dot{\hat{X}}_{n+1}(t) = A_{n+1}\hat{X}_{n+1}(t) + \hat{b}B_{n+1}u(t-\tau) + L_{n+1}\left(x_1(t) - \hat{x}_1(t)\right) \tag{4.1}$$

Though the modification is simple, it enhances the regular ADRC design by allowing higher observer bandwidth to be achieved. With appropriate tuning, the proposed method also provides a unified solution to a variety of systems with time delay, not matter they have stable poles, pure integrators, or even unstable poles, as will be demonstrated in the next section.

4.3 Simulation and Experimental Results

The following FOPTD and SOPTD systems have been widely studied and will be used to test the proposed method in this section.

$$G_{FOPTD}(s) = \frac{b}{s+a}e^{-\tau s} \tag{4.2}$$

$$G_{SOPTD}(s) = \frac{b}{s^2 + a_1 s + a_0} e^{-\tau s} \tag{4.3}$$

In most cases, there are $a > 0$, $a_1 > 0$ and $a_0 > 0$, i.e. all the poles are stable. With $a = 0$ and $a_0 = 0$, system (4.2) and (4.3) become integral processes with time delay, which has caught much attention. Furthermore if for (4.2) $a < 0$, and for (4.3) $a_1 < 0$ or $a_0 < 0$, the poles become unstable, which makes the problem more challenging.

4.3.1 Simulation Results

Example 4.1: The fuel dynamics of a boiler turbine unit can be considered as a FOPTD system [76] with the following transfer function.

$$G_{fuel}(s) = \frac{0.2}{145s + 1} e^{-60s} = \frac{1.38 \times 10^{-3}}{s + 6.90 \times 10^{-3}} e^{-60s} \tag{4.4}$$

Three different ADRC designs are carried out. The first one is a standard first order ADRC by ignoring the time delay; the second design is a standard second order ADRC approximating the time delay with a first order dynamic; the last is the modified ADRC. The parameters of the three ADRC designs are chosen as: for the regular first order ADRC, $\hat{b} = 1.38 \times 10^{-3}$, $\omega_c = 0.015$ and $\alpha = 1$; for the regular second order ADRC, $\hat{b} = 6.90 \times 10^{-5}$, $\omega_c = 0.02$ and $\alpha = 2$; for the modified first ADRC, $\hat{b} = 1.38 \times 10^{-3}$, $\omega_c = 0.015$ and $\alpha = 10$. A disturbance of magnitude 1 is added at 1000 seconds. The simulation results are shown in Figure 15.

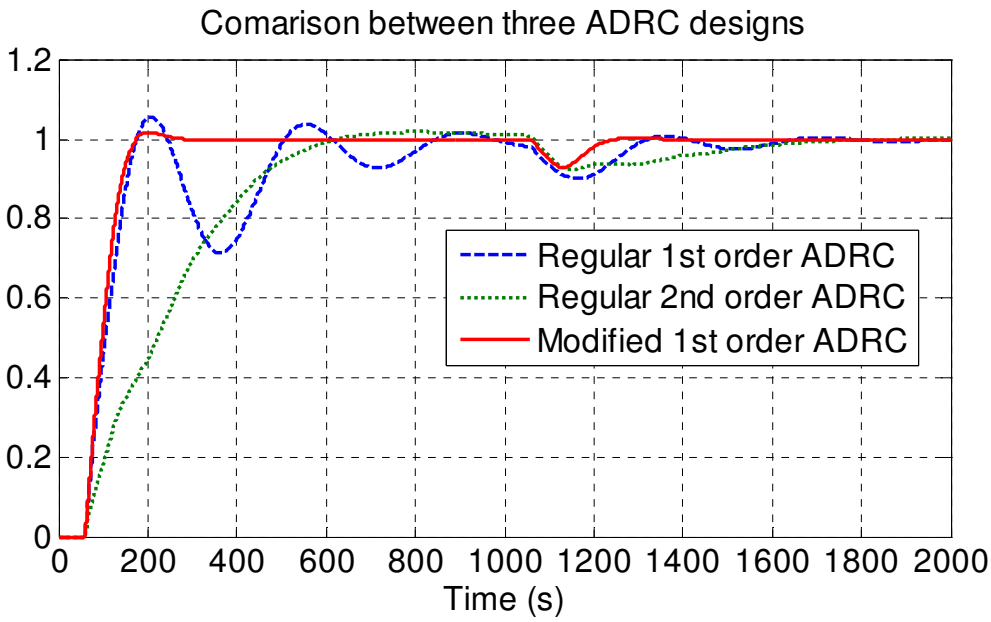

Figure 15 Simulation results of three ADRC designs for system with time delay.

As can be seen from above, since the modified ADRC allows higher observer bandwidth, better disturbance estimation and rejection is achieved. This demonstrates the advantages of the modified ADRC over the regular ADRC for systems with time delay.

Example 4.2: In this example, we test the ability of the proposed ADRC to deal with different types of time-delay systems. The systems studied are all in the form of (4.2) with parameters $\tau = 5$, $b = 1$ and $a = 0.05$, 0 and -0.05 respectively. The design parameter $\hat{b} = b = 1$ is the same for all three cases, and the tuning parameters are chosen as: for $a = 0.05$, $\omega_c = 0.14$ and $\alpha = 10$; for $a = 0$, $\omega_c = 0.09$ and $\alpha = 10$; for $a = -0.05$, $\omega_c = 0.06$ and $\alpha = 30$. A disturbance of magnitude 0.1 is added at 70 seconds. The simulation results are shown in Figure 16.

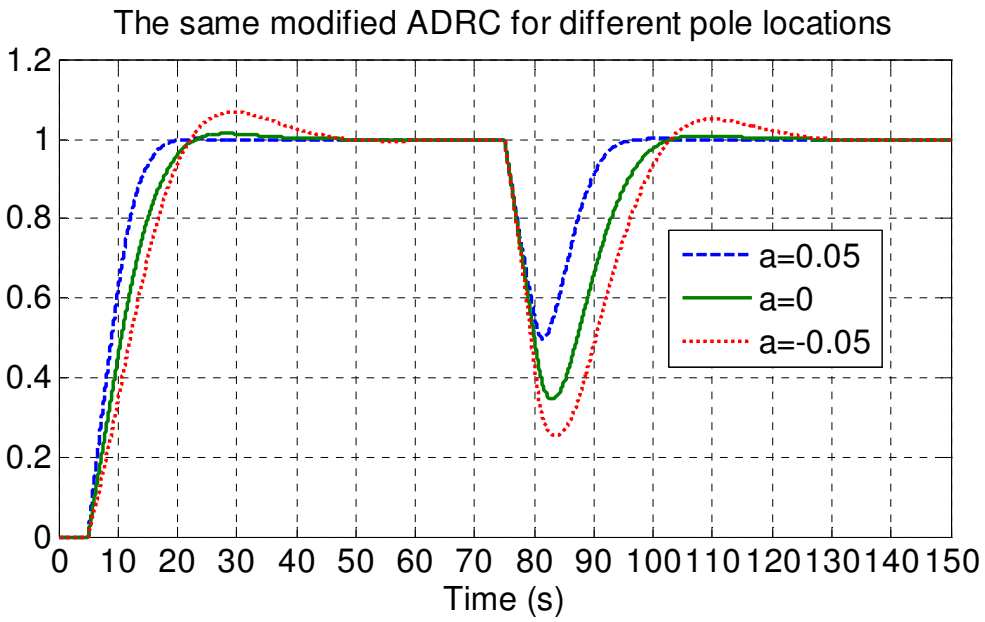

Figure 16 Simulation results of ADRC accommodating different system dynamics.

From above, it is demonstrated that the same ADRC design works for time-delay systems with stable, critical stable and unstable poles. Notice that, for the $a=0$ case, similar performance as given in [68] is achieved, but our method is much easier to tune. Basically only one tuning parameter needs to be adjusted, whereas in [68], there are three parameters for the filter and an additional for the controller.

4.3.2 Experimental Results

The distillation column benchmark problem [77] is studied here. The system has two inputs and two outputs, and the system dynamics is represented by the following transfer function matrix.

$$\begin{bmatrix} Y_1(s) \\ Y_2(s) \end{bmatrix} = \begin{bmatrix} P_{11}(s) & P_{12}(s) \\ P_{21}(s) & P_{22}(s) \end{bmatrix} \begin{bmatrix} U_1(s) \\ U_2(s) \end{bmatrix} \tag{4.5}$$

where $P_{11}(s)=\frac{12.8e^{-1s}}{16.7s+1}$, $P_{12}(s)=\frac{-18.9e^{-3s}}{21.0s+1}$, $P_{21}(s)=\frac{6.6e^{-7s}}{10.9s+1}$ and $P_{22}(s)=\frac{-19.4e^{-3s}}{14.4s+1}$.

Then it is modeled in MATLAB SIMULINK as shown in Figure 17, and running in real-time workshop to mimic the dynamics of a real distillation column. The virtual distillation column interacts with the outside through a multi-function analog and digital I/O card (PCI-DAS1602-16) from Measurement Computing Corporation.

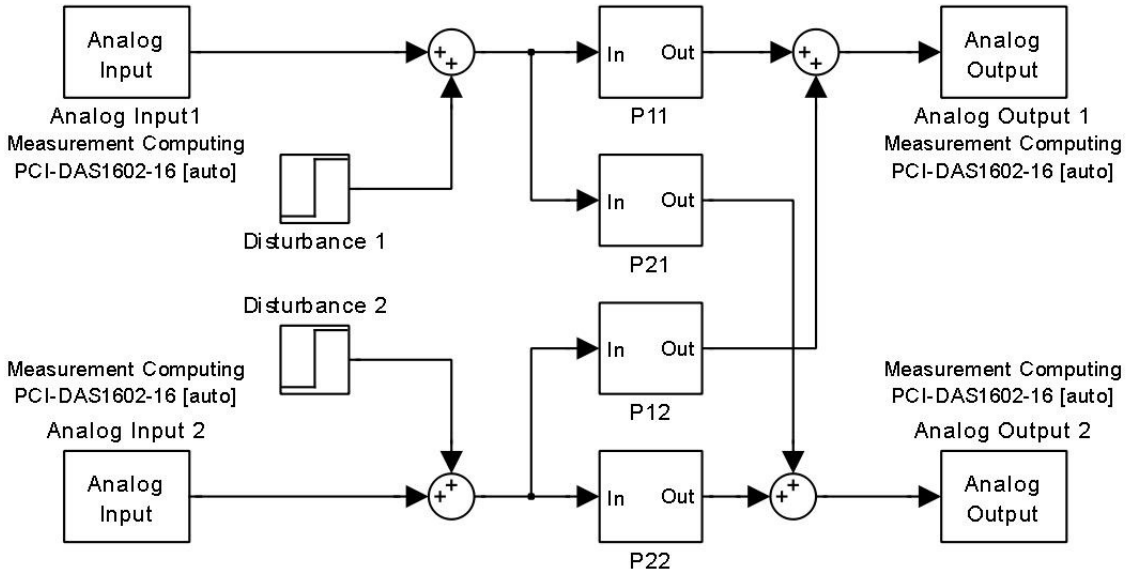

Figure 17 SIMULINK model of the distillation column.

According to the disturbance decoupling control proposed in [26], two modified first order ADRC are designed to control $P_{11}(s)$ and $P_{22}(s)$ respectively. The control algorithm is coded and compiled in OpenPCS, an IEC (International Electrotechnical Commission) 61131-3 compatible PLC (Programmable Logic Controller) programming environment as shown in Figure 18, and then downloaded to and executed on the UPAC (Universal Programmable Automation Controller) platform as shown in Figure 19, a product from UniControl Inc., which interfaces with the virtual distillation column.

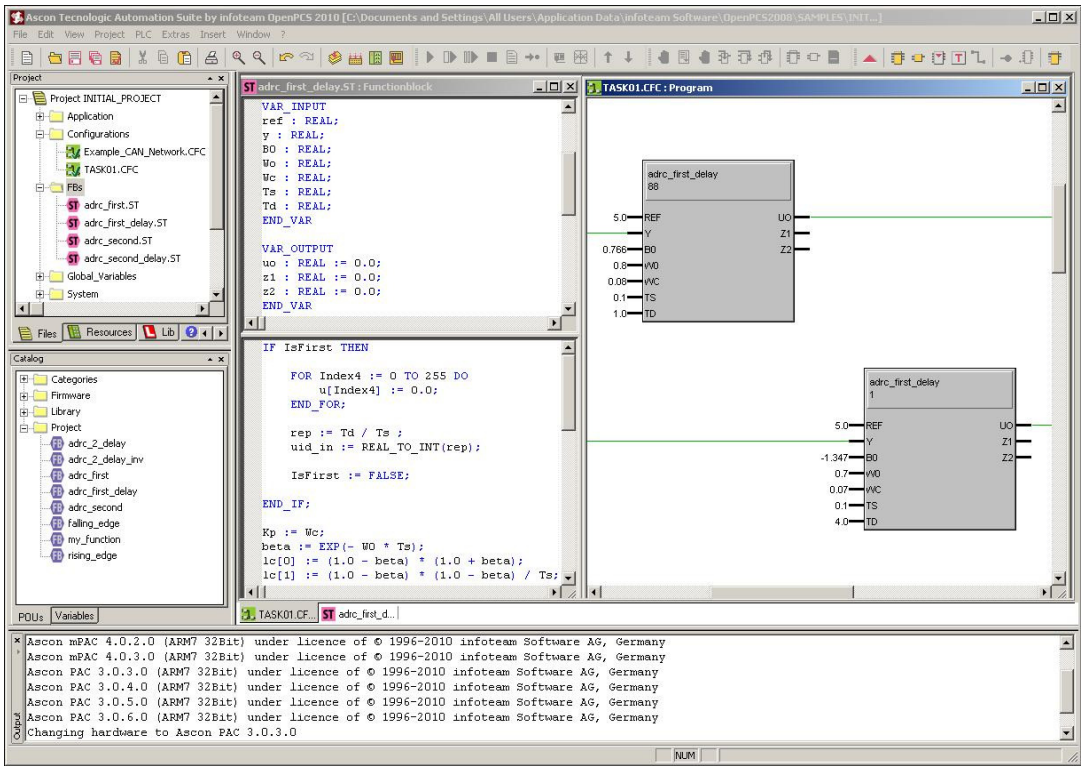

Figure 18 OpenPCS programming environment.

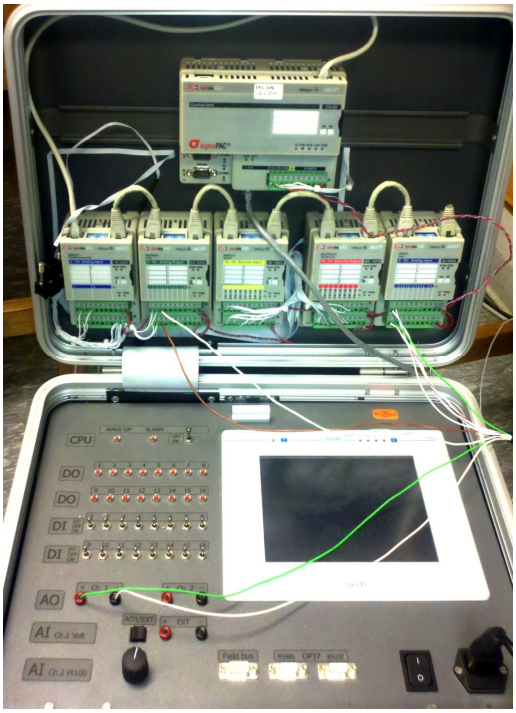

Figure 19 UPAC platform.

The test is done with the following parameters: $\hat{b}_1 = 0.766$, $\omega_{c1} = 0.08$, $\alpha_1 = 10$, $\hat{b}_2 = -1.347$, $\omega_{c2} = 0.1$ and $\alpha_2 = 10$. The set-points for both loops are set to 5. At 100 seconds a disturbance of magnitude of 0.1 is added to loop 1 and another disturbance of the same magnitude is added to loop 2 at 200 seconds. The dynamics of the distillation column is simulated at a rate of 100 Hz, and the controller runs at a rate of 10 Hz. The test results are shown in Figure 20 and Figure 21.

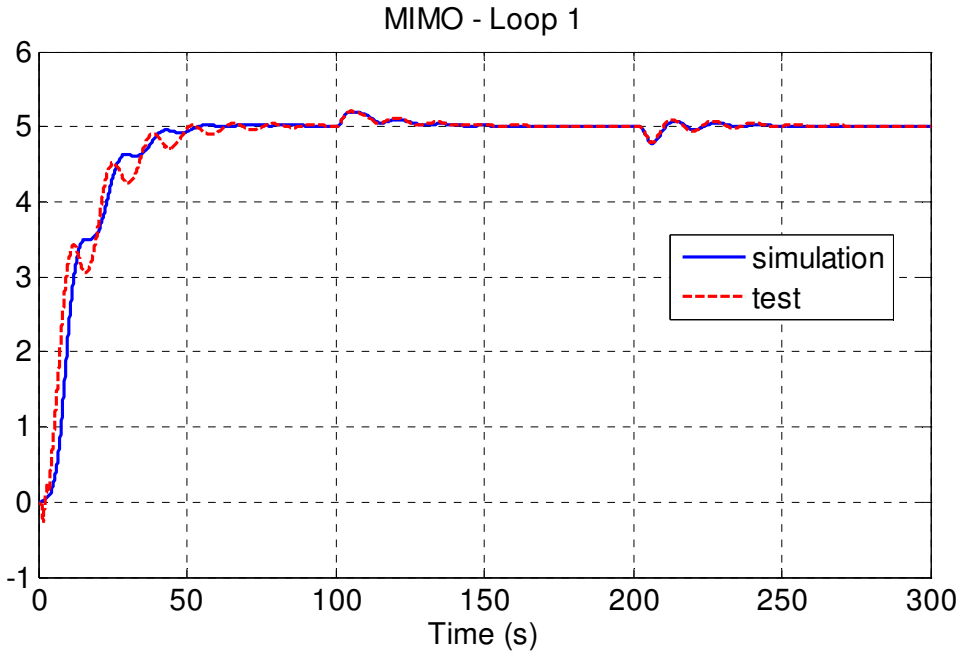

Figure 20 Simulation and test results of loop 1 of the distillation column.

From the results we see that the simulation and test results match well, and the disturbances are well rejected. The discrepancy between the simulation and the hardware test at the beginning is caused by the different initial conditions. In this experiment, we demonstrate the feasibility of the implementation of the proposed method. Also its ability to deal with MIMO system with time delay, which is common in real industrial

applications, is verified. The tuning for such systems needs more consideration of the trade-off between the performances of each loop.

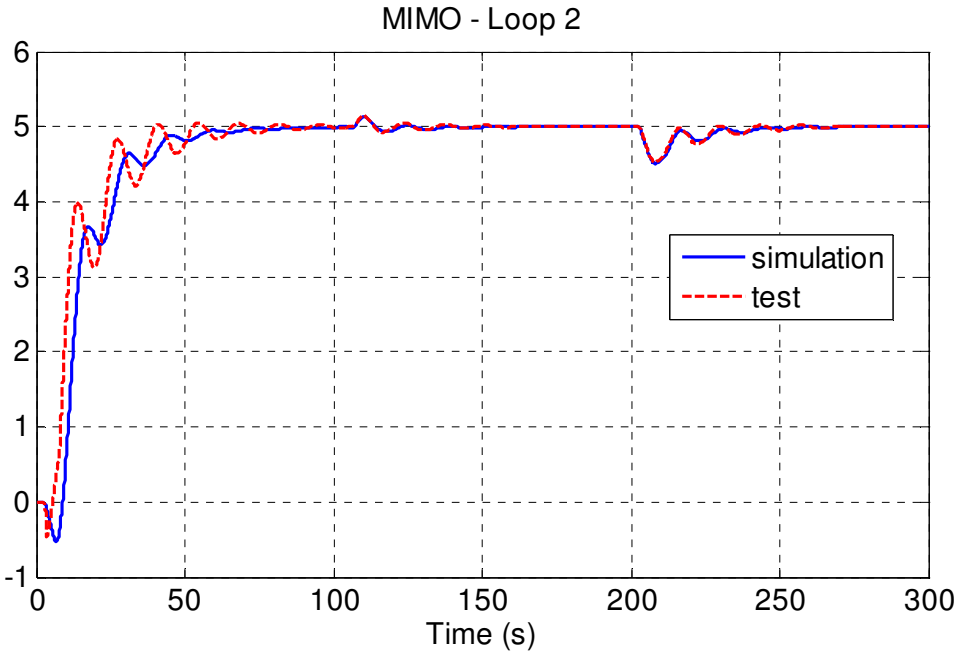

Figure 21 Simulation and test results of loop 2 of the distillation column.

4.4 Stability Analysis

The stability analysis for the above design can be carried out following the idea presented in [78] by means of linear matrix inequality (LMI). Applying the modified ADRC design, the overall closed-loop system can be written as

$$\begin{aligned} \dot{x}(t) &= Ax(t) + A_d x(t-\tau),\ t>0 \\ x(t) &= \xi(t),\ t\in[-\tau,0] \end{aligned} \tag{4.6}$$

where $\xi(t)$ is a vector-valued continuous function of time and τ is the constant time delay. For the FOPTD system (4.2) there are

$$x=\begin{bmatrix} y \\ \hat{y} \\ \hat{f} \end{bmatrix},\ A=\begin{bmatrix} -a & -k_1 b/\hat{b} & -b/\hat{b} \\ 0 & -l_1 & 1 \\ 0 & -l_2 & 0 \end{bmatrix} \text{ and } A_d=\begin{bmatrix} 0 & 0 & 0 \\ l_1 & -k_1 & -1 \\ l_2 & 0 & 0 \end{bmatrix};$$

and for the SOPTD system (4.3) there are

$$x=\begin{bmatrix} y \\ \dot{y} \\ \hat{y} \\ \hat{\dot{y}} \\ \hat{f} \end{bmatrix},\ A=\begin{bmatrix} 0 & 1 & 0 & 0 & 0 \\ -a_0 & -a_1 & -k_1 b/\hat{b} & -k_2 b/\hat{b} & -b/\hat{b} \\ 0 & 0 & -l_1 & 1 & 0 \\ 0 & 0 & -l_2 & 0 & 1 \\ 0 & 0 & -l_3 & 0 & 0 \end{bmatrix} \text{ and } A_d=\begin{bmatrix} 0 & 0 & 0 & 0 & 0 \\ 0 & 0 & 0 & 0 & 0 \\ l_1 & 0 & 0 & 0 & 0 \\ l_2 & 0 & -k_1 & -k_2 & -1 \\ l_3 & 0 & 0 & 0 & 0 \end{bmatrix}.$$

The following lemmas will be used for the analysis.

Lemma 4.1 (Jensen's Inequality) [79]**:** *For any constant matrix* $S>0$, *scalars* $t_2>t_1$, *vector function* $x:[t_1,t_2]\to R^m$ *such that the integrations in the following are well defined, then*

$$(t_2-t_1)\int_{t_1}^{t_2} x(t)^T Sx(t)\,dt \geq \left[\int_{t_1}^{t_2} x(t)\,dt\right]^T S\left[\int_{t_1}^{t_2} x(t)\,dt\right] \tag{4.7}$$

Lemma 4.2 (Finsler's Lemma) [78]**:** *Let* $x\in R^n$, $P=P^T\in R^{n\times n}$ *and* $H\in R^{m\times n}$ *such that* $\operatorname{rank}(H)=r<n$. *The following are equivalent:*

1. $x^T Px<0,\ \forall Hx=0,\ x\neq 0$;
2. $\exists X\in R^{n\times m}$ *such that* $P+XH+H^T X^T<0$.

Lemma 4.3 (Schur complements) [80]**:** *For any symmetric matrix* $\Psi=\begin{bmatrix} A & B \\ B^T & C \end{bmatrix}$, *where* $C>0$ *and is invertible, then* $\Psi>0$ *if and only if* $A-BC^{-1}B^T>0$.

Theorem 4.1: *System (4.6) is asymptotically stable, if there exist symmetric matrices* $P>0$, $Q>0$ *and* $M>0$ *such that the following LMI holds.*

$$\begin{bmatrix} PA+A^TP+Q-M & PA_d+M & \tau A^TM \\ A_d^TP+M & -Q-M & \tau A_d^TM \\ \tau MA & \tau MA_d & -M \end{bmatrix} < 0 \tag{4.8}$$

Proof. Choosing the following Lyapunov functional

$$V\left(x(t)\right) = x^T(t)Px(t) + \int_{t-\tau}^{t} x^T(s)Qx(s)ds + \tau\int_{-\tau}^{0}\int_{t+s}^{t} \dot{x}^T(\sigma)M\dot{x}(\sigma)d\sigma ds \tag{4.9}$$

The time derivative of $V\left(x(t)\right)$ along the trajectory of system (4.6) can be calculated as

$$\begin{aligned} \dot{V}\left(x(t)\right) = {} & 2x^T(t)P\dot{x}(t) + x^T(t)Qx(t) - x^T(t-\tau)Qx(t-\tau) \\ & + \tau^2\dot{x}^T(t)M\dot{x}(t) - \tau\int_{t-\tau}^{t}\dot{x}^T(\sigma)M\dot{x}(\sigma)d\sigma \end{aligned} \tag{4.10}$$

From Lemma 4.1, the following is true.

$$-\tau\int_{t-\tau}^{t}\dot{x}^T(\sigma)M\dot{x}(\sigma)d\sigma \le -\tilde{x}^T(t)M\tilde{x}(t) \tag{4.11}$$

where $\tilde{x}(t) = x(t) - x(t-\tau)$. Then

$$\dot{V}\left(x(t)\right) \le \phi^T(t)\Lambda\phi(t) \tag{4.12}$$

where $\phi(t) = \left[\dot{x}^T(t), x^T(t), x^T(t-\tau), \tilde{x}^T(t)\right]^T$ and

$$\Lambda = \begin{bmatrix} \tau^2M & P & 0 & 0 \\ P & Q & 0 & 0 \\ 0 & 0 & -Q & 0 \\ 0 & 0 & 0 & -M \end{bmatrix}.$$

According to (4.6), there is $\bar{A}\phi(t) \equiv 0$, where $\bar{A} = \begin{bmatrix} I & -A & -A_d & 0 \\ 0 & -I & I & I \end{bmatrix}$. Then the closed-loop system (4.6) is asymptotically stable if for all $\bar{A}\phi(t) = 0$, $\phi^T(t)\Lambda\phi(t) < 0$.

With $\bar{A}^{\perp} = \begin{bmatrix} A^T & I & 0 & I \\ A_d^T & 0 & I & -I \end{bmatrix}^T$, which is orthogonal to $\bar{A}$ and $\bar{A}\bar{A}^{\perp} = 0$, from Lemma 4.2, the following holds.

$$\phi^T(t)\Lambda\phi(t) < 0 \Leftrightarrow \bar{A}^{\perp T}\Lambda\bar{A}^{\perp} < 0 \tag{4.13}$$

$$\bar{A}^{\perp T}\Lambda\bar{A}^{\perp} = \begin{bmatrix} \tau^2 A^T MA + PA + A^T P + Q - M & \tau^2 A^T MA_d + PA_d + M \\ \tau^2 A_d{}^T MA + A_d^T P + M & \tau^2 A_d^T MA_d - Q - M \end{bmatrix} < 0 \tag{4.14}$$

By Lemma 4.3, (4.14) is equivalent to (4.8). Thus, we can always find a sufficiently small $\varepsilon > 0$ such that $\dot{V}(x(t)) < -\varepsilon \|x(t)\|^2$, which ensures the asymptotic stability of system (4.6). Q.E.D.

The MATLAB code for finding a feasible solution of (4.8) can be found in the Appendix A.2. The analysis above can be used as a guide for selecting controller parameters. For example, we can choose the maximum controller bandwidth which ensures a feasible solution of (4.8) as a starting point, i.e. the closed-loop system is guaranteed to be stable; then gradually increase the bandwidth until a satisfactory performance is achieved, since the solution from (4.8) may be conservative.

4.5 Summary

The main contributions of this chapter are: 1) proposed a simple and easy to implement ADRC solution for systems with time delay; 2) provided, for the first time, the stability analysis of ADRC applied to systems with time delay. The proposed solution has been demonstrated to be very effective through both simulations and experiments.

CHAPTER V

THE VIBRATION SUPPRESSION IN MOTION CONTROL

The vibration due to the resonance mode, which is a part of the internal dynamics, is a widely recognized problem in motion control applications. In this chapter, we try to provide an alternative solution to this problem using our unique ADRC design, which requires very little system model information and makes the control system tolerant of unknown changes in system dynamics. With the proposed method, the effect of the resonant mode to motion, i.e. the ripples in torque, is estimated and canceled in real time using the motor torque, after which the motion dynamic behaves largely like a rigid body.

The chapter is organized as follows. First, the literature review is presented in Section 5.1, while the specific problem studied and the existing solutions are described in Section 5.2. In Section 5.3, the ADRC design for the vibration problem is carried out. Simulation and experimental results are presented in Section 5.4 and Section 5.5 respectively. Section 5.6 summarizes the chapter.

5.1 Background

Vibration suppression is important in motion control applications because vibration causes dynamic stresses, energy wastes and performance degradations [81]. By law of physics, mechanical resonance is unavoidable in every system involving motion, but the natural frequencies of such systems are usually quite high and not excited during most common motion maneuvers, where a simple proportional-integral-derivative (PID) controller is often sufficient to meet the design requirements. Control design becomes an issue, however, when the performance improvements push the loop bandwidth to its limit where the resonant modes come into play. The most common resonance seen in industry can be attributed to the compliant couplings, such as gear boxes, long shafts and belts, which can be treated as springs [82].

To deal with resonance, there are mechanical and electrical means. Since the resonance is caused by compliance, a stiffer transmission, i.e. a direct coupling in place of a belt, will be an obvious solution. Adding more mechanical damping will surely be helpful. In addition, increasing the motor inertia is found to be an effective way to alleviate the resonance [82]. These mechanical methods are costly, which leads us to electrical options, consist of low-pass filter, notch filter [83] and bi-quad filter [84], all for the objective of attenuating the loop gain amplitude at the resonant frequency so that the resonance is suppressed. Some of the electrical methods are equivalent mathematically to the mechanical methods mentioned above. Active resonance damping control [84] actually increases the effective physical damping by adding a torque that is proportional to the speed difference between the motor and load. Acceleration feedback control [84, 85], however, increases the motor inertia equivalently. There are still other

control methods available, such as center of mass control [82, 84] and resonance ratio control [86, 87].

All of the above control methods predicate on the detailed mathematical model of the physical process that may or may not be readily available. Even if such a model is obtained at considerable cost, the parameters of the model often change during operation, which may lead to variations in the resonant frequency, leaving the notch filter approach, for example, vulnerable. The attempt to address this flaw leads to solutions such as the adaptive notch filter [88], which is designed to tune the filter parameters on the fly based on adaptive control theory, adding complexity and cost to the design, implementation, and tuning of the control system. It is in this background that an alternative ADRC solution is proposed in this chapter.

5.2 Problem Description and Existing Solutions

The compliant resonance problem can be simplified and represented by the two-inertia system model [82, 87] as shown in Figure 22.

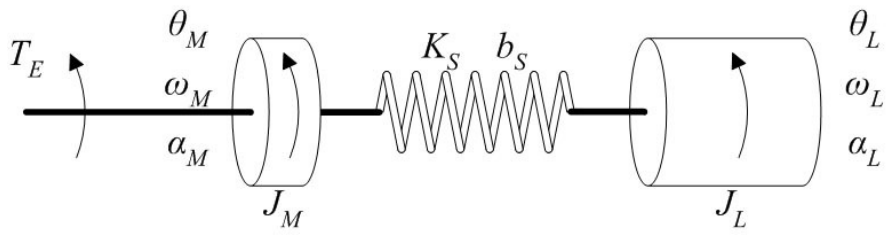

Figure 22 Two-inertia system model.

Motor inertia J_M is connected to load inertia J_L by a spring with spring constant K_S and damping ratio b_S. A torque T_E is applied on the motor side to drive the system.

Angular acceleration, angular velocity and angular position of the motor and the load are denoted as α_M, ω_M, θ_M and α_L, ω_L, θ_L respectively. Through simple analysis, we can derive the transfer functions from input (T_E) to different outputs (ω_M, ω_L, θ_M and θ_L). The transfer function from T_E to ω_M is

$$\frac{\omega_M}{T_E} = \frac{1}{(J_M + J_L)s} \cdot \frac{J_L s^2 + b_S s + K_S}{J_P s^2 + b_S s + K_S} \tag{5.1}$$

where $J_P = J_M J_L / (J_M + J_L)$. Similarly, the other three transfer functions are

$$\frac{\theta_M}{T_E} = \frac{1}{(J_M + J_L)s^2} \cdot \frac{J_L s^2 + b_S s + K_S}{J_P s^2 + b_S s + K_S} \tag{5.2}$$

$$\frac{\omega_L}{T_E} = \frac{1}{(J_M + J_L)s} \cdot \frac{b_S s + K_S}{J_P s^2 + b_S s + K_S} \tag{5.3}$$

$$\frac{\theta_L}{T_E} = \frac{1}{(J_M + J_L)s^2} \cdot \frac{b_S s + K_S}{J_P s^2 + b_S s + K_S} \tag{5.4}$$

The first term of each transfer function is exactly the same as the transfer function for the rigid body model; the second term which contains resonance is introduced by the compliance. In both motor and load transfer functions, the denominators of the resonance term will produce a resonant frequency ω_R, and the numerator of the resonance term in motor transfer functions will produce an anti-resonant frequency ω_{AR} [82]. They can be calculated by following equations.

$$\omega_R = \sqrt{K_S / J_P} \tag{5.5}$$

$$\omega_{AR} = \sqrt{K_S / J_L} \tag{5.6}$$

The Bode plots of velocity transfer functions of rigid body model and compliant model (two-inertia system model) are shown in Figure 23 for comparison. At low

frequency (below the anti-resonant frequency) the two models behave the same. The motor and load are connected as a whole just like the rigid body. As frequency goes higher, the motor and load become disconnected and behave differently. Around resonant frequency there is a 180 degree phase difference between the motor and load, which to some extent represents the resonance as well.

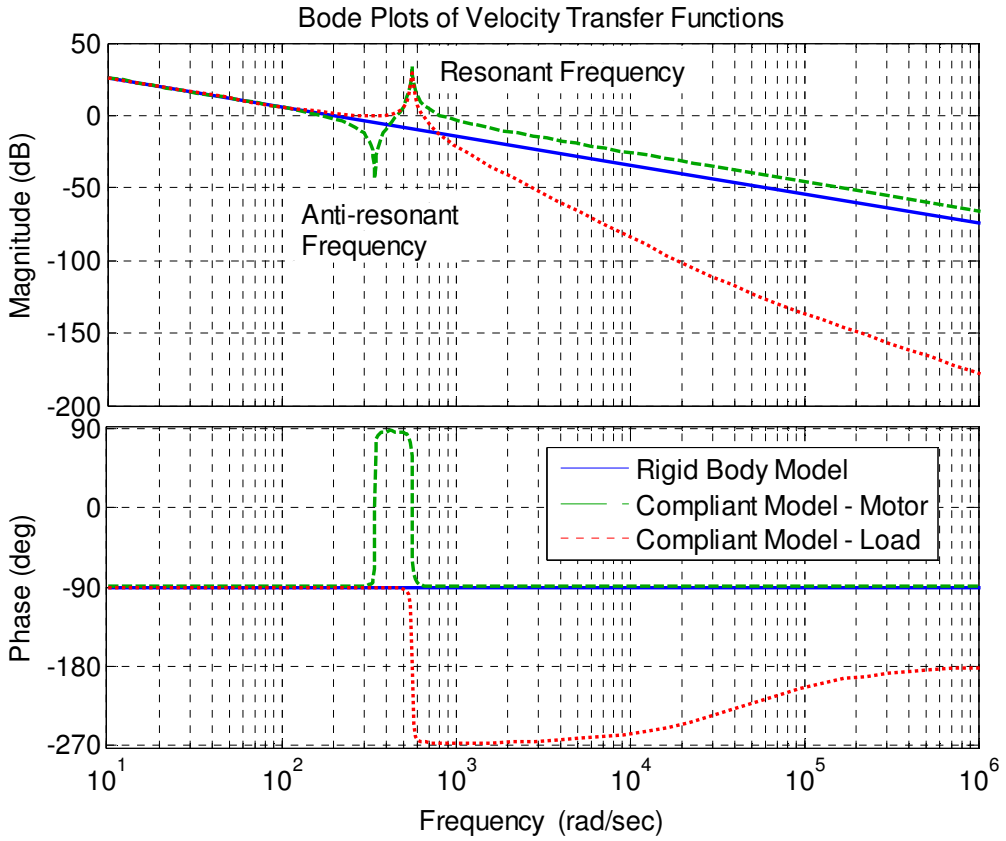

Figure 23 Bode plots of velocity transfer functions - Rigid vs. Compliant.

Several existing methods are described in [84] that deal with the resonance. A notch filter in the form of

$$F_N(s) = \frac{s^2 + \omega_R^2}{s^2 + 2\zeta\omega_R s + \omega_R^2} \tag{5.7}$$

is often used to attenuate the open loop gain at the resonant frequency. The bi-quad filter

$$F_{BQ}(s) = \frac{s^2 + 2\zeta_R \omega_R s + \omega_R^2}{s^2 + 2\zeta_{AR} \omega_{AR} s + \omega_{AR}^2} \tag{5.8}$$

as another solution, not only attenuates the open loop gain at the resonant frequency but also increases the open loop gain at the anti-resonant frequency making it more like a rigid body system. The acceleration feedback method employs a rigid-body Luenberger observer to estimate the motor acceleration and uses it as a feedback for the purpose of increasing the motor inertia, as shown in Figure 24.

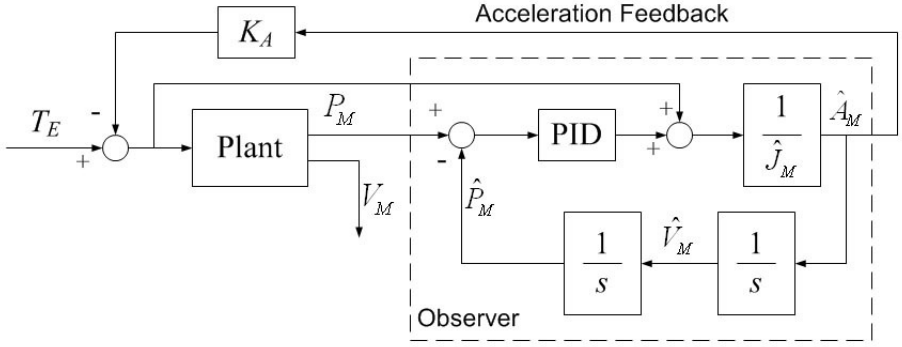

Figure 24 Diagram of the acceleration feedback design.

In a typical configuration of two-inertia system, the sensor is normally mounted at the motor end, where only the motion of the motor is measured and fed back. We denote this set up as motor feedback and this is the common practice in industry. In most cases seen in industry, however, the objective is to control the motion of the load. Consequently, we will also investigate the alternative where we mount the sensor at the load end and use the measurement of the load as feedback, which is denoted as the load feedback. Although the load feedback provides the direct information on how the load behaves, there is a considerable amount of phase lag, comparing to the motor feedback,

which makes the control design more challenging. One may suspect that this might be a main reason why the motor feedback configuration is widely used in industry.

Different applications may have different design objectives. Some regulate velocity, others position. To show the generality of the proposed method, both velocity control and position control are addressed.

5.3 ADRC Solution

The main idea of ADRC is to treat any unknown dynamics of the system together with external disturbance as a total disturbance, use an extended state observer (ESO) to estimate this total disturbance in real time, and then cancel it in the control law [4]. In this manner we do not have to know the exact system model in order to control it, and particularly in this application we can treat the resonance, no matter what the frequency is, as part of the total disturbance.

For completeness, we consider two types of motion control, velocity control and position control, and two feedback options, motor feedback and load feedback. Since the only difference between velocity control and position control is that the plant has one more integrator in position control, we will only present the problem reformulation for velocity control in the ADRC structure with both feedback options.

Velocity Control with Motor Feedback

With $b_2 = 1/J_M$, $b_1 = b_S/(J_M J_L)$, $b_0 = K_S/(J_M J_L)$, $a_2 = b_S/J_P$, $a_1 = K_S/J_P$, and considering an external disturbance w, (5.1) can be rewritten as

$$\dddot{y} + a_2\ddot{y} + a_1\dot{y} = b_2\ddot{u} + b_1\dot{u} + b_0 u + w \tag{5.9}$$

where y is the motor velocity ω_M, and u is torque T_E applied to the motor. Integrating (5.9) twice on both sides, the third-order system with a relative degree of one becomes a first order system [89] as below

$$\begin{aligned}\dot{y} &= b_2 u + \left(-a_2 y - a_1 \int y dt + b_1 \int u dt + b_0 \iint u dt + \iint w dt\right) \\ &= b_2 u + f\left(y, \int y dt, \int u dt, \iint u dt, \iint w dt\right)\end{aligned} \tag{5.10}$$

Hence the standard first order ADRC design is adopted for this case. Similarly, a second order ADRC can be applied to the position control with motor feedback.

Velocity Control with Load Feedback

Considering an external disturbance w, (5.3) can be rewritten as

$$\dddot{y} + a_2 \ddot{y} + a_1 \dot{y} = b_1 \dot{u} + b_0 u + w \tag{5.11}$$

where y is the load velocity ω_L, and u is torque T_E applied to the motor. Integrating (5.11) once on both sides, the third-order system with a relative degree of two becomes a second order system

$$\begin{aligned}\ddot{y} &= b_1 u + \left(-a_2 \dot{y} - a_1 y + b_0 \int u dt + \int w dt\right) \\ &= b_1 u + f\left(\dot{y}, y, \int u dt, \int w dt\right)\end{aligned} \tag{5.12}$$

Hence the standard second order ADRC design is adopted. Similarly, a third order ADRC can be applied to the position control with load feedback.

5.4 Simulation Results

In this section, the ADRC solution is tested in simulation and compared to the three existing methods described in [84], using the motor feedback configuration as in [84]. The more practical load feedback configuration is also explored.

5.4.1 Parameters and Profile Selection

The proposed method is tested in simulations using the same system parameters as those in [84], with $K_S = 372$ N·m/rad, $b_S = 0.008$ N·m·s/rad, $J_M = 1.88\times10^{-3}$ kg·m^2, $J_L = 3.13\times10^{-3}$ kg·m^2, $J_P = 1.17\times10^{-3}$ kg·m^2. In this case, the anti-resonant frequency ω_{AR} is 345 rad/s (or 55 Hz), and resonant frequency ω_R is 563 rad/s (or 90 Hz).We also compare our method with those discussed in [84] applying their fine tuned parameters in velocity control with motor feedback. The comparison is not done for other cases because only velocity control with motor feedback is considered in [84].

Step reference is a commonly used profile in simulations and real tests, but it is too aggressive and contains components with very broad bandwidth, which will excite the resonant mode of the system. So in industry the trapezoidal profile, which is less aggressive and also energy saving, is widely used instead of step reference.

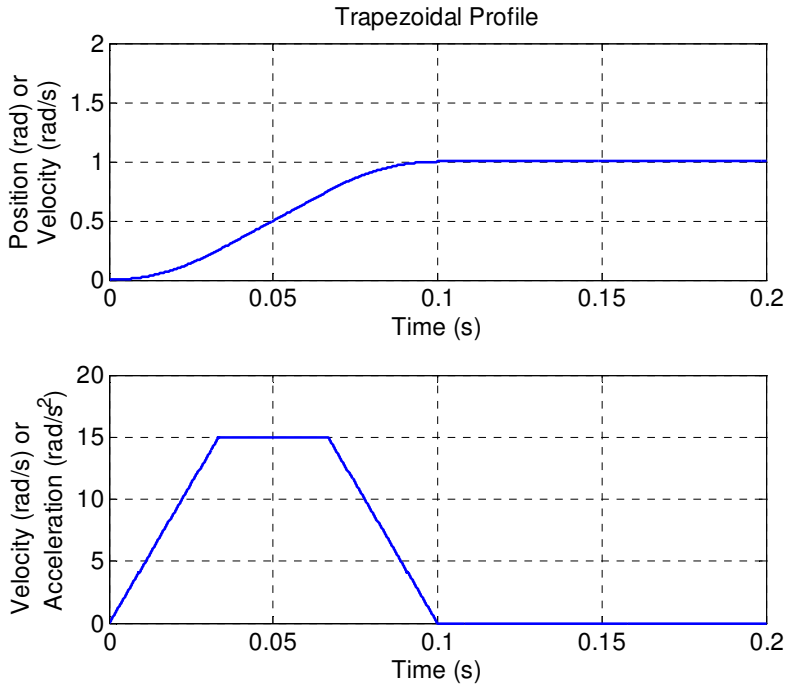

Figure 25 Trapezoidal profile.

Even if a trapezoidal profile is used, the rising time of the profile is still crucial to the system performance. The faster the rising time is, more possible the system is going to have resonance. In order to avoid the resonance, the rising time is chosen between 0.05 seconds and 0.1 seconds in the simulations.

5.4.2 Results Comparison for Velocity Control with Motor Feedback

Table I MOTOR RESPONSES: TRACKING PERFORMANCE

		Overshoot (%)	**5‰ Settling Time** (ms)
Notch Filter		4.2	132
Bi-quad Filter		1.4	112
Acceleration Feedback		6.6	139
ADRC with different ω_c (Hz)	50	0.8	110
	100	0.3	96
	200	0.1	96

Table II MOTOR RESPONSES: DISTURBANCE REJECTION PERFORMANCE

		Maximum Error (rad/s)	**5‰ Settling Time** (ms)
Notch Filter		1.35	>1000
Bi-quad Filter		0.82	>1000
Acceleration Feedback		0.66	101
ADRC with different ω_c (Hz)	50	0.68	73
	100	0.40	80
	200	0.22	115

The proposed ADRC solution is simulated and compared to the notch filter, bi-quad filter and acceleration feedback methods, with the rising time set to 100 ms (0.1

s), the profile starting time set to 0.5 s and a disturbance of 1 N·m applied to the motor at 1 second. The ratio between the observer and controller bandwidth α is set to 2 for the rest of the chapter. The results are shown in Table I and Table II , as well as in Figure 26.

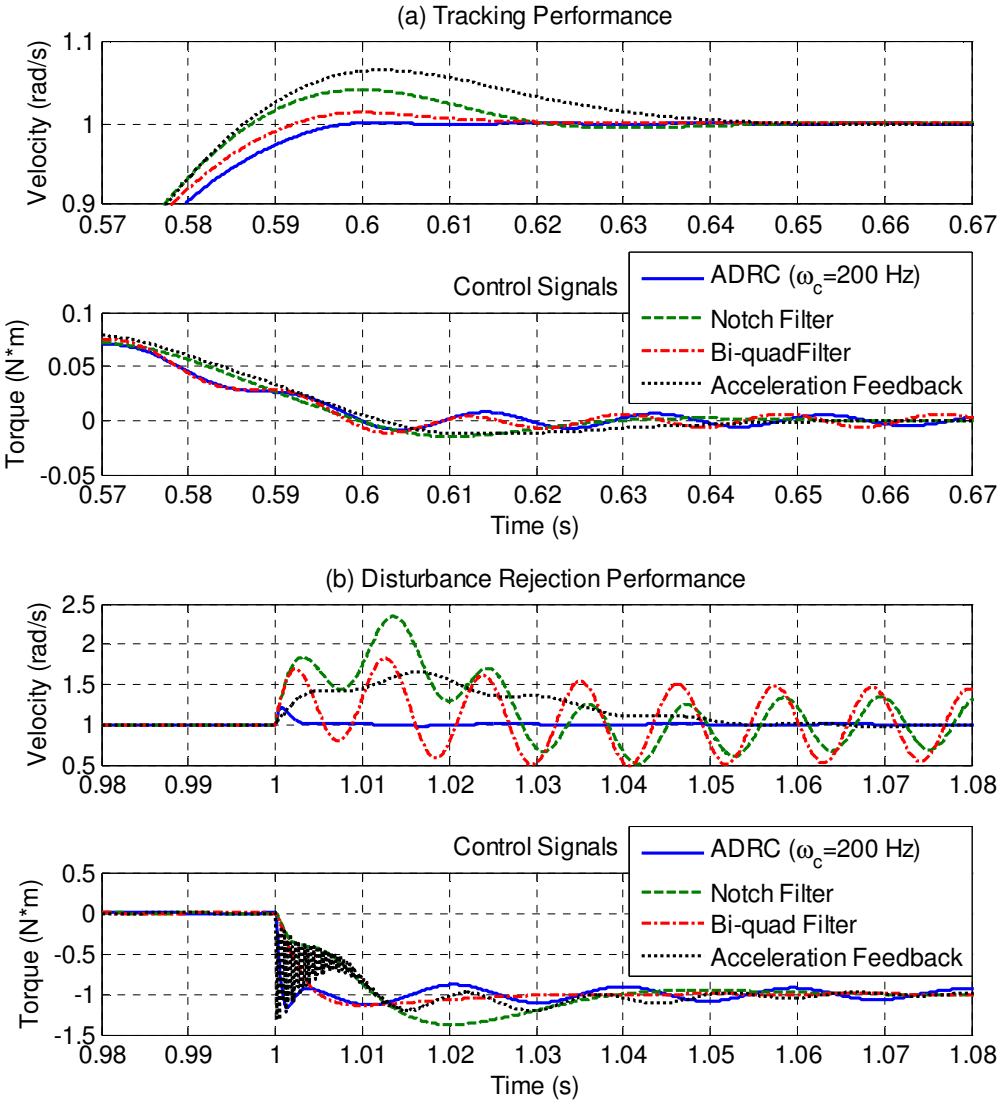

Figure 26 Motor responses of velocity control with motor feedback.

It is observed that acceleration feedback has the biggest overshoot. Bi-quad filter has less overshoot because it cancels out both resonant and anti-resonant terms in the transfer function. ADRC has even less overshoot and the overshoot decreases as the

bandwidth increases. The disturbance rejection ability of acceleration feedback is better than both notch filter and bi-quad filter, which have big errors and oscillate. The ADRC has the best disturbance rejection ability which increases as the bandwidth increases.

Note that the bandwidth of ADRC can go well beyond the resonant frequency, which is quite difficult to achieve with other methods. As shown in [84] the closed-loop bandwidths associated with the notch filter, the bi-quad filter and acceleration feedback design are 32 Hz, 47 Hz and 37 Hz, respectively, well below the resonant frequency (90 Hz). With ω_c set to 200 Hz, however, the closed-loop bandwidth of ADRC is found to be 192 Hz, which is well beyond the resonant frequency, unlike the existing methods.

The robustness of each controller is also tested by varying the load inertia without changing the controller parameters. The tests are performed with the load changing to 0.9, 1.1, 2 and 5 times of its original value. The bi-quad filter is found to be the most fragile, because the system becomes unstable for all four load changes. With the notch filter, the system is stable for the first two changes but becomes unstable for last two in the presence of external disturbances. Acceleration feedback and ADRC are stable for all four cases, but the former results in a bigger overshoot of 17% when the load increases to 5 times of its original value. The motor overshoot in ADRC remains mostly unchanged, but the load oscillation becomes more pronounced with the increasing load.

5.4.3 More Results on Load Response Regulation

In Section 5.4.2, we were concerned with only the response of the motor, as in the existing methods mentioned above. In reality, however, load response is equally important. The good response from the motor in Figure 26 may be a bit misleading,

considering that the load may experience significant oscillations, as shown in Figure 27. Following we will discuss how to better regulate the load response.

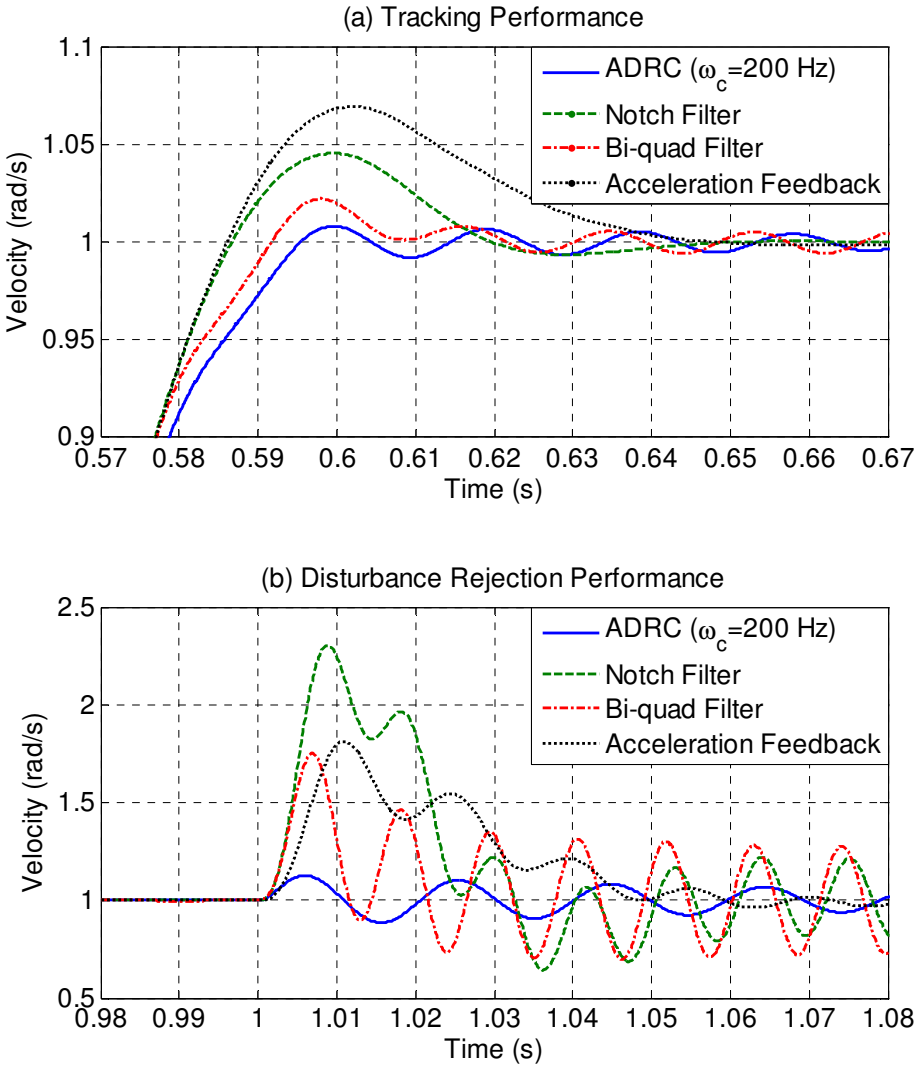

Figure 27 Load responses of velocity control with motor feedback.

Load Control with Motor Feedback

With motor feedback, since it is open loop from the motor to the load, all we can do is to control the motor. From the simulation we found that if the motor is perfectly controlled, more oscillation is found in load response. In this situation, we are left with

the only option of either manipulating the motion profile to influence the load response indirectly, or to degrade the motor response performance to avoid load oscillation.

Table III and Table IV summarize load responses of all four methods considering velocity control with motor feedback. Note that the best load response performance is obtained at $\omega_c = 100$ Hz, proving that the optimal performance is not corresponding to the highest bandwidth. The reason is rather intuitive: higher bandwidth in the motor loop leads to faster movement of the motor shaft, which in turn leads to more stimulation of the resonant mode.

Table III LOAD RESPONSES: TRACKING PERFORMANCE

		Overshoot (%)	**5‰ Settling Time** (ms)
Notch Filter		4.6	134
Bi-quad Filter		2.2	226
Acceleration Feedback		7.0	139
ADRC with different ω_c (Hz)	50	1.1	110
	100	0.7	104
	200	0.8	149

Table IV LOAD RESPONSES: DISTURBANCE REJECTION PERFORMANCE

		Maximum Error (rad/s)	**5‰ Settling Time** (ms)
Notch Filter		1.30	>1000
Bi-quad Filter		0.75	>1000
Acceleration Feedback		0.81	116
ADRC with different ω_c (Hz)	50	0.84	73
	100	0.38	154
	200	0.13	308

For position control, the results are similar as shown in Table V . The best performance is obtained at the medium bandwidth of 40 Hz; when bandwidth goes beyond 75 Hz the system becomes unstable. The load still has some oscillation but the amplitude is relative small. The performance of disturbance rejection is also quite good. To further reduce load oscillation, we investigate the alternative load feedback configuration below.

Table V LOAD RESPONSES OF POSITION CONTROL WITH MOTOR FEEDBACK

Controller Bandwidth (Hz)	**Overshoot** (%)	**5‰ Settling Time** (ms)
20	0.4	158
30	0.3	133
40	0.1	114
50	0.4	123
60	0.7	154

Load Control with Load Feedback

In this configuration, the output measurement, i.e. position or velocity, is taken at the load side, leading to significantly more phase lag, as shown in (5.3) and (5.4). Note that comparing to the motor feedback, there is one less zero in the transfer function and the remaining zero moves to the frequency of 7 KHz. This means that at the resonant frequency (90 Hz), there is additional 180 degree phase lag, making the control design more challenging. But it turns out that the benefits of measuring the load response directly outweigh disadvantage in the phase lag.

Applying the proposed ADRC solution to this configuration at the sampling frequency of 50 KHz, excellent performance is obtained. With ω_c set to 100 Hz and

rising time set to 50 ms, the overshoot is only 0.1%, and the settling time is 52 ms as shown in Figure 28. With load feedback the load response gets better and the oscillation migrates to the motor response. It is evident that ADRC has the ability to remove the oscillation from whichever response that is the main concern.

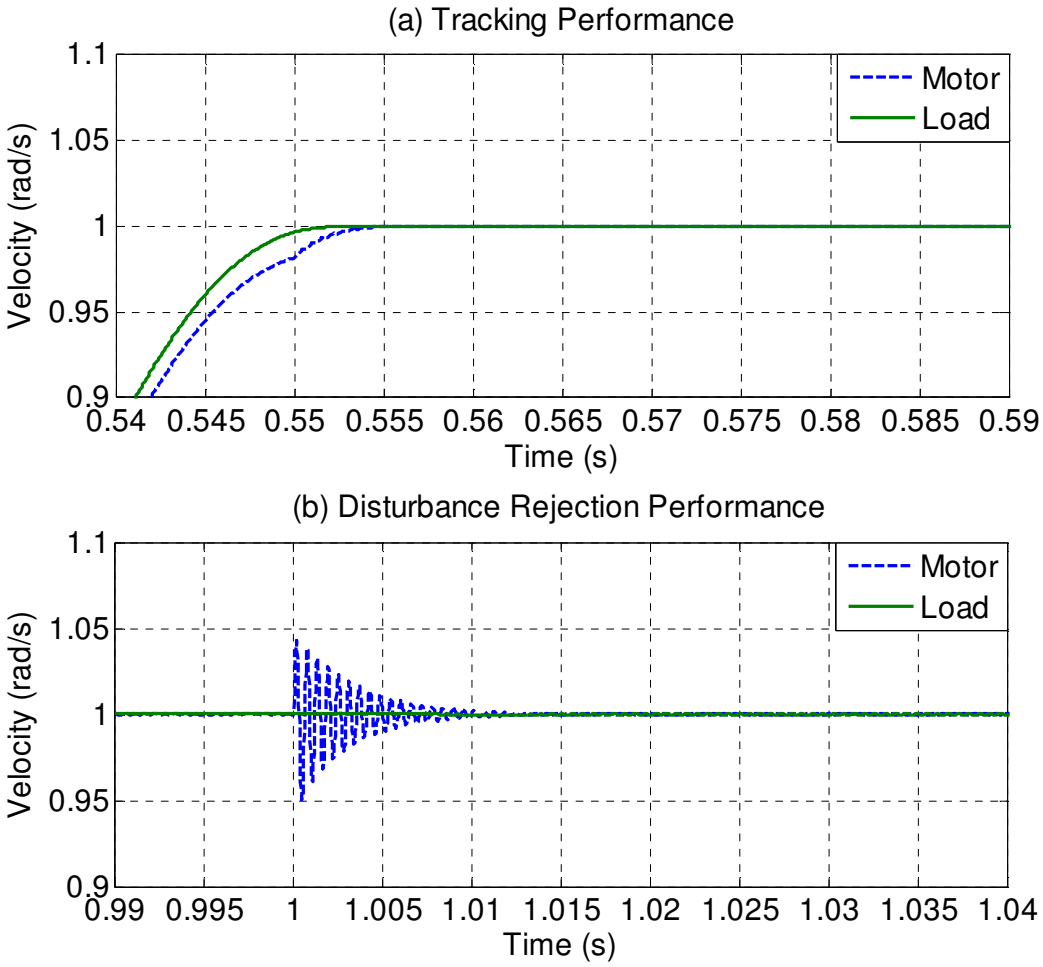

Figure 28 Motor and load responses of velocity control with load feedback.

The simulation results for the position control with load feedback are listed in Table VI . Note that the overshoot is basically nonexistent. Excellent disturbance rejection is also observed.

Table VI LOAD RESPONSES OF POSITION CONTROL WITH LOAD FEEDBACK

Controller Bandwidth (Hz)	**Overshoot** (%)	**5‰ Settling Time** (ms)
25	0.2	104
50	0.3	60
100	0.0	55

5.5 Experiment Verification

In addition to the simulation comparison with other methods, the proposed control solution to the vibration problem is also verified in hardware tests for the velocity control with motor feedback case. The experiments are conducted on the torsional apparatus Model 205 from Educational Control Products. For a fast validation, the control algorithm is implemented using the MATLAB real-time workshop. For application purpose, the implementation of the proposed algorithm can be found in [23].

5.5.1 Test Setup

The torsional apparatus Model 205 has a flexible vertical shaft connecting three disks (lower, middle and upper), with an encoder mounted on each disk for the purpose of position measurement. The lower disk is driven by a DC servo motor via the belt and pulley system with a 3 to 1 speed reduction ratio. In this experiment since we only consider the vibration in a two-inertia system, the upper disk is not used and the belt is tightened to provide a rigid connection that matches the simulation model. There are also brass weights that can be added to the middle disk to test the effect of changing the inertia of the load.

A personal computer, with MATLAB real-time workshop installed, is used to implement the proposed control algorithm. A four-channel quadrature encoder input card (PCI-QUAD04) and a multi-function analog and digital I/O card (PCI-DAS1002), both from Measurement Computing, are install in the computer to interface with the torsional apparatus. A photo of the experimental system is shown in Figure 29. A diagram is also given (see Figure 30) to clearly show the mechanical and electrical connections of the system.

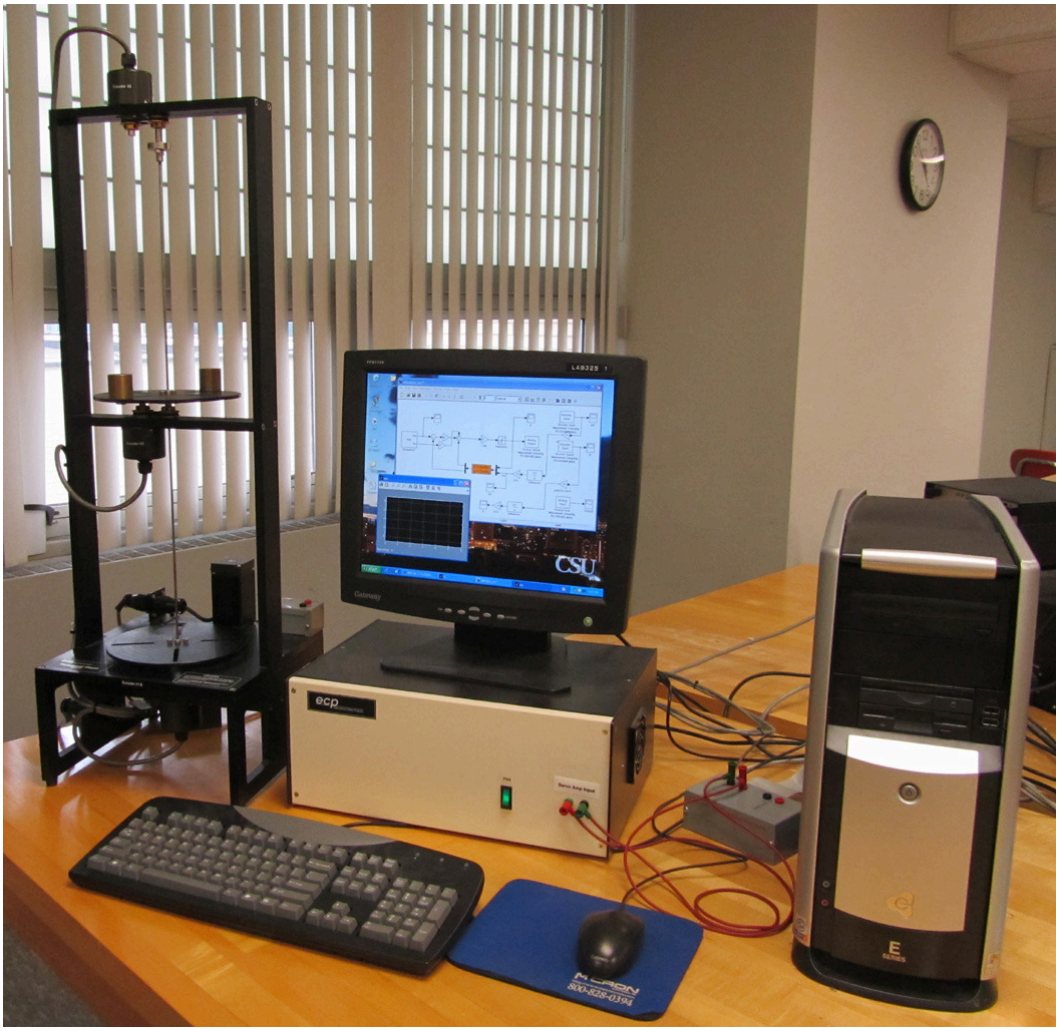

Figure 29 Photo of the test setup.

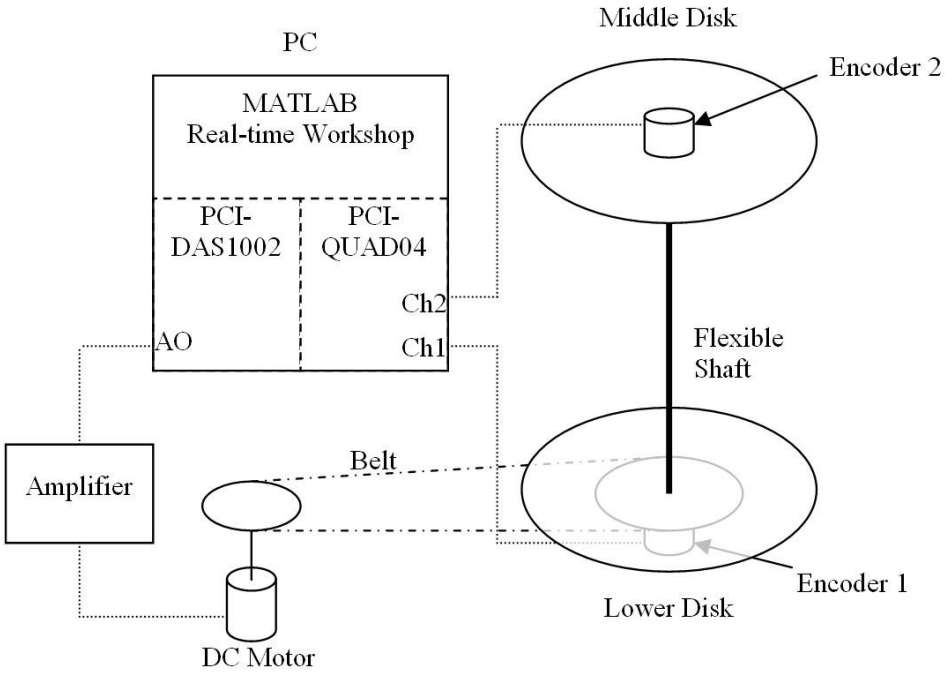

Figure 30 Diagram of the test setup.

5.5.2 System Parameters

The torque constant ($K_T = T_E / U$) of the motor is 0.058 N·m/V. The encoders generate 16000 pulses per round. Therefore the resolution for position measurement is 3.927×10^{-4} rad (6.25×10^{-5} round). The resolution for velocity measurement depends on the sampling rate, and is 0.196 rad/s (0.03125 round/s) at 500 Hz and 0.393 rad/s (0.0625 round/s) at 1 KHz, i.e. higher the sampling rate lower the resolution. To get a better resolution, a sampling rate of 500 Hz is adopted for velocity control.

To determine the parameters of the test equipment, a frequency sweep test is run by applying a chirp signal with amplitude of 2 volts to the amplifier. The frequency changes from 0.1 Hz to 15 Hz in 30 seconds. Figure 31 shows the motor velocity response. The anti-resonant frequency ω_{AR} and the resonant frequency ω_R are observed

at 37.6 rad/s (or 5.99 Hz) and 48.1 rad/s (or 7.65 Hz) respectively from the test. The peak velocity at the resonant frequency is 3.08 round/s.

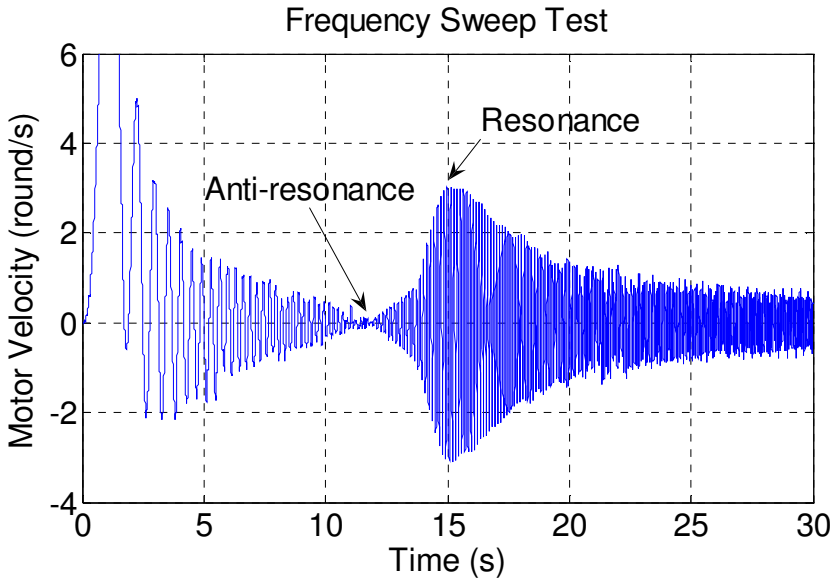

Figure 31 Motor velocity response of the frequency sweep test.

From Figure 23 we can see that at low frequency the motor response and the load response are consistent and the whole system behaves like a rigid body. Thus another test is run with a 0.3 Hz sinusoid input to determine the total inertia ($J_T = J_M + J_L$) of the system. The gain at 0.3 Hz is found to be 107.76 round/s/N/m. From (5.1) J_T is calculated to be $4.92\times10^{-3}\ \text{kg}\cdot\text{m}^2$. Together with the above frequency sweep test results, from (5.5) and (5.6), we get $J_M = 3.01\times10^{-3}\ \text{kg}\cdot\text{m}^2$, $J_L = 1.91\times10^{-3}\ \text{kg}\cdot\text{m}^2$, $J_P = 1.17\times10^{-3}\ \text{kg}\cdot\text{m}^2$, $K_S = 2.71$ N·m/rad, $b_S = 0.006$ N·m·s/rad.

According to the equipment manual the motor inertia, which includes the inertial of the DC motor, pulley and the lower disk, is around $2.65\times10^{-3}\ \text{kg}\cdot\text{m}^2$ and the load inertia is around $2.00\times10^{-3}\ \text{kg}\cdot\text{m}^2$, which matches the test results quite well.

5.5.3 Test Results

A trapezoidal profile, as mentioned in Section 5.4.1, with a magnitude of 8 round/s is used to run the tests. The rising time is chosen to be 0.5 seconds which is slower, due to a relative lower resonant frequency compared to the simulation case. The controller under test is described in Section 5.3, with the controller bandwidth set to 160 rad/s. The results are shown in Figure 32.

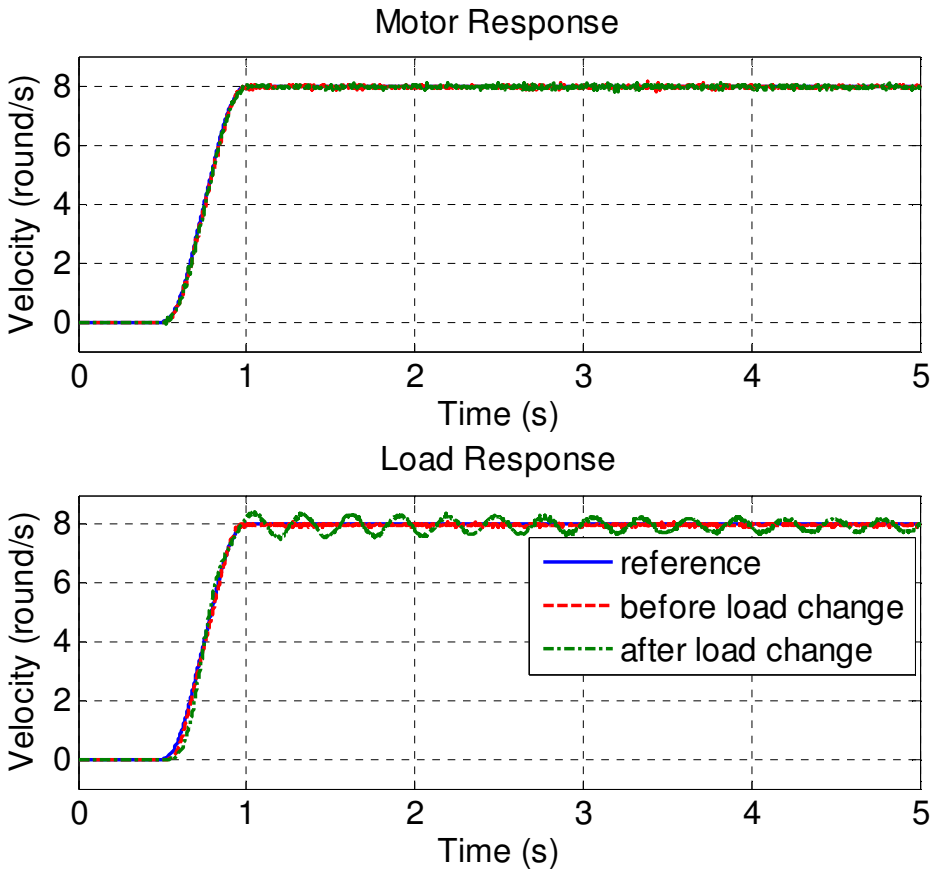

Figure 32 Velocity control hardware test results.

Both motor response and load response track the reference very well before the load change. A load with inertia of 3.29×10^{-3} $kg\cdot m^2$ is added to the middle disk, which is equivalent to 2.7 times load change, to test the robustness of the control method. The

motor velocity remains well controlled with the load change. But the load exhibits oscillations as expected, since resonant frequency is lowered with the load increase and the previous profile is a little fast compare to the new resonance. Test results show that decreasing the rising time to one second will greatly reduce the oscillations.

Based on the system model, the open loop and closed-loop transfer functions are derived using the above system and controller parameters and the Bode plots are given in Figure 33 and Figure 34. From Figure 33 the phase margin of the system is found to be 50 degrees. The closed-loop bandwidth is read from Figure 34 to be 158 rad/s, which is well beyond the resonant frequency of the system (48.1 rad/s). The resonant mode of the system is attenuated by applying the proposed ADRC design.

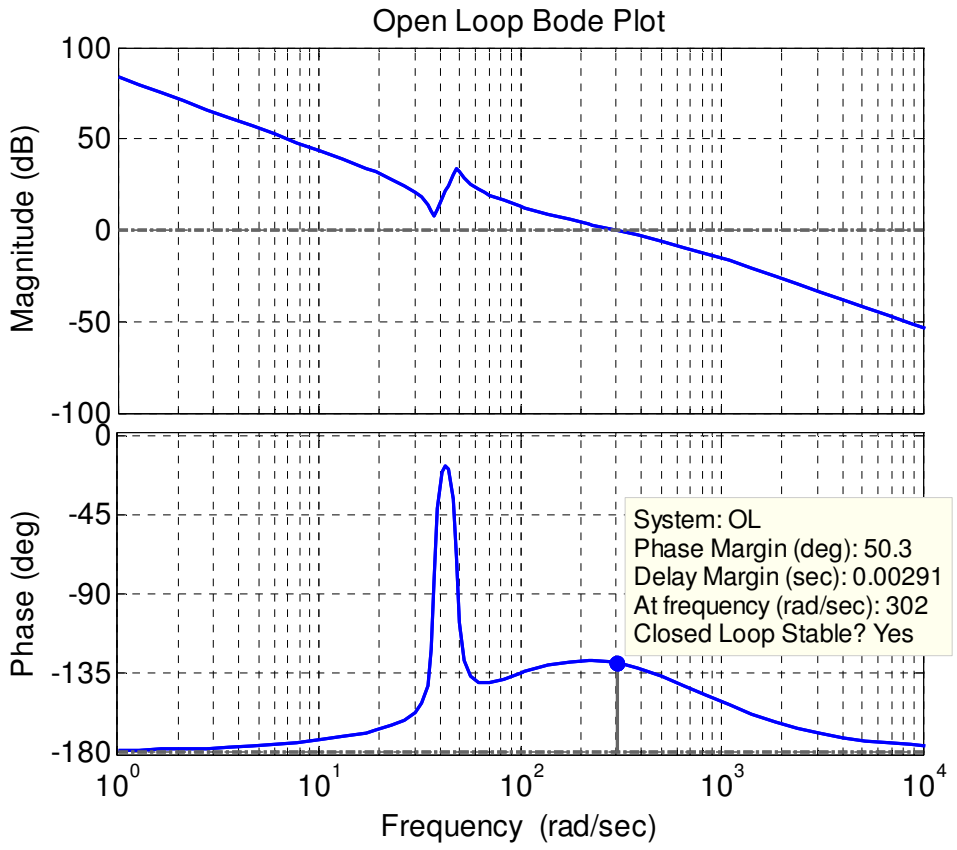

Figure 33 Open loop Bode plot for hardware test.

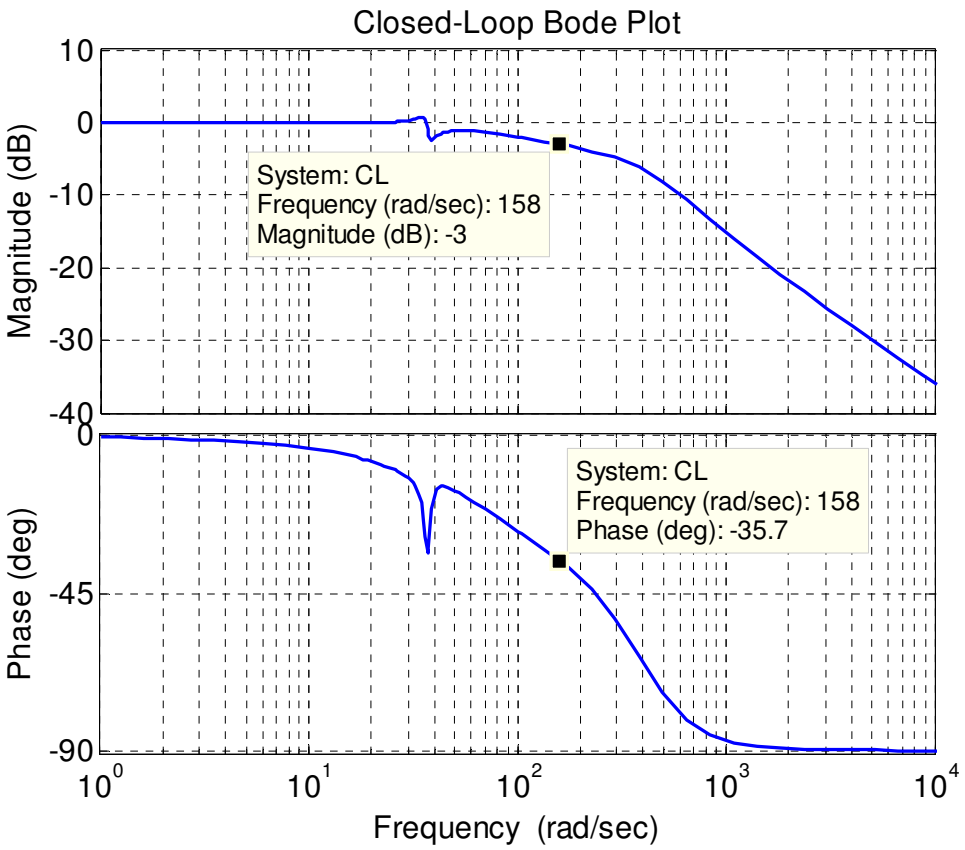

Figure 34 Closed-loop Bode plot for hardware test.

5.6 Summary

In this chapter, the vibration suppression problem is reformulated as a disturbance rejection problem. The ADRC design as an alternative solution to the problem is thoroughly studied through both simulations and experiments. The results demonstrate the method to be very effective and practical.

CHAPTER VI

CURE FOR MICROPHONICS IN SUPERCONDUCTING RADIO FREQUENCY CAVITY CONTROL[2]

Microphonics in the superconducting radio frequency (SRF) cavity control are external vibrations from the environment. In this chapter, the ADRC is applied to solve the microphonics problem in the SRF cavity application. The chapter is organized as follows. Section 6.1 introduces the background of the problem. The dynamics of the SRF cavity is described in Section 6.2, followed by a new problem formulation and the corresponding control design presented in Section 6.3. Simulation and hardware test results are provided in Section 6.4. The actuator nonlinearity problem as an extension is studied in Section 6.5. Section 6.6 summarizes the chapter.

[2] This work was supported in part by the National Science Foundation under Grant no. PHY-06-06007. It has been published in an Elsevier journal [96]. The author retains the right to include it in the dissertation.

6.1 Background

The National Superconducting Cyclotron Laboratory (NSCL) is currently constructing a 3 MeV/u re-accelerator (ReA3), expandable to 12 MeV/u, using SRF cavities [90]. The project is cooperatively funded by Michigan State University (MSU) and the National Science Foundation (NSF). In addition, MSU has been selected to build the Facility for Rare Isotope Beams (FRIB) national user facility that features a 400 kW, 200 MeV/u SRF linear accelerator (LINAC) requiring over 340 SRF cavities [91]. FRIB is funded through a cooperative agreement between MSU and the Office of Nuclear Physics in the Department of Energy (DOE) Office of Science. Maximizing the performance and decreasing the overall costs of these systems is an ongoing goal of both projects.

Figure 35 NSCL facility at MSU[3].

The control of lightly loaded SRF cavities is an ongoing topic in the accelerator community due to the extreme sensitivity of these cavities to disturbances and other

[3] ©Copyright by Michigan State University. Reprinted with permission.

detuning forces. A dominant method applied is to over-couple these cavities thereby reducing the sensitivity by increasing the bandwidth and applying standard PID controls [92]. Advanced control algorithms are sought that can minimize the required drive power and improve the overall performance of these systems.

Figure 36 A 7-cell SRF cavity under test at NSCL[4].

In accelerator applications, the cavity voltage must be precisely controlled in the presence of vibrations referred to as "microphonics". The problem is acute here at NSCL since the ReA3 accelerator has been mounted on a balcony, making it even more susceptible to microphonics disturbances from the environment. The previously explored adaptive feedforward cancellation method [93] is found to be not sufficient in this case. Thus the motivation to explore more effective disturbance rejection technology beyond a standard PID leads to our ADRC solution.

The nature of many, if not most, control problems is disturbance rejection, particularly the microphonics problem discussed here, and the key question in design is

[4] ©Copyright by Michigan State University. Reprinted with permission.

how to deal with it. The PID control strategy, by default, deals with the disturbances in a passive way as it merely reacts to the tracking errors caused by the disturbances. An alternative, and better, solution is to reject the disturbances actively by estimating the disturbances directly and cancelling it out, before it affect the system in a significant way, and this is at the core of ADRC.

6.2 Dynamics of the SRF cavity

The cavity dynamics can be represented by a parallel RLC circuit [94] as shown in Figure 37, where $\vec{V}_c$ is the cavity voltage and $\vec{I}_g$ is the generator current.

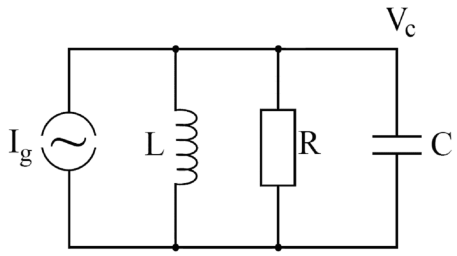

Figure 37 Equivalent circuit model for the SRF cavity dynamics.

According to Kirchhoff's law, the following second order differential equation holds.

$$\frac{d^2\vec{V}_c}{dt^2}+\frac{\omega_0}{Q}\frac{d\vec{V}_c}{dt}+\omega_0^2\vec{V}_c=\frac{R\omega_0}{Q}\frac{d\vec{I}_g}{dt} \tag{6.1}$$

where $\omega_0=1/\sqrt{LC}$ is the cavity resonant frequency and $Q=R\sqrt{C/L}$ is the quality factor.

For a fixed frequency radio frequency (RF) system, transforming the cavity voltage and the driving current to a reference frame that rotates at the generator frequency ω_g can greatly simplify the calculation [95]. The transformations are given below.

$$\vec{V}_c(t) = \left[V_{cI}(t) + jV_{cQ}(t) \right] e^{j\omega_g t} \tag{6.2}$$

$$\vec{I}_g(t) = \left[I_{gI}(t) + jI_{gQ}(t) \right] e^{j\omega_g t} \tag{6.3}$$

where V_{cI} and I_{gI} are in-phase components; V_{cQ} and I_{gQ} are quadrature components.

The amplitude of the cavity voltage and generator current are slowly changing compared to the RF component, thus $\dot{V}_c << \omega_g V_c$ and $\dot{I}_g << \omega_g I_g$. Together with $\omega_0 \approx \omega_g$ and $1/2Q << 1$, (6.1) can be simplified to the following two first order differential equations.

$$\dot{V}_{cI} + \omega_{1/2} V_{cI} + \Delta\omega V_{cQ} = \omega_{1/2} V_{gI} \tag{6.4}$$

$$\dot{V}_{cQ} + \omega_{1/2} V_{cQ} - \Delta\omega V_{cI} = \omega_{1/2} V_{gQ} \tag{6.5}$$

where $\omega_{1/2} = \omega_0 / 2Q$ is the cavity half bandwidth; $\Delta\omega = \omega_0 - \omega_g$ is the cavity detuning frequency; $V_{gI} = I_{gI} R$ and $V_{gQ} = I_{gQ} R$.

Note that the quadrature components in (6.4) and the in-phase components in (6.5) represent the coupling between the two channels which is ignored in the existing PID design. This microphonics induced coupling is what makes the control design challenging for the SRF cavities.

6.3 The Total Disturbance Rejection Formulation

The key problem in SRF cavity control is to maintain the constant amplitude and phase in V_c, which is a very challenging task as the resonant frequency ω_0 changes due to Lorenz force and microphonics. Here the microphonics are part of external disturbances, denoted as d and the Lorenz force is field induced within the cavities and

is a function of the system variable V_c. Therefore, the controller must mitigate both the external disturbances and internal dynamics. Since the cavity resonant frequency $\omega_0(d,V_c)$ is actually a function of both the external disturbance (primarily microphonics) and the cavity voltage, a more realistic model of the cavity is

$$\dot{V}_{cI} + \omega_{1/2} V_{cI} + \Delta\omega(d,V_c) V_{cQ} = \omega_{1/2} V_{gI} \tag{6.6}$$

$$\dot{V}_{cQ} + \omega_{1/2} V_{cQ} - \Delta\omega(d,V_c) V_{cI} = \omega_{1/2} V_{gQ} \tag{6.7}$$

For such a nonlinear, time-varying and coupled system (6.6)-(6.7), the control design using regular methods could be very complicated. In the ADRC framework, however, all the nonlinear, time-varying and coupling terms are parts of the total disturbance to be estimated and mitigated greatly simplifying the design task.

Considering the realistic model (6.6) and defining the output as $y = V_{cI}$, input as $u = V_{gI}$ and the total disturbance as $f = -\omega_{1/2} V_{cI} - \Delta\omega(d,V_c) V_{cQ}$, the dynamics of the in-phase (I) component can be reformulated as

$$\dot{y} = bu + f \tag{6.8}$$

where $b = \omega_{1/2}$. Similarly, for the quadrature (Q) component, (6.7) can also be rewritten as (6.8) by defining $y = V_{cQ}$, $u = V_{gQ}$ and $f = -\omega_{1/2} V_{cQ} + \Delta\omega(d,V_c) V_{cI}$. Since no zero and time delay exist in both loops, the standard first order ADRC design described in Section 2.4 is adopted.

As shown above, the cavity dynamics can be clearly described by the IQ model. However, in the real operation environment, the set-point for the electric field is normally given in terms of amplitude and phase. The relationship between the IQ components and amplitude/phase is merely an algebraic coordinate transformation, from Cartesian to

polar. For the sake of convenience and without loss of generality, the proposed ADRC solution is implemented to control the amplitude and phase directly instead of the IQ components, as the transformation does not affect the cavity dynamics. However, a difficulty that is referred to as the "wrap-around" problem exists in the phase control, since the phase can jump between -180 degrees and 180 degrees. The problem is addressed in more detail in Section 6.5.

6.4 Simulation and Test Results

A MATLAB simulation model is built to test the control design as shown in Figure 38. The cavity half bandwidth is 219 rad/s (35 Hz). The sampling rate is 54.6 kHz; the ADRC parameters are chosen as: $\hat{b} = 219$, $\omega_c = 600$ rad/s and $\alpha = 5$. For comparison, a PI controller is tuned with a proportional gain of 3 and an integral gain of 5474. The parameters were tuned to achieve the best stable response. The same values were used for simulations and measurements.

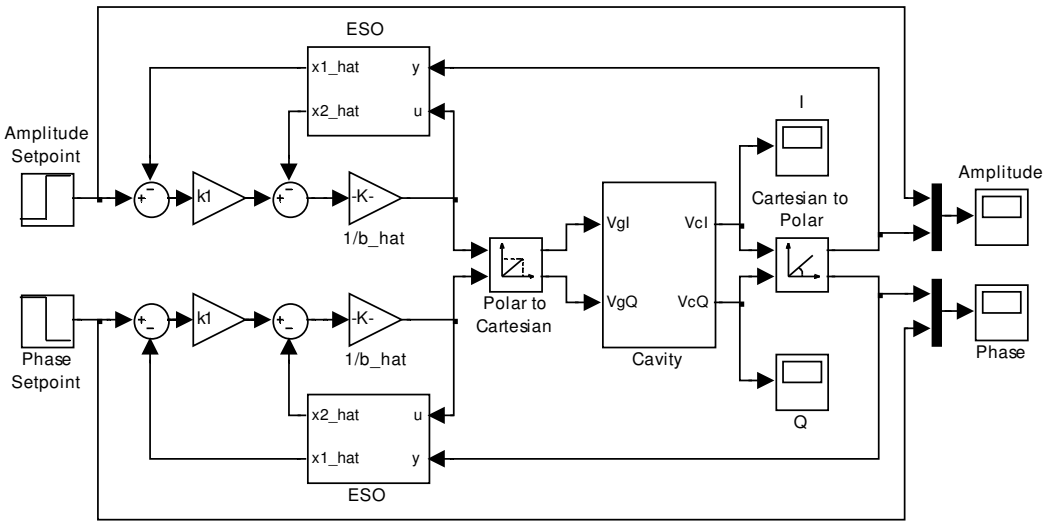

Figure 38 SRF cavity simulation model with ADRC control.

The RF control is implemented on a digital low-level RF (LLRF) controller developed at the NSCL. The controller produces a LLRF output at the cavity drive frequency and directly controls the phase and amplitude of the output. This LLRF signal is fed into a solid-state linear amplifier and the output of the amplifier is coupled to the cavity. The cavity used for the tests is a SRF quarter wave resonator with a loaded bandwidth of 70 Hz (438 rad/s). This particular cavity is especially susceptible to microphonics because its mechanical damper does not work as well as anticipated. During tests, intermittent microphonics was present that detuned the cavity by more than 40 Hz. The discrete implementation of the ADRC control algorithm can be found in [23].

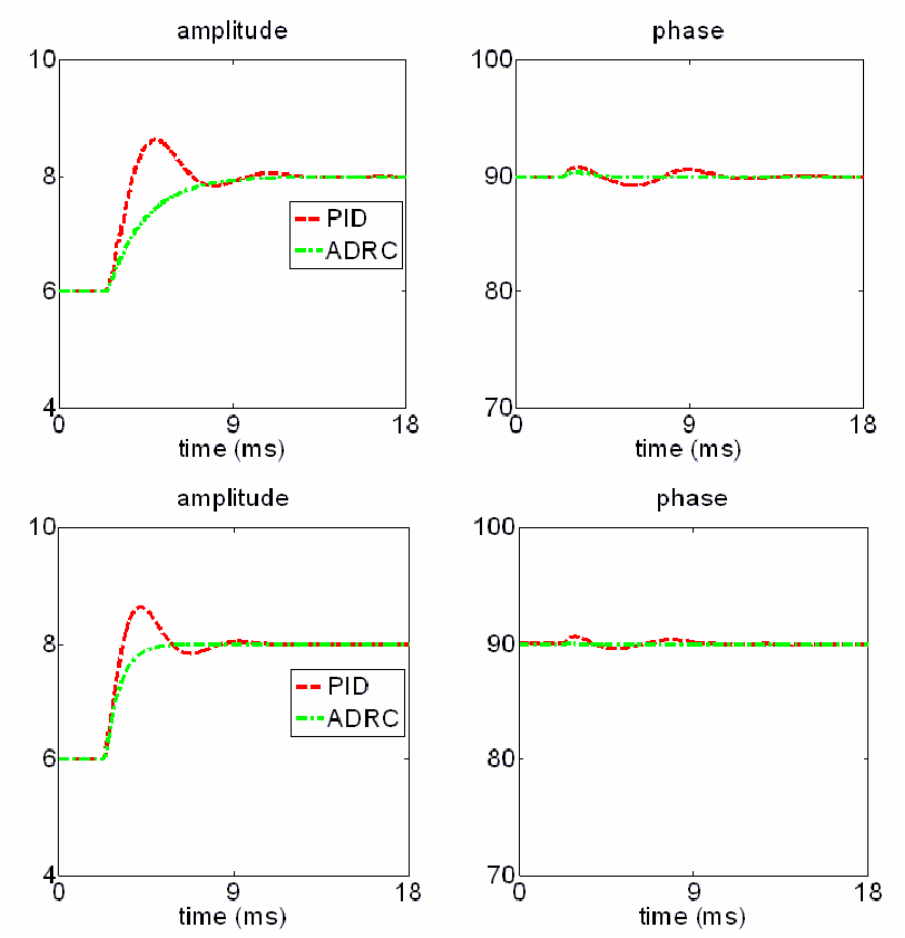

Figure 39 Cavity amplitude step response - Simulation (top) vs. Measured (bottom).

Step signals were introduced as the references for both amplitude and phase components. For the simulations, a constant detuning frequency of 40 rad/s was used. The simulated and measured response curves for a step in amplitude (from 6MV/m to 8MV/m) are shown in Figure 39. The response curves for a step in phase (from 75° to 90°) are shown in Figure 40. With the ADRC controller, the coupling between the amplitude and phase loops is greatly reduced, and the overshoot in both loops while tracking a set-point change is eliminated.

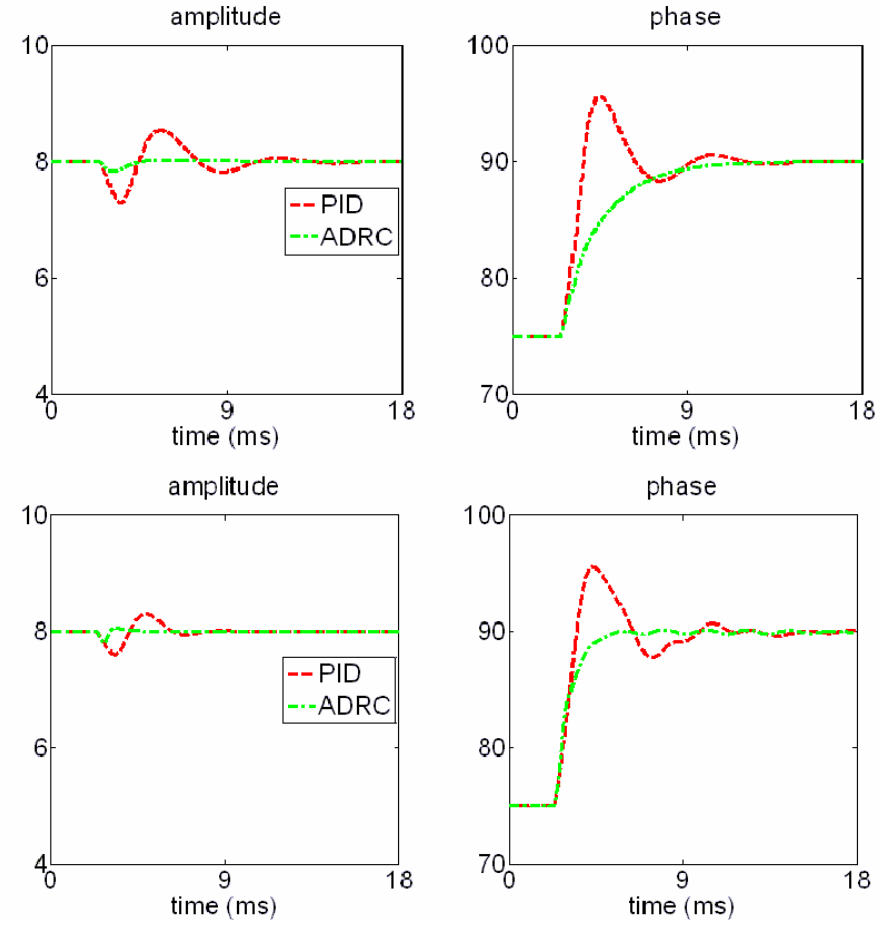

Figure 40 Cavity phase step response - Simulation (top) vs. Measured (bottom).

The steady state probability density functions for amplitude and phase are shown in Figure 41. The steady state model includes a Gaussian detuning frequency which was varied in order to match the measured data. Two times of performance improvement in simulation and four times of performance improvement in hardware test are observed.

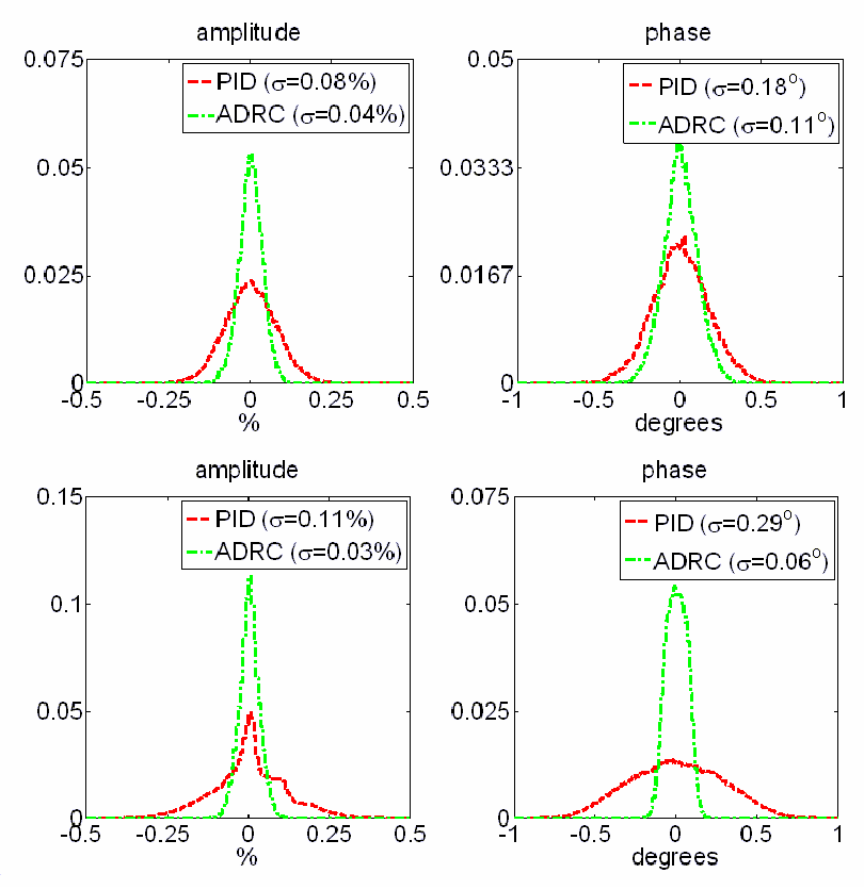

Figure 41 Steady state probability density function - Simulation (top) vs. Measured (bottom).

6.5 Actuator nonlinearities

As mentioned in Section 6.3, there is a wrap-around problem associated with the phase loop. In fact, it can be treated as a type of actuator nonlinearity, similar to the

saturation effect. Other types of actuator nonlinearity includes dead-zone, backlash and hysteresis. A previous study [24] suggests that taking the signal after the saturation and sending it back to ESO will improve the performance. It is not true, however, for the wrap-around effect in this application. Ignoring the wrap-around effect totally and using the disturbance rejection ability of ADRC to handle it is found to be the solution, which has been documented in [96]. This leads us to the investigation of the ADRC's ability to handle actuator nonlinearities. The general analysis is provided below.

The main idea is that a nonlinear actuator can be represented by a linear one plus the difference between the two and the difference can be treated as a disturbance to be estimated and rejected in the ADRC framework. In particular, suppose that the controller outputs a control signal u to the actuator. Due to the nonlinear effect of the actuator, the effective control that acts on the system dynamic becomes $F(u)$, where $F(\cdot)$ is an unknown nonlinear function whose specific form depends on the actuator. If system (2.1) has a nonlinear actuator, ignoring the input disturbance w, (2.1) becomes

$$y^{(n)} + a_{n-1}y^{(n-1)} + \cdots + a_1\dot{y} + a_0 y = bF(u) \tag{6.9}$$

From the ADRC design point of view, (6.9) can still be rewritten as (2.2) with $f = bF(u) - bu - \sum_{i=0}^{n-1} a_i y^{(i)}$. In other words, the difference between the nonlinear actuator represented as $bF(u)$ and its linear counterpart bu is treated as a disturbance to be rejected. Note that in most cases $bF(u) - bu$ will be bounded and previous analysis has shown the convergence of ESO under the condition that f is bounded. In addition, experimental results have shown that such disturbance can be readily estimated and cancelled, forcing the actuator to behave like a linear one [97].

It is worthwhile to notice that the specific form of $F(\cdot)$ as well as its parameters are assumed unknown, and they do not affect the problem formulation, i.e. the ADRC design shares the same solution for different types of actuator nonlinearities.

6.6 Summary

The main contributions of this chapter are: 1) provided a cost effective solution to the microphonics problem for NSCL; 2) provided a general analysis for ADRC when dealing with actuator nonlinearities. The ADRC solution proposed in this chapter has been applied to control the SRF cavities at NSCL since January, 2011. Similar performance improvement as shown in the test has been reported. As the FRIB project moves forward hundreds more SRF cavities will be installed in the near future.

CHAPTER VII

CONCLUSION AND FUTURE WORK

7.1 Conclusion

In this dissertation, we investigated the generally challenging control design for two kinds of NMP systems, namely systems with RHP zeros and systems with time delay, which has not been well addressed under the DRP, especially in the frame work of ADRC. The results of the investigation show that with appropriate modifications made to the existing ADRC design both problems can be solved effectively and enhanced performance is obtained. For the control of systems with RHP zeros, the tracking performance obtained merely by applying ADRC is still limited due to the complexity of the problems. Hence we resort to feedforward design to improve the tracking performance further. A unique feedforward design with practical undershoot constraint

consideration is accomplished. For the control of systems with time delay, the stability analysis for the modified ADRC also fills in a blank on theoretical analysis of ADRC.

The two specific industrial applications, the vibration suppression in motion control and the microphonics control in SRF cavities, show that ADRC is capable of handling vibrations caused both internally and externally, demonstrating again the benefit of the DRP. Through thorough simulation study and experimental verification, the ADRC solution as an alternative to existing solutions is demonstrated to be superior, not only because of the performance improvement but also the simple and easy implementation. As an extension to the SRF cavity control problem, the analysis shows that ADRC can deal with unknown actuator nonlinearities despite of type of the nonlinearity.

7.2 Future Work

Though a lot has been accomplished in this dissertation, there are still unsolved problems or other possible topics to work on. In Chapter 3, a hypothesis on the synthesis of the minimum settling time control signal subject to undershoot constraint for the general m RHP zeros case is raised. The mathematical proof of it will be very meaningful. The systematic ADRC design for systems with RHP zeros can be explored further as well.

The problem studied in Chapter 4 is restricted to the constant time delay case. The ability of ADRC applied to systems with uncertainty in the time delay or with time varying delay needs to be tested and can be a future research topic. Also the relay tuning [98] based auto-tuning function can be added to the ADRC function blocks developed, making it readily available for industrial applications.

Since the systems with RHP zeros is closely related to the systems with time delay, the methods proposed for one can be tested to see if it applies to the other. This cross validation is interesting and could be a research topic as well.

Other problems such as the transfer function based decoupling analysis for coupled systems, the online estimation of $\hat{b}$ using adaptive control techniques are all very interesting topics.

REFERENCES

[1] F. L. Lewis, *Applied optimal control & estimation : digital design & implementation*. Englewood Cliffs, N.J.: Prentice Hall, 1992.

[2] R. C. Dorf and R. H. Bishop, *Modern control systems*, 11th ed. Upper Saddle River, NJ: Pearson/Prentice Hall, 2008.

[3] S. Bennett. (1984) Nicholas Minorsky and the automatic steering of ships. *Control Systems Magazine, IEEE*. 10-15.

[4] Z. Gao, Y. Huang, and J. Han, "An alternative paradigm for control system design," in *Decision and Control, Proceedings of the 40th IEEE Conference on*, 2001, pp. 4578-4585.

[5] Z. Gao, "Active disturbance rejection control: a paradigm shift in feedback control system design," in *American Control Conference*, 2006, pp. 2399-2405.

[6] Z. Gao, "On disturbance rejection paradigm in control engineering," in *29th Chinese Control Conference*, Beijing, China, 2010, pp. 6071-6076 (in Chinese).

[7] K. J. Åström and T. Hägglund, *PID Controllers: Theory, Design and Tuning*, 2nd ed. Research Triangle Park, NC: Instrument Society of America, 1995.

[8] C. Johnson, "Accomodation of external disturbances in linear regulator and servomechanism problems," *Automatic Control, IEEE Transactions on,* vol. 16, pp. 635-644, 1971.

[9] G. H. Hostetter and J. S. Meditch, "On the generalization of observers to systems with unmeasurable, unknown inputs," *Automatica,* vol. 9, pp. 721-724, 1973.

[10] T. Umeno and Y. Hori, "Robust speed control of DC servomotors using modern two degrees-of-freedom controller design," *Industrial Electronics, IEEE Transactions on,* vol. 38, pp. 363-368, 1991.

[11] E. Schrijver and J. van Dijk, "Disturbance Observers for Rigid Mechanical Systems: Equivalence, Stability, and Design," *Journal of Dynamic Systems, Measurement, and Control,* vol. 124, pp. 539-548, 2002.

[12] J. Han, "A class of extended state observers for uncertain systems," *Control and Decision,* vol. 10, pp. 85-88, 1995 (in Chinese).

[13] S. Kwon and W. K. Chung, "Robust performance of the multiloop perturbation compensator," *Mechatronics, IEEE/ASME Transactions on,* vol. 7, pp. 190-200, 2002.

[14] S. Kwon and W. K. Chung, "A discrete-time design and analysis of perturbation observer for motion control applications," *Control Systems Technology, IEEE Transactions on,* vol. 11, pp. 399-407, 2003.

[15] X. Liu, *History of Chinese Mechanical Engineering Inventions*. Beijing: Science Press, 1962 (in Chinese).

[16] J. Needham, *Science and Civilization in China: Volume 4, Part 2.* Taipei: Caves Book Ltd., 1986.

[17] S. Bennett, *A history of control engineering, 1800-1930*. Stevenage ; New York: Peregrinus for the Institution of Electrical Engineers, 1979.

[18] L. Finkelstein, "The theory of invariance," *Control,* pp. 96-98, 1960.

[19] J. Han, "Active disturbance rejection controller and its applications," *Control and Decision,* vol. 13, pp. 19-23, 1998 (in Chinese).

[20] J. Han, *Active disturbance rejection control technique: the technique for estimating and compensating the uncertainties*, 1st ed. Beijing: National Defense Industry Press, 2008 (in Chinese).

[21] Z. Gao, "Scaling and bandwidth-parameterization based controller tuning," in *American Control Conference*, New York, 2003, pp. 4989-4996.

[22] G. F. Franklin, J. D. Powell, and M. L. Workman, *Digital control of dynamic systems*, 3rd ed. Menlo Park, Calif.: Addison Wesley, 1998.

[23] R. Miklosovic, A. Radke, and Z. Gao, "Discrete implementation and generalization of the extended state observer," in *American Control Conference*, 2006, p. 6 pp.

[24] A. Radke, "On disturbance estimation and its applications in health monitoring," Dissertation, Cleveland State University, 2006.

[25] G. Tian, "Reduced-order extended state observer and frequency response analysis," Thesis, Cleveland State University, 2007.

[26] Q. Zheng, Z. Chen, and Z. Gao, "A practical approach to disturbance decoupling control," *Control Engineering Practice,* vol. 17, pp. 1016-1025, 2009.

[27] J. Csank and Z. Gao, "Uncertainty reduction through Active Disturbance Rejection," in *American Control Conference*, 2008, pp. 3689-3694.

[28] Y. Hou, Z. Gao, F. Jiang, and B. T. Boulter, "Active disturbance rejection control for web tension regulation," in *Decision and Control, Proceedings of the 40th IEEE Conference on*, 2001, pp. 4974-4979 vol.5.

[29] W. Zhou and Z. Gao, "An Active Disturbance Rejection Approach to Tension and Velocity Regulations in Web Processing Lines," in *Control Applications, IEEE International Conference on*, 2007, pp. 842-848.

[30] B. Sun and Z. Gao, "A DSP-based active disturbance rejection control design for a 1-kW H-bridge DC-DC power converter," *Industrial Electronics, IEEE Transactions on,* vol. 52, pp. 1271-1277, 2005.

[31] F. J. Goforth and Z. Gao, "An Active Disturbance Rejection Control solution for hysteresis compensation," in *American Control Conference*, 2008, pp. 2202-2208.

[32] F. J. Goforth, Q. Zheng, and Z. Gao, "A novel practical control approach for rate independent hysteretic systems," *ISA Transactions,* to be published, available online at http://www.sciencedirect.com/science/article/pii/S0019057812000079.

[33] Q. Zheng, L. Dong, D. H. Lee, and Z. Gao, "Active Disturbance Rejection Control for MEMS Gyroscopes," *Control Systems Technology, IEEE Transactions on,* vol. 17, pp. 1432-1438, 2009.

[34] Y. Xia, P. Shi, G. P. Liu, D. Rees, and J. Han, "Active disturbance rejection control for uncertain multivariable systems with time-delay," *IET Control Theory & Applications,* vol. 1, pp. 75-81, 2007.

[35] G. Tian and Z. Gao, "Frequency response analysis of active disturbance rejection based control system," in *Control Applications, Proceedings of IEEE Conference on*, 2007, pp. 739-743.

[36] Q. Zheng, L. Q. Gao, and Z. Gao, "On stability analysis of active disturbance rejection control for nonlinear time-varying plants with unknown dynamics," in *Decision and Control, 46th IEEE Conference on*, 2007, pp. 3501-3506.

[37] Q. Zheng, L. Q. Gao, and Z. Gao, "On Validation of Extended State Observer Through Analysis and Experimentation," *Journal of Dynamic Systems, Measurement, and Control,* vol. 134, pp. 024505-6, 2012.

[38] X. Yang and Y. Huang, "Capabilities of extended state observer for estimating uncertainties," in *American Control Conference*, 2009, pp. 3700-3705.

[39] L. B. Freidovich and H. K. Khalil, "Performance Recovery of Feedback-Linearization-Based Designs," *Automatic Control, IEEE Transactions on,* vol. 53, pp. 2324-2334, 2008.

[40] W. Zhou, S. Shao, and Z. Gao, "A stability study of the active disturbance rejection control problem by a singular perturbation approach," *Applied Mathematical Sciences,* vol. 3, pp. 491-508, 2009.

[41] G. Tian and Z. Gao, "From Poncelet's invariance principle to Active Disturbance Rejection," in *American Control Conference*, 2009, pp. 2451-2457.

[42] C. Zhao, "Capability of ADRC for minimum-phase plants with unknown orders and uncertain relative degrees," in *29th Chinese Control Conference*, 2010, pp. 6121-6126.

[43] B. Guo and Z. Zhao, "On the convergence of an extended state observer for nonlinear systems with uncertainty," *Systems & Control Letters,* vol. 60, pp. 420-430, 2011.

[44] Y. Huang and W. Xue, "Active Disturbance Rejection Control: Methodology and Theoretical Analysis," *Journal of Systems Science and Mathematical Sciences,* vol. 31, pp. 1111-1129, 2011 (in Chinese).

[45] J. B. Hoagg, J. Chandrasekar, and D. S. Bernstein, "On the Zeros, Initial Undershoot, and Relative Degree of Collinear Lumped-Parameter Structures," *Journal of Dynamic Systems, Measurement, and Control,* vol. 129, pp. 493-502, 2007.

[46] J. B. Hoagg and D. S. Bernstein. (2007) Nonminimum-phase zeros - much to do about nothing - classical control - revisited part II. *Control Systems Magazine, IEEE*. 45-57.

[47] S. Skogestad and I. Postlethwaite, *Multivariable feedback control : analysis and design*. Chichester ; New York: Wiley, 1996.

[48] K. J. Åström, P. Hagander, and J. Sternby, "Zeros of sampled systems," *Automatica,* vol. 20, pp. 31-38, 1984.

[49] T. Mita and H. Yoshida, "Undershooting phenomenon and its control in linear multivariable servomechanisms," *Automatic Control, IEEE Transactions on,* vol. 26, pp. 402-407, 1981.

[50] M. Vidyasagar, "On undershoot and nonminimum phase zeros," *Automatic Control, IEEE Transactions on,* vol. 31, pp. 440-440, 1986.

[51] B. A. Leon de la Barra S, "On undershoot in SISO systems," *Automatic Control, IEEE Transactions on,* vol. 39, pp. 578-581, 1994.

[52] B. L. De La Barra, M. El-Khoury, and M. Fernández, "On undershoot in scalar discrete-time systems," *Automatica,* vol. 32, pp. 255-259, 1996.

[53] K. Lau, R. H. Middleton, and J. H. Braslavsky, "Undershoot and settling time tradeoffs for nonminimum phase systems," *Automatic Control, IEEE Transactions on,* vol. 48, pp. 1389-1393, 2003.

[54] D. P. Looze and J. S. Freudenberg, "Limitations of feedback properties imposed by open-loop right half plane poles," *Automatic Control, IEEE Transactions on,* vol. 36, pp. 736-739, 1991.

[55] L. Qiu and E. J. Davison, "Performance limitations of non-minimum phase systems in the servomechanism problem," *Automatica,* vol. 29, pp. 337-349, 1993.

[56] B. P. Rigney, L. Y. Pao, and D. A. Lawrence, "Nonminimum Phase Dynamic Inversion for Settle Time Applications," *Control Systems Technology, IEEE Transactions on,* vol. 17, pp. 989-1005, 2009.

[57] M. Tomizuka, "Zero Phase Error Tracking Algorithm for Digital Control," *Journal of Dynamic Systems, Measurement, and Control,* vol. 109, pp. 65-68, 1987.

[58] S. Devasia, C. Degang, and B. Paden, "Nonlinear inversion-based output tracking," *Automatic Control, IEEE Transactions on,* vol. 41, pp. 930-942, 1996.

[59] A. Piazzi and A. Visioli, "Minimum-time system-inversion-based motion planning for residual vibration reduction," *Mechatronics, IEEE/ASME Transactions on,* vol. 5, pp. 12-22, 2000.

[60] J. T. Wen and B. Potsaid, "An experimental study of a high performance motion control system," in *American Control Conference*, 2004, pp. 5158-5163.

[61] R. H. Middleton, "Trade-offs in linear control system design," *Automatica,* vol. 27, pp. 281-292, 1991.

[62] D. E. Kirk, *Optimal control theory : an introduction*. Mineola, NY: Dover Publications, 2004.

[63] D. V. Widder, "The Inversion of the Laplace Integral and the Related Moment Problem," *Transactions of the American Mathematical Society,* vol. 36, pp. 107-200, 1934.

[64] Y. Zhang, "Load Frequency Control of Multiple-Area Power Systems," Thesis, Cleveland State University, 2009.

[65] D. E. Seborg, T. F. Edgar, and D. A. Mellichamp, *Process dynamics and control*, 2nd ed. Hoboken, NJ: Wiley, 2004.

[66] O. J. M. Smith, "A controller to overcome dead time," *ISA Journal,* vol. 6, pp. 28-33, 1959.

[67] J. E. Normey-Rico and E. F. Camacho, "Dead-time compensators: A survey," *Control Engineering Practice,* vol. 16, pp. 407-428, 2008.

[68] K. J. Astrom, C. C. Hang, and B. C. Lim, "A new Smith predictor for controlling a process with an integrator and long dead-time," *Automatic Control, IEEE Transactions on,* vol. 39, pp. 343-345, 1994.

[69] M. R. Matausek and A. D. Micic, "A modified Smith predictor for controlling a process with an integrator and long dead-time," *Automatic Control, IEEE Transactions on,* vol. 41, pp. 1199-1203, 1996.

[70] J. E. Normey-Rico and E. F. Camacho, "Robust tuning of dead-time compensators for processes with an integrator and long dead-time," *Automatic Control, IEEE Transactions on,* vol. 44, pp. 1597-1603, 1999.

[71] M. R. Stojic, F. S. Matijevic, and L. S. Draganovic, "A robust Smith predictor modified by internal models for integrating process with dead time," *Automatic Control, IEEE Transactions on,* vol. 46, pp. 1293-1298, 2001.

[72] Q. C. Zhong and L. Mirkin, "Control of integral processes with dead-time. 2. Quantitative analysis," *Control Theory and Applications, IEE Proceedings,* vol. 149, pp. 291-296, 2002.

[73] Q. C. Zhong and J. E. Normey-Rico, "Control of integral processes with dead-time. 1. Disturbance observer-based 2 DOF control scheme," *Control Theory and Applications, IEE Proceedings,* vol. 149, pp. 285-290, 2002.

[74] Q. C. Zhong, "Control of integral processes with dead time.3. Deadbeat disturbance response," *Automatic Control, IEEE Transactions on,* vol. 48, pp. 153-159, 2003.

[75] B. Wang, D. Rees, and Q. C. Zhong, "Control of integral processes with dead time. Part IV: various issues about PI controllers," *Control Theory and Applications, IEE Proceedings,* vol. 153, pp. 302-306, 2006.

[76] W. Tan, F. Fang, L. Tian, C. Fu, and J. Liu, "Linear control of a boiler–turbine unit: Analysis and design," *ISA Transactions,* vol. 47, pp. 189-197, 2008.

[77] R. K. Wood and M. W. Berry, "Terminal composition control of a binary distillation column," *Chemical Engineering Science,* vol. 28, pp. 1707-1717, 1973.

[78] Y. Xia, M. Fu, and S. Peng, *Analysis and Synthesis of Dynamical Systems with Time-Delays*. Berlin, Heidelberg: Springer-Verlag, 2009.

[79] K. Gu, V. Kharitonov, and J. Chen, *Stability of time-delay systems*. Boston Mass.: Birkhäuser, 2003.

[80] F. Zhang, *The Schur complement and its applications*. New York: Springer Science, 2005.

[81] C. F. Beards, *Vibration analysis and control system dynamics*. New York: Halsted Press, 1981.

[82] G. Ellis, *Control system design guide : a practical guide*, 3rd ed. Amsterdam ; Boston: Elsevier Academic Press, 2004.

[83] P. Schmidt and T. Rehm, "Notch filter tuning for resonant frequency reduction in dual inertia systems," in *Industry Applications Conference*, 1999, pp. 1730-1734.

[84] G. Ellis and R. D. Lorenz, "Resonant load control methods for industrial servo drives," in *Industry Applications Conference*, 2000, pp. 1438-1445.

[85] G. Ellis and Z. Gao, "Cures for low-frequency mechanical resonance in industrial servo systems," in *Industry Applications Conference*, 2001, pp. 252-258.

[86] K. Yuki, T. Murakami, and K. Ohnishi, "Vibration control of 2 mass resonant system by resonance ratio control," in *Industrial Electronics, Control, and Instrumentation, International Conference on*, 1993, pp. 2009-2014.

[87] Y. Hori, H. Sawada, and C. Yeonghan, "Slow resonance ratio control for vibration suppression and disturbance rejection in torsional system," *Industrial Electronics, IEEE Transactions on,* vol. 46, pp. 162-168, 1999.

[88] Y. Zhou, F. Peng, and B. Li, "Adaptive Notch Filter Control for the Torsion Vibration in Lead-Screw Feed Drive System Based on Neural Network," in *Proceedings of the First International Conference on Intelligent Robotics and Applications: Part II*, Wuhan, China, 2008, pp. 803-812.

[89] J. Han, "From PID to Active Disturbance Rejection Control," *Industrial Electronics, IEEE Transactions on,* vol. 56, pp. 900-906, 2009.

[90] O. Kester and e. al., "The MSU/NSCL Re-Accelerator ReA3," in *International Conference on Radio Frequence Superconductivity*, Berlin, Germany, 2009, pp. 57-61.

[91] R. C. York and e. al., "FRIB: A New Accelerator Facility for the Production of Rare Isotope Beams," in *International Conference on Radio Frequence Superconductivity*, Berlin, Germany, 2009, pp. 888-894.

[92] C. Hovater, "RF Control of High QL Superconducting Cavities," in *Linear Accelerator Conference*, Victoria, Canada, 2008, pp. 704-708.

[93] T. H. Kandil, H. K. Khalil, J. Vincent, T. L. Grimm, W. Hartung, J. Popielarski, R. C. York, and S. Seshagiri, "Adaptive feedforward cancellation of sinusoidal disturbances in superconducting RF cavities," *Nuclear Instruments and Methods in Physics Research Section A: Accelerators, Spectrometers, Detectors and Associated Equipment,* vol. 550, pp. 514-520, 2005.

[94] S. Simrock, G. Petrosyan, A. Facco, V. Zviagintsev, S. Andreoli, and R. Paparella, "First demonstration of microphonic control of a superconducting cavity with a fast piezoelectric tuner," in *Particle Accelerator Conference*, Portland, OR, 2003, pp. 470-472.

[95] M. G. Minty and R. H. Siemann, "Heavy beam loading in storage ring radio frequency systems," *Nuclear Instruments and Methods in Physics Research Section A: Accelerators, Spectrometers, Detectors and Associated Equipment,* vol. 376, pp. 301-318, 1996.

[96] J. Vincent, D. Morris, N. Usher, Z. Gao, S. Zhao, A. Nicoletti, and Q. Zheng, "On active disturbance rejection based control design for superconducting RF

cavities," *Nuclear Instruments and Methods in Physics Research Section A: Accelerators, Spectrometers, Detectors and Associated Equipment,* vol. 643, pp. 11-16, 2011.

[97] S. Zhao, Q. Zheng, and Z. Gao, "On Model-free Accommodation of Actuator Nonlinearities," in *World Congress on Intelligent Control and Automation*, Beijing, China, 2012, Accepted.

[98] C. C. Hang, K. J. Astrom, and Q. G. Wang, "Relay feedback auto-tuning of process controllers — a tutorial review," *Journal of Process Control,* vol. 12, pp. 143-162, 2002.

APPENDICES

A.1 Permission for Reusing Copyrighted Photos

RE: Request for permission to reuse copyrighted photos

From: **Kingery, Ken** (kingery@nscl.msu.edu)
Sent: Wednesday, March 07, 2012 12:38:53 AM
To: Shen Zhao (teddy__zhao@hotmail.com)

Sure! Go right ahead and good luck with your dissertation!

ken

From: Shen Zhao [mailto:teddy__zhao@hotmail.com]
Sent: Tuesday, March 06, 2012 10:31 AM
To: Kingery, Ken
Subject: Request for permission to reuse copyrighted photos

Ken,

I am a doctoral student at Cleveland State University. We had a collaboration with NSCL in 2010 on a project to solve the microphonics problem in the SRF cavity control. I will include this research work in my dissertation and would like to reuse the attached two photos, which I found online, in both my dissertation (print and electronic form) and presentation. I believe the photos are copyrighted and am asking for the permission to reuse them. The title of my dissertation is "FROM THE DISTURBANCE REJECTION PARADIGM IN CONTROL DESIGN: PRACTICAL SOLUTIONS TO THE NON-MINIMUM PHASE AND VIBRATION PROBLEMS" and the research work mentioned above will be the sixth chapter of the dissertation.

Thank you for your consideration.

Sincerely,

Shen Zhao
216.502.1204

A.2 MATLAB Files Used in the Dissertation

All simulation files and MATLAB codes to regenerate the results in this dissertation can be downloaded at the Center for Advanced Control Technologies website: http://cact.csuohio.edu/index.php?option=com_content&view=article&id=51&Itemid=58.

A.3 List of Publications

1. S. Zhao and Z. Gao, "An active disturbance rejection based approach to vibration suppression in two-inertia systems," in *American Control Conference*, 2010, pp. 1520-1525.

2. S. Zhao and Z. Gao, "Active disturbance rejection control for non-minimum phase systems," in *Chinese Control Conference*, 2010, pp. 6066-6070.

3. J. Vincent, D. Morris, N. Usher, Z. Gao, S. Zhao, A. Nicoletti and Q. Zheng, "On Active Disturbance Rejection Based Control Design for Superconducting RF Cavities," *Nuclear Instruments and Methods in Physics Research Section A*, vol. 643, pp. 11-16, 2011.

4. S. Zhao and Z. Gao, "An active disturbance rejection based approach to vibration suppression in two-inertia systems," *Asian Journal of Control*, accepted.

5. S. Zhao, Q. Zheng and Z. Gao, "On Model-free Accommodation of Actuator Nonlinearities," in *World Congress on Intelligent Control and Automation*, 2012, accepted.

6. S. Zhao, W. Xue and Z. Gao, "Achieving Minimum Settling Time Subject to Undershoot Constraint in Systems with One or Two RHP zeros," *ASME Journal of Dynamic Systems, Measurement and Control*, submitted.